FOUR-DIMENSIONAL RADIATION THERAPY FOR THORACIC CARCINOMA

—

Dosimetric Evaluation Using Deformable Image Registration

Thesis submitted in accordance with the
requirements of the University of Liverpool
for the degree of Doctor in Philosophy

By

Victy Yee Wa Wong

September 2012

CONTENTS

To my father, the smartest and most inspirational man I know. Although he is no longer with us, his influence has never faded. His curiosity and enthusiasm towards the universe and adventurous spirit, that I have followed grounding me the courage to commit to this study.

To my mentor, Dr Thien How, who has been my mentor for twenty years. He exemplifies hard work and pride in his profession, and encourages my love of science, research and music. The time he spent, the opportunities he provided and the instruction he gave continue to bless my life. The attitude and care he put into all of his students has set an example I hope to follow.

To my nephew and nieces, Cruz, Portia, Chloe, Sinead and Kristal, you were the spark that kindled my dream. Your natural, simple and cheerful essence often reassured me from anxiety during study. I hope you will always know how proud I am of you, how grateful I am for you, and all how much I love you.

To my family and my friends, you have supported me in the darkest of times and believed in me even when I did not believe in myself. Your tireless efforts not only sustained my work but made the past three years some of the best of my life. The pleasurable environment you helped to maintain provided the boost that made even the longest hours enjoyable. Words cannot express how grateful I am for your love and support.

To the person who loves Physics, "Life is like riding a bicycle. To keep your balance you must keep moving – Albert Einstein"

ACHOWLEDGEMENTS

(To whom this thesis is dedicated)

I would like to offer special thanks to Dr. Colin R. Baker, who has provided supervision and thought-provoking guidance to this research to a successful completion. The opportunities Dr Baker provided to broaden my professional experience and prepare me for future challenges are gratefully acknowledged.

I would like to thanks Dr. Thien V. How for his patient guidance on this study. Special thanks to Dr. How for his careful review and numerous revisions provided on the manuscript.

I would like to express my gratitude to Dr. To-Wai Leung, the Chief-of-Service of the Department of Clinical Oncology, Queen Mary Hospital, Hong Kong, for his countless acts of support in this study.

I would like to thank Dr. Stewart Y. Tung, the Chief-of-Service of the Department of Clinical Oncology, Tuen Mun Hospital, Hong Kong, for his kind support in this study and permission of using the clinical data.

I am grateful to Dr. Alice, W. Y. Ng for the provision of the clinical data and useful discussions on the updated treatment techniques.

I would like to express my gratitude to Brainlab AG (Feldkirchen, Germany) for the retrieval of the morphed vector which relates the changes in morphology between different phases of the 4D CT dataset.

The research study has been approved by the Ethical Committee of Hospital Authority, Hong Kong

ABSTRACT

Respiratory motion remains a significant challenge for radiation therapy in targeting the tumour. The use of planning margins to avoid geometrical miss of the target volume during respiration results in excessive lung tissue irradiation that limits the prescribed dose to be safely delivered and escalated for better therapeutic gain. The purpose of this study was to develop effective dose planning techniques for treatment to be performed under natural patient breathing. The techniques accounted for the dosimetric influences of tumour movement and aimed to provide an optimized treatment volume by minimizing the internal target volume (ITV) without compromising the target coverage.

In the study, the accumulated 4D dose distribution over the tumour volume was calculated using deformable image registration (DIR). A DICOM-RT based tool-box was specially developed for automated 4D dose calculation and evaluations. A new concept of defining the internal target volume from 4D dose coverage, namely inverse ITV (iITV) was introduced via the dose volume enclosed by the minimum accumulated dose in the tumour during the respiratory cycle. The dosimetric advantages of using this iITV with reference to the conventional ITV were confirmed in nine clinical cases by an average dose volume reduction of 16.4% (ranging from 2.3% to 29.9%). 4D radiotherapy involves complex dose distribution which was found to be affected by a number of factors including tumour size, magnitude of tumour displacement, tumour motion characteristics and the reference phases selected for dose planning. Our findings indicate that optimal dose planning was generally, but not always, achieved with the planning CT performed at the temporal mean tumour position and the degree of target coverage maximization strongly depends on the nature of tumour movement. Moreover, the conventionally geometric defined treatment margin could over estimate the treatment volume for a required target coverage.

In conclusion, 4D dose calculation based on DIR offers realistic dose estimation, as both geometric and temporal factors are considered, and also provides optimal dose plans by minimizing the treatment volume. However, 4D radiation planning involves a number of factors resulting from the properties of tumours (eg. tumour

size, amplitude and characteristics of tumour motion, etc) and from the procedure of treatment planning (eg. reference phase for dose planning, penumbra of dose beam, employed treatment volume etc) that interactively affect the resultant dosimetry. Since these factors vary patient-by-patient, there is no single formula or universal solution that can be used to obtain optimal dose planning. The 4D dose toolbox developed in this study could however provide a user friendly platform for 4D dose calculation and analysis, and allow the optimal treatment modalities and planning techniques to be determined for individuals.

CHAPTER 1

INTRODUCTION

1.1 Lung Cancer

1.1.1 Overview of Lung Cancer

Lung Cancer is the most common cancer in the world with 1.61 million new cases diagnosed every year. In 2005 there were 172,570 new lung cases diagnosed in the United States, an estimated 94.7% of whom died as a result of their lung cancer. The UK cancer registry in 2008 also reported that lung cancer was the most common cause of death from cancer for both men and women, and was responsible for approximately 22% of all cancer deaths and 6% of all deaths in UK (Office for National Statistics 2008; ISD Online 2009; Northern Ireland Cancer Registry 2009). With a 5-year survival in the range 10-14%, lung cancer is the leading cause of cancer death and accounts for about 1 million deaths worldwide every year (Williams et al. 2001).

Lung cancer is a disease caused by the rapid growth and division of cells that make up the lungs. Under normal circumstances, lung cells reproduce in an orderly fashion to maintain tissue health and repair injuries. However, when growth control is lost and cells divide too much and too fast a cellular mass (or tumour) is formed. If the mass is confined to a few cells layers and does not invade the surrounding tissues or organs, it is considered benign. However, if the mass spreads to adjacent tissues or organs, it is considered malignant or cancerous. If the cancerous cells break away from the original tumour, travel and grow within other organs – such as the opposite lung, bone, brain, liver, adrenal glands, or lymph nodes of the chest, the process is known as metastasis.

The risk factors for lung cancer include smoking, exposure to radon gas, industrial carcinogens and air pollution, family history and lifestyle (e.g., lack of physical activity, poor diet, excessive alcohol consumption). Tobacco smoking is the main aetiology causing approximately 90% of cases (Parkin 2011; Lubin et al. 2007; Lukanich 1999). Passive smokers are also at increased risk of lung cancer (Doll et al. 1994; Janssen-Heijnen et al. 2003; Harkness et al. 2002; Taylor et al. 2001).

Radon exposure (Frumkin et al. 2001; Green et al. 2002; Darby et al. 2005) and certain occupational exposure to arsenic, asbestos, chromium, nickel and vinyl chloride also plays an important role in lung cancer (Armstrong et al. 2004; Richiardi et al. 2004).

1.1.2 Types of Lung Cancer

Lung cancer is classified into different types according to its histology and includes small cell carcinoma (SCLC), squamous cell carcinoma, adenocarcinoma, large cell carcinoma, broncho-alveolar carcinoma and undifferentiated pulmonary carcinoma. Squamous cell carcinoma and SCLC often are centrally located and may appear as pneumonia, atelectasis, or pit-like masses. Adenocarcinoma and large cell carcinoma are usually found on the periphery of the lungs and may occur as solitary nodules. Squamous cell cancers frequently are slow growing and can take several years to progress from a confined tumour into invasive cancer. The prognosis of adenocarcinoma and large cell cancer tend to have a worse prognosis than squamous cell cancer at all stages.

1.1.3 Causes of Lung Cancer

Squamous cell carcinoma, adenocarcinoma and large cell carcinoma account for approximately 35%, 27% and 10% of all lung cancers, respectively (National Institute for Clinical Excellence. 2005), the remainder is SCLC. The small cell carcinoma, squamous cell carcinoma and adenocarcinoma are the three principal histological types associated with smoking-related lung cancer. Adenocarcinoma also account for the lung cancer in non-smokers. In the United States, adenocarcinoma is now the most common type of lung cancer. In Europe the most common type of lung cancer is still squamous cell carcinoma despite increases in the incidence of adenocarcinoma (Harkness et al. 2002). The National Cancer Institute (NCI) also reported that adenocarcinoma is now more common than squamous cell carcinoma in both Caucasian and African American women. In Hong Kong, there is very high rate of lung adenocarcinoma among Chinese women. In addition, the rate of adenocarcinoma in Koreans is increasing in both sexes. The causes for race- and sex-related differences in lung cancer histopathology are unknown. Some experts suggest that adenocarcinoma in women may be increased by hormonal (endocrine) factors. In particular, researchers believe that estrogen replacement

therapy (ERT) increases the risk for adenocarcinoma (Riman et al. 2002). Studies have also indicated that women may have a greater genetic susceptibility to specific types of lung cancer due to female, X-linked inheritance (inheritance of genes located on the X chromosome) (Hemminki et al 2005). However, the increasing incidence of adenocarcinoma has been linked to low-tar cigarettes.

Occupational exposure is also associated with certain histopathologic types of lung cancer. For example, recent findings (Wild et al. 2000) suggest that long-term (20+ years) exposure to mineral and metal dust is related to the growth of both small cell and squamous cell carcinomas. In addition, asbestos exposure may be associated with the development of adenocarcinoma and, to a lesser degree, with squamous cell or anaplastic carcinoma (cancer in which the cells have lost specialized characteristics, including physical placement). Some investigators theorize that household exposure to low-dose radon over long period of time may increase the risk of small cell lung carcinoma (Alavanja et al. 1999).

1.2 Conventional Treatment Methods for Lung Cancer

There are three options for treating the primary lung cancer namely surgery, chemotherapy and radiation therapy and these may be applied alone or in combination. The choice of treatments depends on a number of factors, including the histological type, the stage of the disease and the physical condition of the patient.

For treatment considerations, lung cancer is divided into two groups: Small Cell Lung Carcinoma (SCLC) and Non-Small Cell Lung Carcinoma (NSCLC). The NSCLC which include squamous cell carcinoma, adenocarcinoma and large cell carcinoma accounts for 80-85% of all lung cancers (National Institute for Clinical Excellence. 2005). There are substantial differences between NSCLC and SCLC in both treatment and prognosis. In general, SCLC tends to be more aggressive and spread sooner to distant sites. Studies suggest that 60-70% of patients with SCLC show evidence of distance spread at the time of initial diagnosis. Treatment of SCLC is not based upon surgery. In fact SCLC is considered to be more responsive to the systematic treatment approach such as chemotherapy and radiotherapy. In contrast, NSCLC may not have spread at the time of diagnosis and surgical resection of the tumour is the treatment of choice.

The TNM classification for staging of lung cancer was revised in 1997 (Mountain 1997) (Table 1.0). The stage of the disease is classified according to the size, location of the tumour and whether the cancer has spread to or beyond the lymph nodes. For the early stage NSCLC with no lymph node involvement, surgical resection of the tumour is the principal form of treatment for the patient. If patients are unable to undergo tumour resection, radiotherapy is considered with the aim of eradicating the primary tumour. For the advance stage disease where obvious lymph nodes or/and metastases are involved, a combination treatment involving radiation therapy and chemotherapy is applied. However, it is unclear whether or not disease-free or overall survival is improved when surgery is performed after concurrent combination therapy.

Table 1.0 TMN classification for lung cancer

0	Carcinoma in situ
IA	T1N0MO
IB	T2N0M0
IIA	T1N1M0
IIB	T2N1M0, T3N0M0
IIIA	T3N1M0, T1—T3N2M0
IIIB	T4N0—N3M0, T1—T3N3M0
IV	any T any N M1
TX	Primary tumour cannot be assessed, or tumour proven by the presence of malignant cells in sputum or bronchial washings but not visualized by imaging or bronchoscopy
T0	No evidence of tumour
T1	Tumour < 3 cm in greatest dimension, surrounded by lung or visceral pleura, without bronchoscopic evidence of invasion more
T2	Tumour with any of the following features of size or extent: >3 cm, involves main bronchus >2 cm distal to carina, invades the visceral pleura. Associated with atelectasis or obstructive pneumonitis that extends to the hilar region but does not involve the entire lung.
T3	Tumour of any size that directly invades any of the following: chest wall (including superior sulcus tumours), diaphragm, mediastinal pleura, parietal pericardium; or tumour in the main bronchus < 2 cm distal to carina, but without involvement of the carina; or associated atelectasis or obstructive pneumonitis of the entire lung
T4	Tumour of any size that invades any of the following: mediastinum, heart, great vessels, trachea, oesophagus, vertebral body, carina; or tumour with a malignant pleural or pericardial effusion, or with satellite tumour nodule(s) within the ipsilateral primary tumour lobe of the lung
Nx	Regional lymph nodes cannot be assessed
N0	No evidence of lymph node
N1	Metastasis to ipsilateral peribronchial and/or ipsilateral hilar lymph nodes and intrapulmonary nodes involved by direct extension of the primary tumour
N2	Metastasis to ipsilateral mediastinal and/or subcarinal lymph node(s)
N3	Metastasis to contralateral mediastinal, contralateral hilar, ipsilateral or contralateral scalene, or supraclavicular lymph node(s)
Mx	Presence of distant metastasis cannot be assessed
M0	No distant metastasis
M1	Distant metastasis present

1.3 Enhanced Radiation Treatment for Lung Cancer – Stereotactic Hypo-fractionated Radiation Therapy

The most common types of lung cancer affecting 75%-80% of patients are grouped under NSCLC (Michaiski, et al. 2004). Of these, approximately 15-20% present with early or localized disease, with the primary tumour in the lung and no nodule involvement, or metastases elsewhere. With increasing use of Computed Tomography (CT) for staging cases of secondary lung cancer, the number of patients with the disease is expected to rise significantly in the coming decades.

Surgery is the main curative treatment for the early stage NSCLC patients and is generally accepted as the treatment of choice. Five-year survival rates for early stage patient treated with radical surgery, specially a lobectomy or pneumonectomy, are over 60% (Mountain 1997; Naruke et al 1988) and as high as 80% for very early squamous cells carcinoma (Souhami et al. 2005). The local control rate was reported to be over 90% (Martini et al. 1995). However, some patients are not suitable surgical candidates for a number of reasons including poor pulmonary reserve, cardiac dysfunctions, vascular disease, diabetes mellitus, general frailty or other co-morbidities. In the case of poor pulmonary reserve, extensive surgical resection is restricted especially for patients with centrally located tumours. Moreover, many of the co-morbidities impact on the anaesthetic and peri-operative risk, and thus preclude any surgical procedure. These patients are typically considered for radiation therapy, with the aim of eradicating the primary tumour.

1.3.1 Treatment Rationale

Conventional radiation therapy, however, has inferior results when compared to surgical series; with local control of 56% and 5-year survival rates ranging from 10% to 30% (Haffty et al. 1998; Dosoretz et al. 1992; Morita et al. 1997). The poor outcomes are partly accounted for by the lower rate of tumour eradication and the selection of less fit patient. Conventional radiotherapy typically consists of 50-66 Gy total dose in 1.8-2.5 Gy per fraction, that is equivalent to Biological Effective Dose 10Gy (BED_{10}) ranging from 64.9 – 68.8 Gy. Some studies, however, demonstrate a benefit to local control by dose escalation. Blomgren and Lax

(Blomgren et al. 1998) developed stereotactic radiotherapy for early stage NSCLC and demonstrated that dose escalation was associated with better local control and survival than conventional radiation therapy. The relationship between dose escalation and local control was further demonstrated by Onishi *et al* (2004), McGarry *et al* (2005) and Wulf *et al* (2005). Onishi *et al* showed a lower cancer recurrence rate with $BED_{10} \geqq 100Gy$ compared to $BED_{10} \leqq 100Gy$ (8.1% vs 26.4%, p=0.04) for stage 1 NSCLC using stereotactic radiotherapy. Wulf *et al* reported a steep dose-response curve using $BED_{10.}$ Encouraging treatment results on hypofractionation stereotactic radiotherapy for stage 1 NSCLC have been reported in numerous studies. Ng *et al* (2008) treated patients with dose escalation of BED_{10} ranged from 90 to 151 and reported 2-year local control and cancer specific survival (CSS) rates of 94.7% and 77.6%, which are very close to those obtained by Fukumoto *et al* (2002) of 94% and 73%, respectively. Hoyer *et al* (2006) also reported a 62% 2-year CSS. Onishi *et al* (2004) reported both 3- and 5-year CSS of 78%. Five-year overall survival had been reported to be 30% -83%, significantly higher than the figure of 15% obtained when patients are treated with conventional radiotherapy. This suggests that medically unfit patients would still benefit from the enhanced radiation treatment technique.

The rationale of stereotactic hypo-fractionated radiation therapy (SHRT) is based on the principles and experience gained from stereotactic brain radiosurgery that allows delivery of very high doses of radiation confined to the tumour region, usually in several large fractions (hypofractionated), by multiple co-planar and non-coplanar beam guided by a set of stereotactic coordinates system. SHRT requires a precise definition of the target, assessment and management of target motion, determination of an effective planning target volume according to the accuracy of target localization of individual centre, conformal RT planning and daily quality assurance on treatment setup. SHRT was developed in the early 1990s in the Karolinska Institute in Stockholm, Sweden (Blomgren et al. 1995), and has been used as an accepted alternative treatment for patients with early stage lung cancer in many centres in Japan and Germany, U.S.A. and elsewhere. Large fraction size is essential for effective outcomes of SHRT as it dominates the BED. A number of fractionation schedules have been employed, including single fractions of 20Gy

-26Gy and various fractionated regimens (commonly 3 to 5 fractions).

1.3.2 Implementation Requirements

In addition to the various dose-fractionation schemes, the technical aspects of treatment planning and treatment delivery to make the SHRT more effective are also important as these technical factors clearly influence the dose delivery to the tumour and the organs at risk, and thus, may impact on both local control and the radiation-induced toxicity. A major challenge for implementing the SHRT for patients with lung cancer is the tumour motion caused by breathing. Some studies have reported that up to 40% of lung tumours move by more than 5 mm and of these 10-12% move by more than 1 cm (Liu et al. 2007; Donnelly et al. 2007). However, conventional treatment planning techniques based on CT images performed on free breathing carry no information of tumour movement. To avoid geometrical misses of the target, it is necessary to apply safety margins which are substantially extended beyond the gross tumour volume to create the planning target volume (PTV). This results in excessive lung tissue irradiation and restricts the ability of dose escalation. To mitigate the effect of motion, many treatment methods have been proposed or in current clinical usage (Ohara et al. 1989; Minohara et al. 2000; Kubo et al. 1996; Keall et al. 2001; Mageras G.S 2001). The effect of tumour motion on radiotherapy planning and the different approaches adopted by various researchers to mitigate this are reviewed in the following chapters.

1.4 Treatment Techniques for Stereotactic Hypo-fractionated Radiation Therapy

To address the issue of tumour motion, several sophisticated treatment delivery methods such as respiratory gating, tracking of tumour motion or tumour immobilization using breath-hold have been developed, in an attempt to reduce the treatment margin required and hence allow dose escalation and consequently minimize toxicity caused by the excessive irradiation of healthy tissue (Barnes et al. 2003; Wong et al. 1999; Engelsman et al. 2005; Mageras et al. 2004; Berbeco 2005; Brown et al. 2007).

In respiratory gating, surrogates of tumour motion are used to trigger the therapeutic beam. Shirato *et al* (2000) have established a method for gating the respiratory movement based on the three-dimensional location of a fiducial implanted near the tumour. Continuous multi-view of the fiducial is employed to ensure that the radiation is being delivered accurately. Schweikard *et al* (2000) used infrared external markers and implanted radio-opaque markers to periodically reestablish the correlation between internal and external movement throughout an irradiation session using the Cyberknife system (Accuray, Inc, Sunnyvale, CA, USA). Many institutes have also developed techniques for respiratory gating based on the position of an external surrogate placed on the thorax or abdomen, or with occasional verification of internal anatomy using x-ray if available. In such cases, the desired treatment outcomes are therefore strongly dependent on patients having a repeatable or predictable respiratory pattern; otherwise the results could be adversely affected. However, geometric uncertainty resulting from the poor correlation between internal tumour motion and movement of external surrogates has been the major pitfall for the respiratory gated radiotherapy (RGRT) (Li et al. 2007; Berbeco et al. 2005). RGRT also requires longer treatment delivery time as irradiation only proceed at the respiratory ‘gate’ (20%-30% of the respiratory cycle), which can in turn increase the risk of patient movement during treatment (Korreman et al. 2008). Muirhead *et al* (2010) evaluated the potential clinical benefit of RGRT in lung cancer and showed that the reduction in toxicity parameter was limited in comparison with non-gated (continuous) 4DCT irradiation due to the intrinsic errors involved in RGRT.

On the other hand, instead of tracing tumour motion, tumour immobilization during

irradiation was pioneered by Wong *et al* (1999) using spirometry. The tumour is temporarily immobilized under deep inspiration breath hold using the active breathing control system (ABC). The deep inspiration breath hold (DIBH) technique has the potential benefits of better tumour immobilization and since this maximizes lung capacity, toxicity is minimized thus allowing treatment with potential dose escalation. However, with such a technique, training must be provided prior to treatment and this may not be tolerated by all patients. Unstable breathhold control could induce unsatisfactory target immobilization thereby resulting in possible treatment failure. With these techniques, compliance of the patients to ensure a reproducible breathing pattern is a pre-requisite in achieving a desirable outcome with the enhanced treatment.

The most consistent and stable tumour movement is expected with natural breathing of the patient. Therefore, despite the availability of the advanced delivery techniques, recent studies have re-employed a free-breathing treatment technique with the treatment margin carefully determined to account for the tumour motion. The concept of internal target volume (ITV) has been suggested by the International Commission on Radiation Units and Measurements (ICRU) report 62 (1999). The ITV is defined as the clinical target volume (CTV) plus an additional margin to account for geometric uncertainties due to internal variations in tumour position, size and shape. The CTV cannot be visualized with the current imaging modalities. The ITV is defined by delineation of the gross tumour volume (GTV) on each of the phases that constitute the four-dimensional computed tomography (4D-CT) image date set, followed by expansion of each GTV to account for the microscopic spread of disease. To make the determination of the ITV more applicable, a recent study (Ezhil et al. 2009) modified the determination of ITV by proposing the concept of internal gross tumour volume (IGTV) which explicitly accounts for internal variations in tumour position, size and shape but is directly derived from imaging studies. The ITV was then determined to be the IGTV plus a margin that accounts for microscopic disease. IGTV is therefore generated by contouring the GTV on each binned phase (typically ten) of the 4D-CT dataset. The merging of these individual three-dimensional (3D) volumes into a single 3D volume represents the IGTV, which denotes the volume of the entire moving tumour. To speed up the contouring process, the IGTV can be generated directly on the maximum intensity

projection (MIP) image data set, in which each voxel represents the maximum intensity encountered by corresponding voxels in all individual 3D data sets of the 4D-CT. This avoids the need to perform contouring the tumour volume on every data set. The post processing of MIP images has been commonly applied for defining the ITV for clinical applications. Another alternative to determining the IGTV by using breath-hold CT imaging is to acquire images at the two extremes (end expiration; end inspiration) of the respiratory cycle. The GTV of each phase is then contoured and the GTVs are then combined to form the IGTV. However, both alternated methods were found to be sub-optimal for IGTV determination. The poor visibility of the MIP images and the possible tumour deformation between the two extreme phases of the breathing and the curved motion pathway during breathing may introduce uncertainty. To identify the most effective delineating technique, studies (Ezhil et al 2009; Underberg et al. 2005; Bradley et al. 2006; Cai et al. 2007) have been carried out to evaluate the delineation accuracy of IGTV using the ten-phase IGTV as reference.

1.5 Aims and Objectives of the Thesis

The concept of ITV and IGTV accounts for the tumour motion only from the geometrical aspect but does not take into consideration the temporal movement of the tumour which may lead to excessive irradiation being delivered to the neighbouring healthy tissue. For instance, tumour coverage shown on each phase of the respiratory cycle occurs during only a fraction of the time, but according to the definition of ITV/IGTV, radiation dose is assigned over the whole breathing cycle. A more appropriate ITV would achieve optimal dose coverage by accounting for the dynamic tumour motion. Several studies (Ezhil et al. 2009; Germain et al. 2008; Kang et al. 2007) have proposed a 4D-dose calculation based on the convolution of the static dose distribution with the probability distribution function (PDF) of the organ motion. Such an approach only accounts for translational displacement and the influence of non-rigid anatomical displacement (i.e. deformable anatomical change) on the dose distribution during breathing is not considered.

This thesis is concerned with radiotherapy treatment planning in the presence of significant tumour movement and aims to investigate and develop an optimal treatment planning technique for lung cancer where the treatment is carried out with natural breathing of the patients. The study is based on the realistic treatment doses over the moving tumour which is evaluated in 4D accounting for both spatial and temporal factors.

In this work, the 4D dose distribution over the moving target was calculated using deformable image registration (DIR), which explicitly takes into account the anatomical changes in shape, volume, position and density during respiration. The DIR tracks the displacement of each voxel of the CT image during the respiratory cycle. Summation of the dose along the trajectory of each voxel generates a realistic 4D dose. Since the 4D dose calculation is complex and involves considerable quantities of dose data, a DICOM-RT based tool box was devised as part of this study in order to automate the dose calculation. The tool box literally transforms any DICOM-RT dose plan from 3D to 4D based on deformable voxel-dose registration. Using the tool box, the 4D dose distribution over the target volume was retrospectively evaluated in nine clinical cases. The several aspects which are involved in realizing the optimal 4D dose planning for treatment of lung

cancer were explored. The main pertinent topics are briefly introduced below.

1) By converting the 3D spatial dose distribution to the 4D spatial-temporal dose distribution, the actual accumulated dose received by the tumour can be revealed. In determining the 4D dose distribution over the tumour, a new concept of defining the internal target volume from 4D dosimetry is proposed. The inverse ITV (iITV) is introduced in this study. [discussed in Chapter 5, section 2]

2) The planning target volume is considered to be the crucial factor for maximizing the therapeutic ratio, as it affects the degree of radiation induced toxicity and hence the potential for dose escalation. Minimizing the internal treatment volume is one of the pathways to achieve the goal. Whether this can be fulfilled by the proposed iITV without compromising the target coverage is one of the concerns which was assessed in the study. [discussed in Chapter 5, section 3, Chapter 5, section 4].

3) In general, the under dosage of an irradiated target is considered to be highly associated with the magnitude of tumour movement. This is conventionally compensated by an additional treatment margin with magnitude directly related to the range of tumour movement. This leads to a substantial irradiated lung volume and the opportunity for increasing prescribed dose is limited. There also remains a controversy (Murphy et al. 2007; Spoelstra et al. 2008.) concerning the threshold of tumour motion where respiratory management of tumour movement should be considered during treatment. Considering that the influence on dose distribution with the same magnitude of movement is far more significant for a small sized target than a large one, then there is a question mark about whether the ITV margin should be applied regardless the target size. Consequently this leads to the question as to how the treatment techniques should be determined for individual cases. The tumour characteristic which may significantly affect the treatment dose are investigated with the aim of identifying the important factors for the optimal treatment planning. [discussed in Chapter 6]

4) In reviewing the numerous studies of lung cancer radiotherapy, the deep

inspiration breath hold technique appears to have potential benefits of better tumour immobility and minimized toxicity due to maximized lung capacity. However, such technique may be poorly tolerated by patients with compromised pulmonary function. The effectiveness of treatment techniques between the 4D treatment planning with free breathing (proposed in this study) and 3D treatment planning with deep inspiration breath hold is compared for optimized dosimetry for selected cases. The most effective and suitable treatment technique for individual patients is determined upon the projected treatment outcomes. [discussed in Chapters 7 and 8]

CHAPTER 2

DICOM-RT BASED TOOL BOX FOR FOUR DIMENSIONAL NON-RIGID DOSE CALCULATION

2.1 Design of DICOM-RT Based Tool box

A toolbox that consists of five main functions was developed for this study. This was written in the MATLAB (Version 7.6, R2008a, The Mathworks Inc.) scientific software environment, in conjunction with CERR, an open source computational environment for radiotherapy research for DICOM images and DICOM-RT data access and analysis. The 4D dose calculation was performed using Image Morphing (IM) (BrainLab, White paper), a deformable image registration tool provided by BrainLab Ltd (Germany). This allows the displacement of each voxel to be tracked during a respiratory cycle and consequently the accumulated dose along the trajectory of each voxel to be generated.

A) Treatment Planning Data Import

A full set of 4D CT images and the dose plans in DICOM-RT format were imported into the computation environment for Radiotherapy Research software (CERR) where the dose value and its corresponding position were contained in a 3D array. The positions of the dose points in the transverse plane were defined according to the CT pixels in a 512 x 512 matrix (Figure 2.1). The position along the cranio-caudal direction was indicated by the CT slice number. For example A (1, 2, 1) indicates dose point located at the 1^{st} row, 2^{nd} column and 1^{st} CT slice. The spatial dose resolution (grid interval) defined by the pixel size and the size of the scanning field (520 mm was employed in the study) was 1.01 mm in the lateral and the anterior-posterior directions and 3 mm in the caudal- cranial direction as determined by the CT slice thickness.

Figure 2.1 The dose points presented in 3D array with CERR

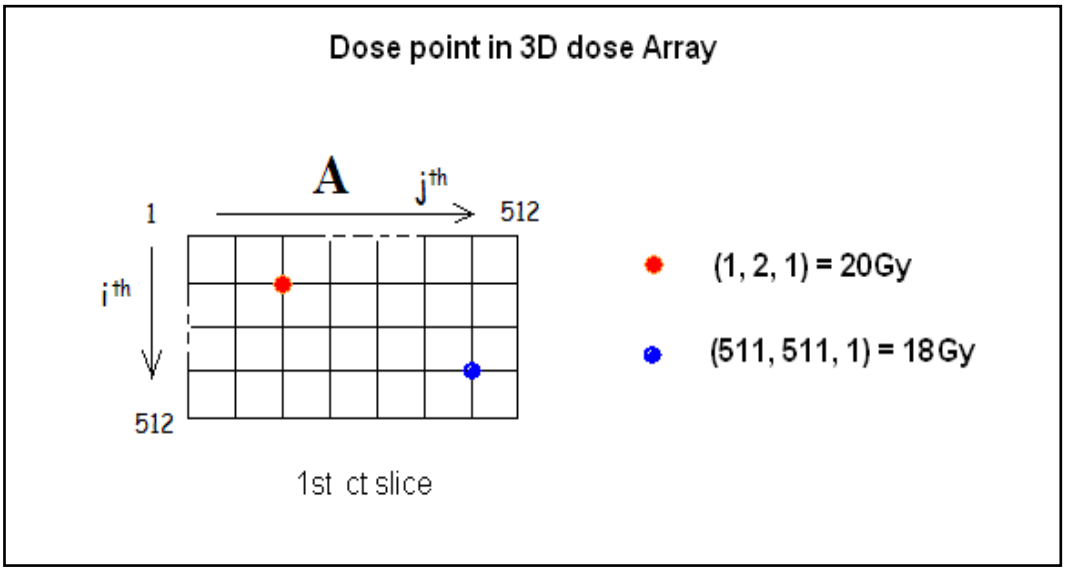

B) Deformable Image Registration – Image Morphing

To identify the displacement trajectory of each voxel during breathing, the deformable image registration tools, Image Morphing (IM) provided by the iPlan (BrainLab Ltd) treatment planning system was used. IM employs a knowledge-based segmentation approach (Chao, Schreibmann, et al. 2006) in which the anatomical structures are morphed from the source images to the target images by comparing the image data. The source data is deformed based on similarity calculation using mutual information and cross correlation algorithm to improve the similarities in voxel density until a match is found. Once the similarity measure is defined, the registration algorithm optimizes the similarities by adjusting the transformation vectors in an iterative process. When the point-to-point correspondence of the two datasets is identified, the software automatically transfers all outlined structures of the source onto the target data set. As a result, the deformation vector field, which defines a unique mapping from the source onto the target data set, is generated. Figure 2.2 illustrates the morphing process; IM creates a virtual grid of points in the source data set and matches them with a grid of points on the target data set. Since each grid point is indexed and its location is recorded in 3D co-ordinates, the voxel displacement caused by breathing can be traced by the position of the corresponding grid point. The output file generated by IM is formatted into a 6D array with the 3D CT co-ordinates of the corresponding grid point for the source data set and the target data set recorded in the 1^{st} – 3^{rd} components and 4^{th} - 6^{th} components of the array, respectively. For example, M

denotes the morph array, and M (1) = [1, 2, 3, 4, 5, 6] implies that the first voxel with the CT coordinates of (1, 2, 3) in the source image was displaced to the CT coordinates of (4, 5, 6) in the target image (figure 2.2). The 3D spatial resolution of the grid point was 1 mm. A sample of M matrix is shown in Table 2.1.

Figure 2.2 Deformable image registration using Image Morphing (IM). Voxels with CT coordinates (x, y, z) in the source image displaced to (x', y', z') in the target image was depicted by the morph matrix "M"

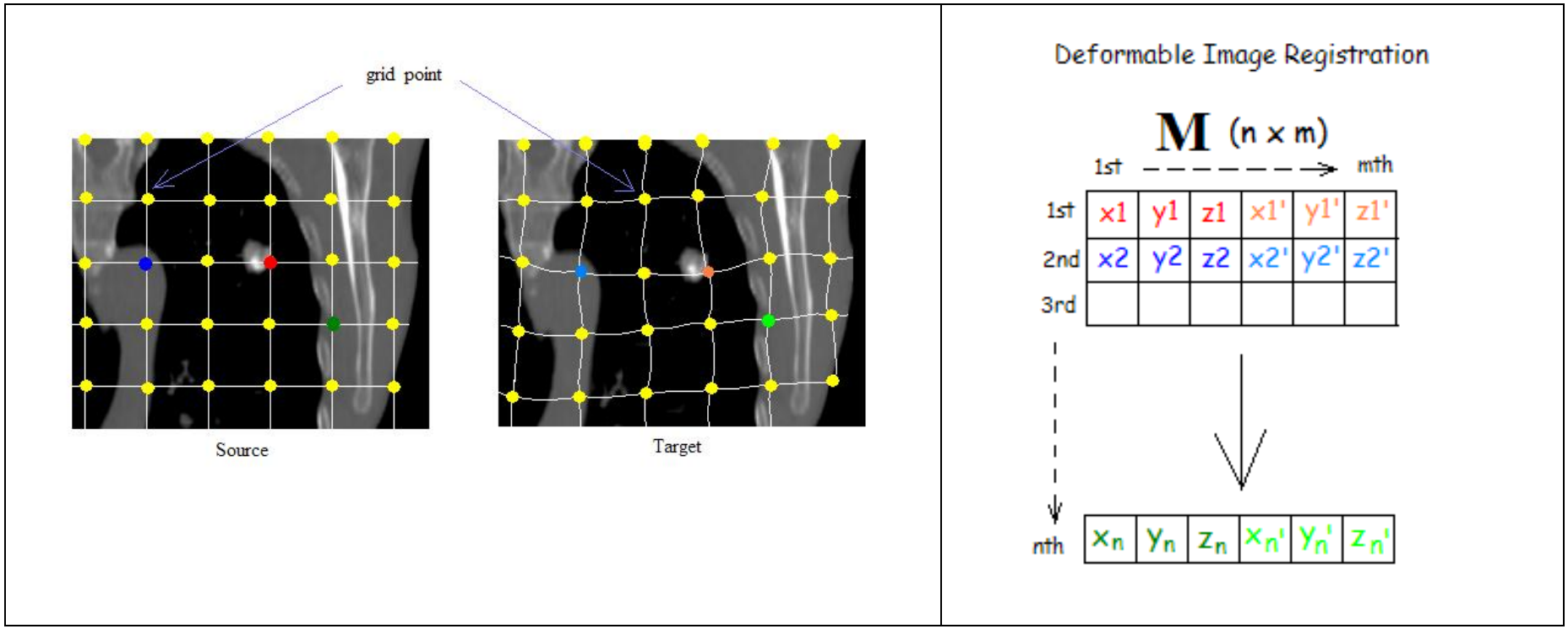

Table 2.1 An example of M matrix containing geometric data of GTV at inhale phase (source) and exhale phase (target) is shown in the table below.

Source data (mm)			Target data (mm)		
x1	**y1**	**z1**	**x1'**	**y1'**	**z1'**
63	-125	-307	62	-123	-306
64	-125	-307	63	-123	-306
65	-125	-307	64	-123	-306
66	-125	-307	65	-123	-306
67	-125	-307	66	-123	-306
68	-125	-307	67	-123	-306
69	-125	-307	68	-123	-306
70	-125	-307	69	-122	-306
71	-125	-307	70	-122	-306
72	-125	-307	71	-122	-306
73	-125	-307	72	-122	-306
74	-125	-307	74	-122	-306
75	-125	-307	75	-122	-305
76	-125	-307	76	-122	-305
77	-125	-307	77	-121	-305
78	-125	-307	78	-121	-305
79	-125	-307	79	-121	-306
80	-125	-307	80	-122	-306
81	-125	-307	81	-122	-306
82	-125	-307	82	-122	-306
83	-125	-307	83	-122	-306
84	-125	-307	84	-122	-306
85	-125	-307	85	-122	-306
86	-125	-307	86	-123	-307
87	-125	-307	87	-123	-306
63	-125	-307	62	-122	-306
64	-125	-307	63	-122	-306

C) DE-DOSE-REG function

The function of DE-DOSE-REG is to register each voxel of the reference CT with the temporal dose received by the corresponding voxel of each individual 4D-CT sets. The corresponding voxels were acquired with the morphed vectors contained in the n x m matrix (M) generated by IM, where n denotes the number of voxels and m their coordinates. The configuration of M is described in figure 2.2. In accordance with the displaced position of the voxel, the temporal dose at each voxel was traced with the 3D dose array (figure 2.1) obtained from the individual 4D-CT plans. In order to match the positioning format between the 3D dose array and M, the 3D dose array containing dose points in grid order was converted into 3D CT coordinates. Moreover, the spatial dose resolution along the cranio-caudal direction which was defined by the slice thickness was refined from 3 mm to 1 mm by linear interpolation between point doses. The temporal doses at each bin of a phase-sorted 4D CT images were finally stored in a 1D dose array, namely TD_x (where x denotes the phase bin; the percentile of the period of the corresponding breathing cycle of the patient), in the order of voxels presented in $M_{1\text{-}n,\ 1\text{-}3}$. The procedures for determining the DE-DOSE-REG function is illustrated in figure 2.3. The Program code of *DE_DOSE_REG* is listed in Appendix I.1

Figure 2.3 Combining the information of dose point (in 3D dose array) with the morphed data (in M matrix) for 4D dose calculation.

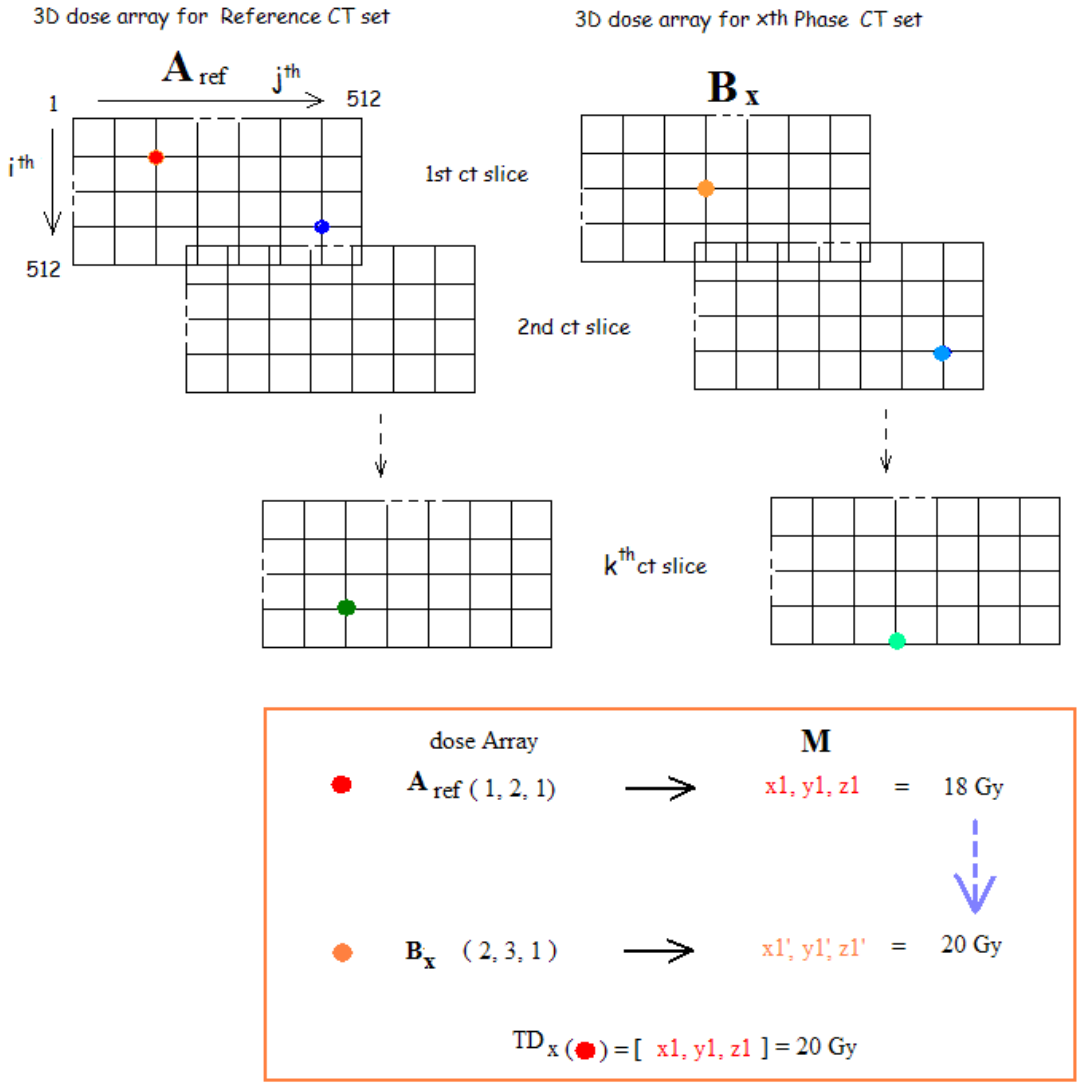

D) AUTO-CERR-DOSE function

This function permits the temporal dose received by each voxel at each respiratory phase to be revealed visually on the reference CT. This was done by replacing the 3D dose array of the reference plan with $TD_{x,,}$ and superimposing the new doses on the reference CT.

E) ADD-ALL-DOSE function

This function derives the complete 4D dose distribution over the entire respiratory cycle by the time-weighted dose summation of TD_x for all phases (figure 2.4). Together with the function AUTO-CERR-DOSE, the resultant 4D dose was displayed and assessed geometrically under the CERR environment. A sample of TD_x is shown in Table 2.2. The complete process of 4D dose calculation using the tool-box is illustrated in Figure 2.5. The Program code of *ADD-ALL-DOSE* is listed in Appendix I.2

Figure 2.4 The accumulated dose distribution over the entire respiratory cycle was obtained by time-weighted dose summation of TD_x for all phases. $TD'_{X\%}$ denotes the amount of tumour doses received only at the x% breathing phase by multiplying a time weighting factor to the TDx.

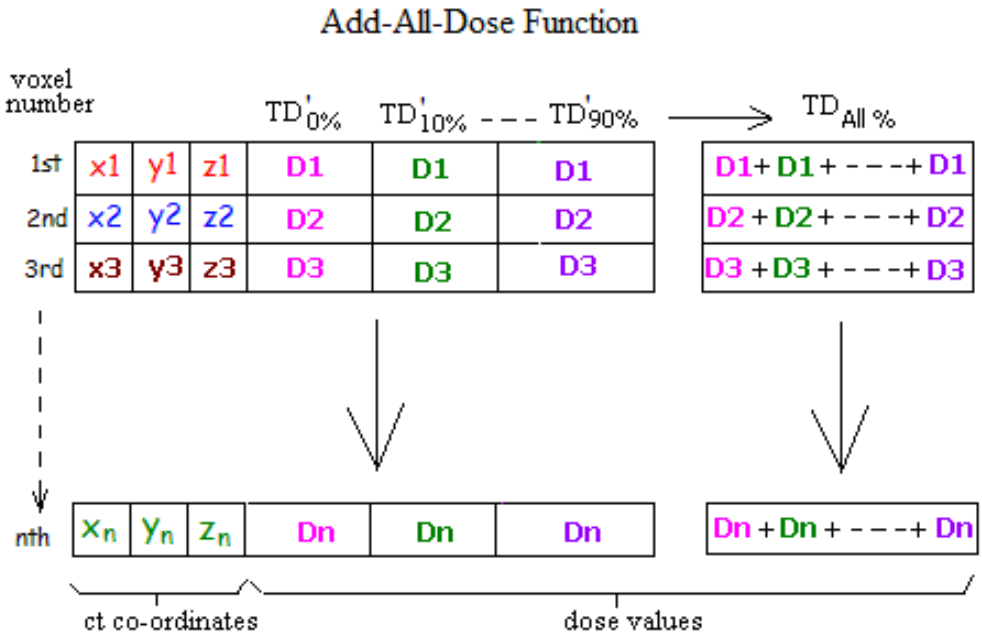

Table 2.2 An example of TD_x. Data extracted from a clinical case (case 3 of the study). Due to the dramatic movement between phase 0% to 10% and phase 60% to 80% (see figure 6.2 for the tumour movement trajectory), the temporal doses at the corresponding voxels are substantially changed. TD_{all} is the time-weighted dose summation of all TD_x

Voxel No	Voxel Dose (Gy)										
	TD_0	TD_10	TD_20	TD_30	TD_40	TD_50	TD_60	TD_70	TD_80	TD_90	TD_all
12527	21.1677	13.1066	3.9216	3.918	3.9204	2.8987	3.9102	3.9456	13.0703	17.8279	8.7687
12528	19.4044	12.9931	8.3529	3.854	3.8546	3.8489	3.8481	3.8875	12.9597	17.724	9.0727
12529	19.1791	12.7968	8.1961	3.7687	3.7726	3.7629	3.7633	3.8051	12.7401	17.4975	8.9282
12530	18.5239	12.3833	8.0191	7.8786	3.6582	3.6475	3.6472	7.9947	12.3249	17.0427	9.512
12531	17.8468	11.8509	7.6904	3.5223	3.5276	3.5197	3.5193	7.6704	11.7943	16.2773	8.7219
12532	16.9972	11.2713	7.3301	3.3701	3.4305	3.3683	7.1736	7.3145	11.2249	15.5369	8.7017
12533	16.5485	10.9668	7.1402	7.0068	7.1489	6.9904	6.9934	7.1238	10.9229	14.7961	9.5638
12534	16.0998	10.6623	10.4358	6.8291	10.4521	6.934	6.9328	10.6041	10.6208	14.3779	10.3949
12535	15.2867	9.5647	10.0962	9.919	9.9349	6.5787	6.2235	10.0624	10.0795	13.6505	10.1396
12536	9.4979	9.4911	7.1066	7.0948	4.8016	4.1729	4.1749	4.7957	7.1343	6.6594	6.4929
12537	10.0152	6.7408	7.4832	4.8048	5.0351	4.523	4.5227	5.03	7.5095	7.3436	6.3008
12538	10.5325	7.0615	4.9525	5.2746	5.2686	4.7252	4.7249	5.2643	7.8847	7.7462	6.3435
12539	11.6855	7.3823	5.42	5.4086	5.7927	2.5765	2.5773	5.7803	8.7126	8.1489	6.3485
12540	13.0737	8.7483	5.9463	5.9309	5.9273	2.7742	2.7753	5.9206	9.715	12.0468	7.2858
12541	14.4982	9.7544	6.5625	6.5509	6.5479	2.9843	2.9866	6.5363	10.7331	14.4691	8.1623
12542	17.744	10.7693	7.2186	7.2074	7.2042	3.2037	3.2063	7.1907	11.7623	15.9279	9.1434
12543	18.5438	11.8023	7.7377	7.7199	7.718	3.4113	3.4109	7.6983	12.4338	16.8632	9.7339

Figure 2.5 A flow-chart for 4D dose calculation using the tool-box

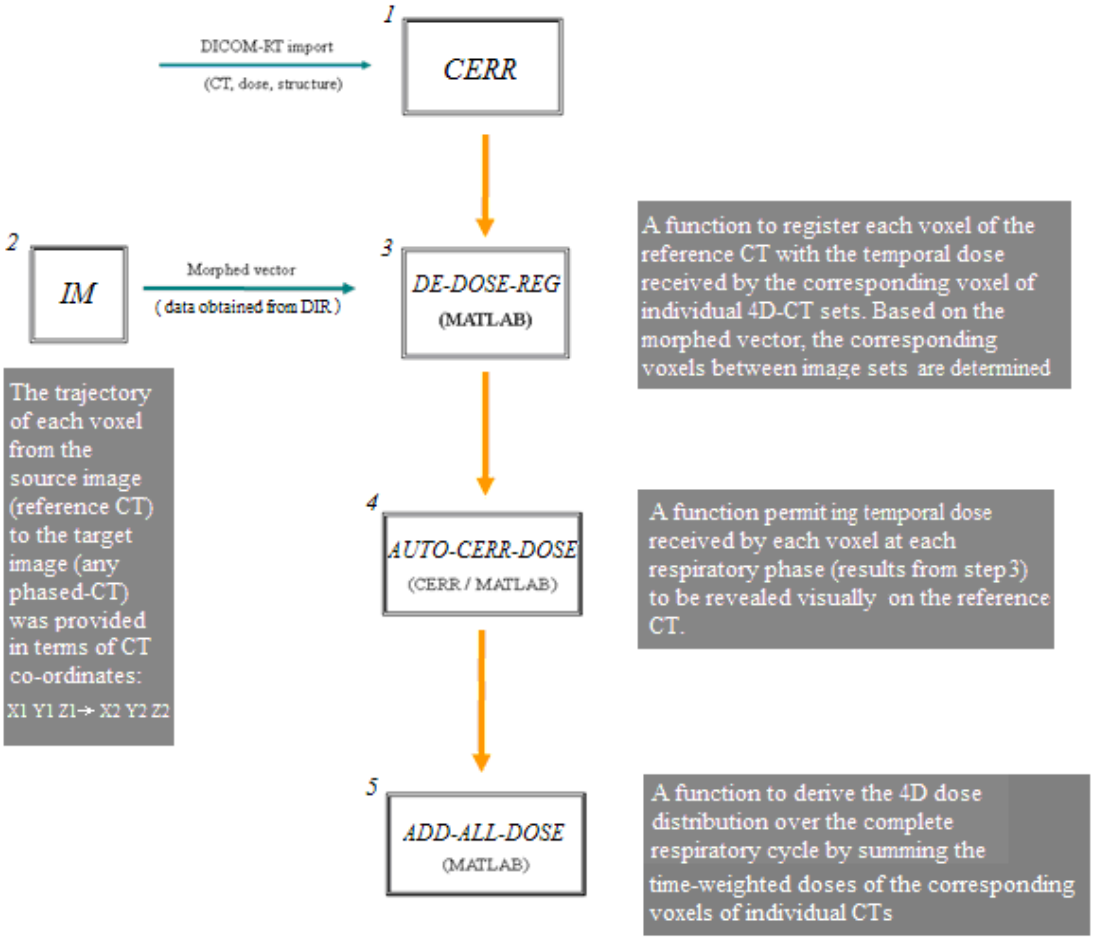

2.2 Evaluation of Deformable Image Registration of IM

The performance of image morphing using IM was evaluated by calculating the Matching Index (Lin, Shi., et al. (2008). The Matching Index is defined as the ratio of the intersected volume between the morphed contour and the manual contour to the union of the two volumes. Using CT lung window, the GTV was manually delineated and the lung volume using auto-segmentation (iPlan) with manual correction where necessary. The contours were initially delineated on the planning CT selected at end-inhale ($PLCT_{in}$) as the source contours and were morphed onto the planning CT selected at end-exhale ($PLCT_{ex}$) defining the morph_contour which was then compared with the contours manually delineated on the $PLCT_{ex.}$ The contouring was performed by a physicist, and confirmed by an oncologist if any uncertainty was found.

$$\textit{Matching Index} = \frac{morph\_contour \cap manual\_contour}{morph\_contour \cup manual\_contour}$$

The matching indices between the manual_contour and the morph_contour of lung volume and of the GTV for all cases were found to be between 0.93 and 0.98 (mean = 0.95 ± 0.01) and between 0.74 and 0.98 (mean = 0.84 ± 0.08), respectively. The index values are listed in table 2.3. The matching indices for lung mapping were comparable with those (range: 0.94 – 0.95) reported in Lin et al's (2008) study. The lower matching index for the GTV may be due to the limitation of image spatial and contrast resolution which would affect manual contouring particularly when the tumour volume is small.

Table 2.3 Matching indices between the manual_contour and the morph_contour of lung volume and of the GTV for all cases

	Matching Indices manual_contour ($PLCT_{ex}$) vs morph_contour ($PLCT_{in} \rightarrow PLCT_{ex}$)	
	GTV	Lung
1	0.79	0.95
2	0.81	0.98
3	0.74	0.96
4	0.94	0.93
5	0.75	0.95
6	0.94	0.93
7	0.90	0.95
8	0.84	0.96
9	0.98	0.96
Mean ± std	0.84 ± 0.08	0.95 ± 0.01

CHAPTER 3

RETROSPECTIVE CLINICAL STUDY ON 4D DOSIMETRY

3.1 Clinical Background

Hypofractionated stereotactic radiotherapy has been used to treat lung cancer at the Tuen Mun Hospital in Hong Kong since 2000. Due to the roll out of the radiation delivery systems at the stage of treatment, several treatment techniques with different delivery modalities were developed and applied. Over the period 2000 - 2010, 49 patients with early stage NSCLC were prescribed with doses ranging from 45 to54 Gy with 1 – 2 fractions per week for a total of 3-4 fractions. The treatment planning technique was modified according to the delivery techniques and was described as following. Cases meeting the research criteria were selected for the study.

3.1.1 Patients Selection

Patients attending a local tertiary oncology centre in Hong Kong who were pathologically proven to have NSCLC according to the WHO criteria were included in this study. Stage I disease as defined by the guidelines given by The American Joint Committee on Cancer (AJCC) was confirmed by CT of the thorax and upper abdomen in all cases. All the patients were considered medically inoperable or had refused surgery after assessment by a physician or thoracic surgeon.

3.1.2 Radiotherapy Planning and Treatment Techniques Applied in Chronological Order

From 2000-2003, patients were simulated and treated with shallow free breathing. The internal margin was estimated according to the CT simulation images by a radiation oncologist who is a specialist in this field. Margins in the range of 1 to 2 cm were added to the GTV depending on the magnitude of tumour movement. These encompass the microscopic extent of the tumour beyond the visible GTV, tumour motion as well as the setup uncertainty to form the PTV.

From 2004, all the selected patients underwent fluoroscopic screening. If tumour movement was greater than 1 cm in cranio-caudal, anterio-posterior or lateral

directions, or with tumour located near to the rib cage (< 2cm), the patient was selected for treatment with the deep inspiration breath-hold technique using active breath control (ABC) system developed by Wong et al (1999). For patients who could not comply with the ABC system, treatment was performed under free breathing. For patients treated with free breathing after 2004, two sets of conventional CT images were obtained during inspiration and expiration guided by the real-time position management system (RPM, Varian). The GTV was delineated using a lung CT window (1000, - 500 Hounsfield units). The IGTV was generated from the sum of GTVs acquired on the inspiratory and expiratory phases which was expanded with 5 mm to form the CTV and further with 2 mm to account for setup error to form the PTV. For the ABC group, the CTV was defined as GTV plus 5 mm margin and a further 3, 5, and 5 mm in the lateral, anterio-posterior and cranio-caudal directions, respectively, to account for internal tumour motion and setup error which form the PTV.

From 2008, 4D-simulation using the Philips Brilliance multi-slice CT scanner was used for tumour movement evaluation and treatment planning lineation. The respiratory phase was tracked using an infra-red optical system (RPM system, Varian). An infra-red marker was placed on the xipoid of the patient for respiratory tracking. A spiral scan was performed to cover the whole lungs. The scan was acquired at a sufficiently low table speed (low pitch) for any scanned voxel to remain within the detector collimation throughout the complete breathing cycle. The source data and the respiratory signal were retrospectively sorted by phase and reconstructed to produce the 4D CT images. Each 4D-CT data set was comprised of ten 3D CT images spaced equally among the respiratory cycle. CT scan with slice thickness of 3 mm with no spacing was performed. As previously stated, suitable patients will be selected for DIBH treatment. For cases with peak to peak tumour movement of less than 1 cm, the IGTV was defined with the MIP image set, and treatment was performed with free breathing. Treatment planning was performed with the iPlan Stereotactic Planning system (BrainLab Ltd). Treatment outcomes of cases performed from 2000 to 2004 were reported by Ng *et al* (2009). The patient disease characteristics and the applied treatment schemes are listed in table 3.1.

Table 3.1 Patient disease characteristics and treatment schemes in TMH from 2000 to 2010.

	Histology	Stage	Admission. year	Screening for tumour motion	Treatment	ITV definition
1	NSCLC	T2N0M0	2000	nil	FB	GTV + max. motion
3	Aden	T1N0	2001	nil	FB	GTV + max. motion
4	Aden	T1N0	2001	nil	FB	GTV + max. motion
6	Aden	T1N0	2002	nil	FB	GTV + max. motion
7	Aden	T1N0	2002	nil	FB	GTV + max. motion
8	SCC	T2N0M0	2002	nil	FB	GTV + max. motion
9	Aden	T1N0	2003	nil	FB	GTV + max. motion
10	Aden	Lung Sec.	2003	nil	FB	GTV + max. motion
11	SCC	T1N0	2003	nil	FB	GTV + max. motion
12	SCC	T2N0M0	2004	nil	FB	GTV + max. motion
13	Aden	T1N0M0	2004	nil	FB	GTV + max. motion
14	NSCLC	T2N0M0	2004	nil	FB	GTV + max. motion
15	Aden		2004	nil	FB	GTV + max. motion
16	Aden	T2N0M0	2004	Flu.	DIBH	GTV + residual motion*
17	NSCLC	T1N0	2004	Flu.	DIBH	GTV + residual motion*
18	Aden	T1N0	2004	Flu.	DIBH	GTV + residual motion*
19	NSCLC	T2N0M0	2004	Flu.	FB	GTV + max. motion
20	SCC	T1N0	2004	Flu.	DIBH	GTV + residual motion*
21	NSCLC		2005	Flu.	FB	GTV + max. motion
22	Aden	Lung Sec.,	2005	Flu.	DIBH	GTV + residual motion*
23	Aden	T1N0	2005	Flu.	DIBH	GTV + residual motion*
24	Aden	T1N0	2005	Flu+RGCT	FB	IGTV (RGCT)
25	Aden	T1N0	2005	Flu+RGCT	FB	IGTV (RGCT)
26	NSCLC		2005	Flu+RGCT	FB	IGTV (RGCT)
27	Aden	T1N0	2005	Flu+RGCT	FB	IGTV (RGCT)
28	NSCLC		2005	Flu+RGCT	FB	IGTV (RGCT)
29	Aden	T1N0	2005	Flu+RGCT	FB	IGTV (RGCT)
30	NSCLC	T1N0	2006	Flu	DIBH	GTV + residual motion*
31	Aden	T2N0	2006	Flu+RGCT	FB	IGTV (RGCT)
32	NSCLC		2006	Flu	DIBH	GTV + residual motion*
33	Aden	T1N0	2006	Flu	DIBH	GTV + residual motion*
34	Aden	T1N0	2006	Flu+RGCT	FB	IGTV (RGCT)
35	SCC	T1N0	2007	Flu+RGCT	FB	IGTV (RGCT)

36	Aden	T1N0	2007	Flu+RGCT	FB	IGTV (RGCT)
37	SCC	T1N0	2007	Flu	DIBH	GTV + residual motion*
38	Aden	T1N0	2007	Flu	DIBH	GTV + residual motion*
39	Aden	T1N0	2007	Flu+RGCT	FB	IGTV (RGCT)
40	Aden	T1N0	2008	Flu+4DCT	FB	IGTV (MIP)
41	SCC	T1N0	2008	Flu+4DCT	FB	IGTV (MIP)
42	Aden	T1N0	2009	Flu+4DCT	DIBH	GTV + residual motion*
43	SCC	T1N0	2009	Flu+4DCT	FB	IGTV (MIP)
44	Aden	T1N0	2009	Flu+4DCT	DIBH	GTV + residual motion*
45	Aden	T1N0	2009	Flu+4DCT	DIBH	GTV + residual motion*
46	Aden	T1N0	2009	Flu+4DCT	FB	IGTV (MIP)
47	Aden	T1N0	2009	Flu+4DCT	DIBH	GTV + residual motion*
48	SCC	T1N0	2009	Flu+4DCT	FB	IGTV (MIP)
49	Aden	T1N0	2010	Flu+4DCT	FB	IGTV (MIP)

NSCLC: non-small cell lung carcinoma

SCC: squamous cell carcinoma

Aden: adenocarcinoma

Flu: assessment of tumour motion using x-ray fluoroscopy

Flu+4DCT: assessment of tumour motion using both fluoroscopy x-ray and 4DCT

DIBH: deep inspiration breath hold

FB: free breathing

GTV + max. motion: treatment margin in range of 1to 2 cm depending on tumour movement is added to GTV to form the CTV/PTV

GTV + residual motion*: The ITV was defined based on the residual tumour motion during DIBH and the PTV margin also accounts for the residual tumour motion as reported in the study by Wong et al 2010

IGTV (RGCT): internal gross target volume (IGTV) was defined with the respiratory gated CT (RGCT) at both inhale and exhale phases.

IGTV (MIP): IGTV was defined with the MIP image set

3.2 4D Dose Study

3.2.1 Case Selection

From 2008 to 2010, ten patients who were diagnosed with stage I lung cancer underwent four-dimensional CT simulation for hypo-fractionated radiation therapy in Tuen Mun Hospital (TMH), Hong Kong (Patients P40-P49 in Table 3.1). When using 4DCT imaging to assess tumour movement and consequently to process 4D dose calculation based on DIR, stable breathing and consistent respiratory performance is a pre-requisite. Cases which were selected for the study were screened according to breathing regularity in order to achieve low-noise CT imaging for delineation of the tumour in various respiratory phases. Since the 4D CT images applied in this study were sorted by the time phase at each respiration cycle, the regularity of breathing rate would be important for the control of imaging reconstruction. The breathing rate regularity was assessed by measuring the length of every respiration cycle during 4D CT scanning. Cases with standard deviation (SD) of the mean breathing rate less than 10% (range: 6.1% - 9.7%) were included in this study. Although the amplitude variation was not assessed in the study, it was however presumed to be correlated with the periodic fluctuation as large variation in amplitude with constant respiratory frequency is rarely observed in practice. Examples of regular and irregular breathing patterns are shown in figure 3.1a and 3.1b, respectively. The studied cases were also chosen for the patient group with well defined GTV, which was usually the case with adenocarcinoma confirmed by histology. As a result, seven out of the ten cases were included (P40, P42-P45, P47, P49 in table 3.1), and of these, four cases were treated with the DIBH technique. Two additional cases (case 8 and 9) were provided by the Clatterbridge Cancer Centre (CCC), UK. For the CCC group, the patients received coaching in order to maintain a regular breathing pattern, which was confirmed during CT scanning. However, the breathing stability was not assessed for the CCC group, as data were anonymized and the respiratory surrogate signal could not be retrieved at the time of study. Each 4D-CT data set of the CCC group comprised six 3D CT images spaced equally among the respiratory cycle. The quality of 4D CT image which was considered may affect the performance of the IM was confirmed by the study of matching index which was performed in Chapter 2.2.

Figure 3.1 a Example of a regular breathing pattern

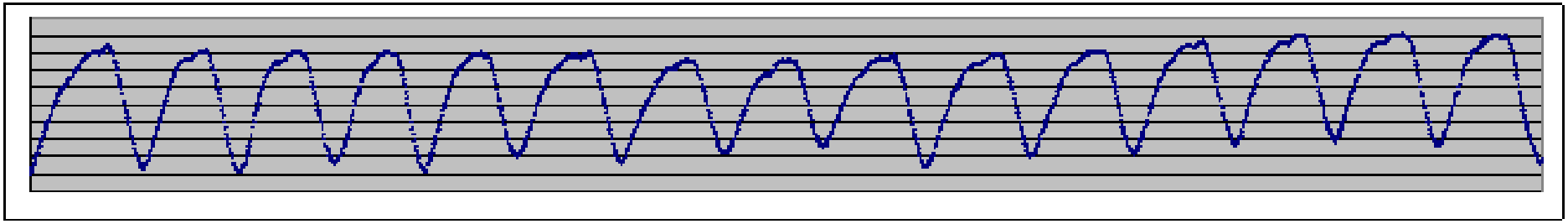

Figure 3.1 b Example of an irregular breathing pattern

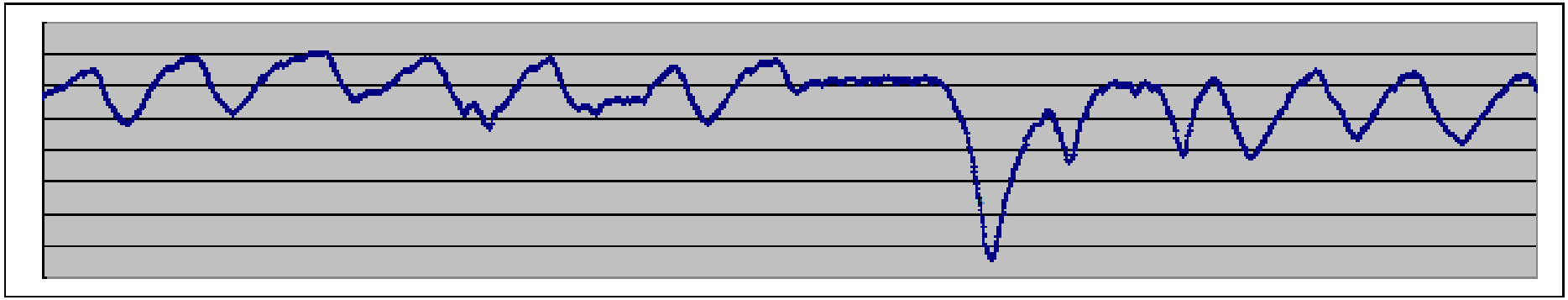

Table 3.2 lists the characteristics of the tumour in terms of tumour size, location, magnitude of movement and histology. The variation of breathing rate obtained over the period of CT scan was also evaluated. For all cases, the mean GTV volumes contoured in 3 different breathing phases (i.e. inhale, exhale and mean tumour position) ranged from 1.42 cc to 17.89 cc (2nd column, Table 1) with small standard deviations (SD). The resultant tumour movements defined by the quadratic sum of the maximum movement along the three axes ranged from 1.2 – 10.5 mm.

Table 3.2 Patients' disease characteristics and treatment parameters for individuals of the study

Patient (patient number of Table 3.1)	* GTV mean ± std (cc)	Tumour Resultant Displacement (mm)	Histology	Location	Breathing rate Variation ($\frac{STD}{Mean} x100\%$)	Treatment Modality
1 (P42)	1.42±0.07	6.0	AC.	LUL	3.4%	DIBH
2 (P40)	1.93±0.06	4.4	AC	LUL	9.5%	FB
3 (P45)	3.00±0.14	4.0	AC	RLL	9.8%	DIBH
4 (P44)	6.74±0.19	1.2	AC	LUL	8.5%	DIBH
5 (P47)	4.06±0.18	4.5	AC	RUL	6.4%	DIBH
6 (P43)	17.89±0.33	6.6	SCC	RLL	9.7%	FB
7 (P49)	12.80±0.54	3.8	AC	LUL	3.3%	FB
8	5.5±0.47	9.2	unknown	LUL	unknown	FB
9	12.40'±1.47	10.5	unknown	LLL	unknown	FB

Histology: AC: adenocarcinoma; SCC: squamous cell carcinoma;

Location: LUL: left upper lobe; RLL: right lower lobe; RUL: right upper lobe; LLL: left lower lobe;

* GTV: The mean volume of GTVs delineated at the inhale and exhale phases and the temporal mean tumour position.

3.2.2 Implementation of 4D Dose Calculation

In principle, the 4D dose over the tumour volume can be calculated by converting the 3D spatial dose distribution to the 4D spatio-temporal dose distribution. Using the GTV as the planning target, by computing the accumulated dose (4D dose) over the GTV volume, the actual dose coverage over the tumour volume resulting from 3D dose planning can be revealed.

The 3D dose planning was performed on the reference CT selected from the 4D-CT set with the GTV as the planning target. The GTV was manually delineated using a lung window (1000, - 500 Hounsfield units) and served as the source data for deformable image registration using IM. In order to minimize the dose volume at the low dose region, the margin of beam aperture was limited to 1 mm – 1.5 mm for dose planning. As the beam penumbra ranged from 3.2 mm – 3.5 mm, the 85% isodose would normally encompassed $\geq$ 99.5% planning target volume. In this study, a prescription of 20Gy was applied at 85% isodose normalized to the isocentre, which was defiend at the geometric centre of the GTV, to enclose $\geq$ 99.5% tumour volume. Treatment planning with radiation dose delivered to the GTV using micro-multileaf collimators (M3, BrainLab Ltd, Germany) with single or multiple coplanar conformal arc/arcs was performed. Since the target dose distribution in terms of dose conformity and dose heterogeneity could be affected by the beam aperture, similar aperture margins ranging from 1.0 - 1.5 mm (larger margin would be required for a less regular shaped target) were applied for all cases. To process 4D dose calculation, the 3D dose distribution at each respiratory phase was formed by re-applying the planning parameters and the monitor units obtained from the reference plan to each set of 4D-CT images, and recalculating the dose with a heterogeneity correction. The pencil beam algorithm implemented in the iPlan planning system (V.4.1.2 BrainLab Ltd, Germany) was applied for dose calculation. An algorithm that account for lateral electronic disequilibrium would be preferable, but was not available at the time of this study. However, since dose plans for comparison were performed under the same conditions, the influence of lateral electronic disequilibrium on the radiation planning using pencil beam between the dose plans was considered to be comparable. The 3D dose plan obtained from each of the 4D-CT data set was imported into the tool box for 4D dose processing as described in Chapter 2.

The procedure for 4D dose calculation is illustrated in figure 3.2. An example is shown with the planning CT taken at the end-exhale phase (50%). Figure 3.2a shows the 3D dose distribution obtained at the end-inhale phase (0%), the blue contour indicates the original location of the GTV captured on the reference CT (50%). The large discrepancy in location between the dose colour-wash and the GTV shown on the CT image clearly demonstrates the effect of tumour motion on the accumulated dose. Using the functions IM, DE-DOSE-REG and AUTO-CERR-DOSE, the 4D doses acquired at each individual temporal phase from 0% to 90% ($TD_{0\%-90\%}$) and the GTV dose volume histogram of each are shown in figure 3.2b. The resultant 4D dose distribution over the tumour in a complete respiratory cycle is presented in figure 3.2c. Figure 3.2d demonstrates the difference on dose coverage of GTV between the original 3D dose plan and the resultant 4D dose using dose volume histogram. Due to the significant tumour movement, the V_{20Gy} which denotes the GTV coverage by the prescription dose (20Gy) was 60% of the GTV volume, and the minimum dose (D_{min}) received by the GTV was 70% (14.02 Gy) of the original planning dose (20 Gy), as a result of 4D dose distribution

Figure 3.2 Procedure of 4D dose calculation. The blue contour indicates the original location of the GTV with dose plan performed at the exhale-phase, tumour shift shown at the inhale-phase (fig. 3.2a). By summing the time-weighted received dose of GTV at different phases (fig.3.2b), the actual resultant doses received by the GTV was obtained (fig.3.3c). DVHs of GTV in 3D and 4D were compared (fig 3.2d).

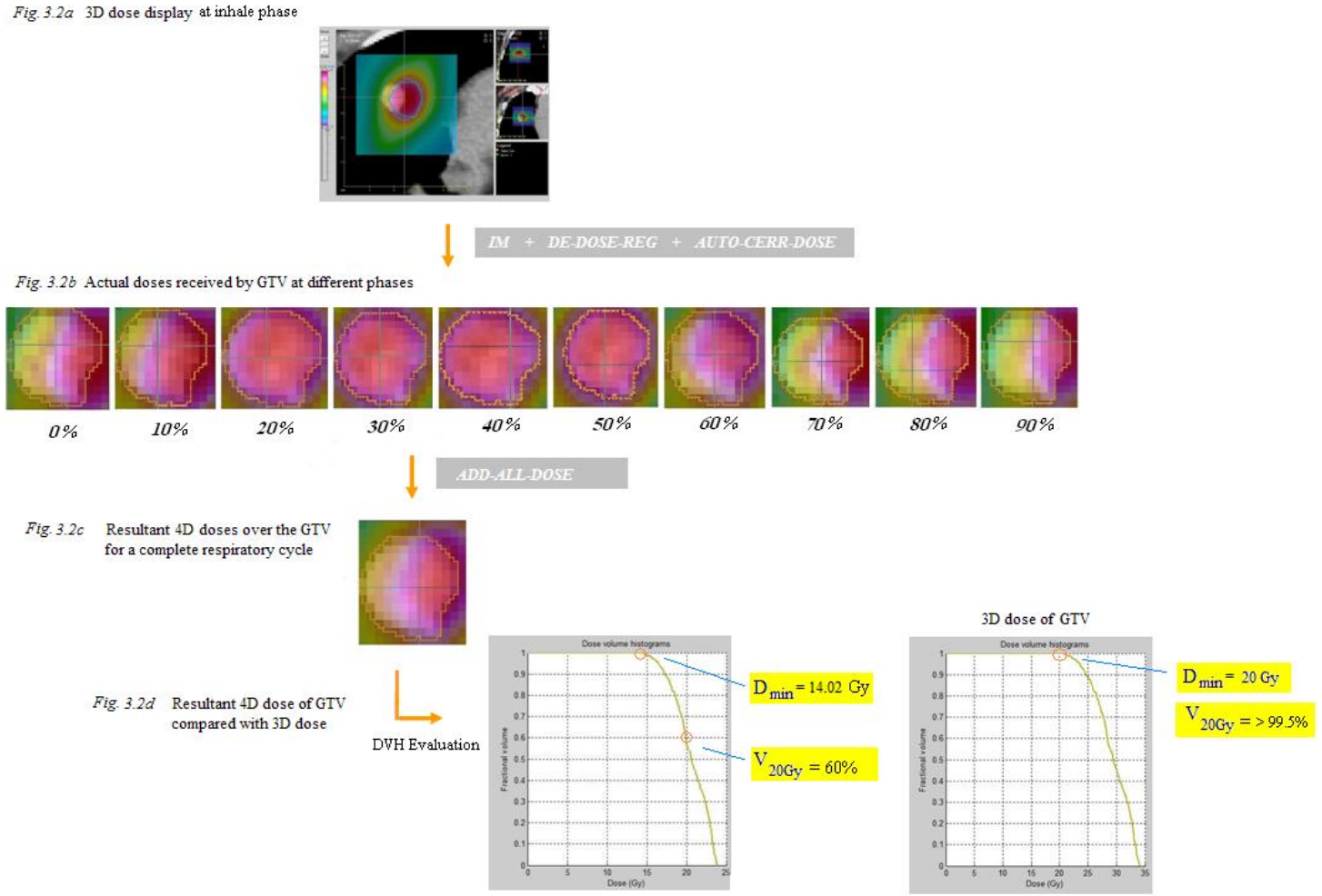

CHAPTER 4

DOSE PLANNING OPTIMIZATION BY MINIMIZING THE INTERNAL TARGET VOLUME

4.1 Definition of Classical Internal Target Volume

The treatment volume is considered to be the crucial factor for maximizing the therapeutic ratio since it affects the degree of radiation induced toxicity and hence the potential for dose escalation. Minimizing the treatment volume is therefore essential for enhanced treatment. The treatment volume is derived from the GTV, ITV, CTV and PTV. The GTV and CTV volumes are restricted by the pathological definition and the PTV which accounts for setup error depends on the technical implementation by individual centres. Reducing the internal margin without compromising dose coverage to the target is the aims in order to minimize the treatment volume. In this study, a new internal target volume was proposed to serve such a purpose; its efficacy was assessed using the classical ITV as a reference. In this study, the classical ITV, namely cITV was defined without microscopic margin. The cITV was defined by summing the volumes of the morphed GTVs generated on the $CT_{10\%\text{ - }90\%}$ using $CT_{0\%}$ as the source image. Since the morphed GTV could be different with various source images, the discrepancies among the cITV volumes using different reference phases as the source images were evaluated. Using the cITV as the planning target, the planning dose volume included >99.5% target coverage denoted as $cITV_{100}\%$. The definitions of cITV and $cITV_{100}\%$ are illustrated in Figure 4.1.

Figure 4.1 Definition of cITV and $cITV_{100\%}$. The cITV was defined by summing the volumes of the morphed GTVs generated on the CT $_{10\%}$ - $_{90\%}$ using CT $_{0\%}$ as the source image. With cITV as the planning target, the planning dose volume included >99.5% target coverage denoted as $cITV_{100}$%.

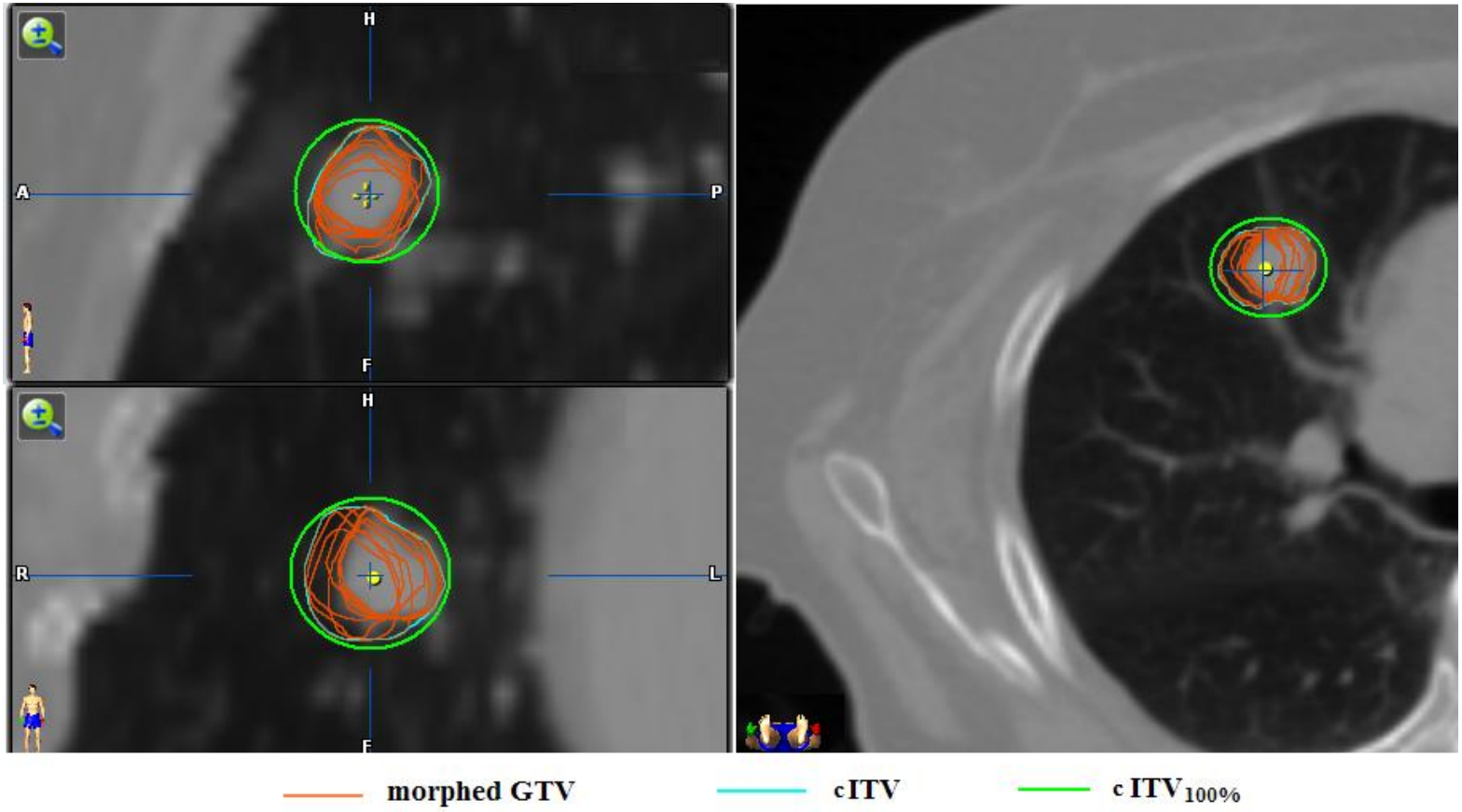

4.2 Introduction of Inverse Internal Treatment Volume (iITV) – A new concept of ITV derived from 4D dosimetry

4D dose calculation using the tool box developed in this work has been described in Chapter 3.2, in which the percentage target coverage by the prescription dose of 20 Gy (V_{20Gy}) and the minimum 4D dose over the target volume (D_{min}) were defined. Since the dose volume enclosed by the D_{min} isodose also determines the dose volume which provides the entire dynamic coverage of the GTV, it corresponds to the conceptual requirement of the classical ITV. Therefore, by applying the prescription dose to D_{min} (ie increasing the prescription dose from 20 Gy to 20/14.02 = 28.6 Gy), 100% coverage of the GTV by 20Gy would be achieved. Thus, the new 3D prescription dose volume (enclosed by the 20Gy isodose level) presented on the renormalized 3D dose plan provides a complete dynamic coverage of the GTV and defines the ITV of the study. In contrast to the classical ITV which is determined before dose calculation, the proposed ITV is derived from the 4D dose calculation and it is therefore denoted as the inverse ITV (iITV). The iITV defined in the 3D dose plan, despite it being initially derived from the 4D dosimetry (from the D_{min}), was intended for enabling comparison with the 3D dose volume generated from the conventional approach for evaluation of potential benefit in terms of a reduction of dose volume. The definition of iITV is illustrated in Figure 4.2. The V_{20Gy} and iITV obtained from dose plans performed at different breathing phases provide a quantitative measure of the dose effects in relation to the magnitude and characteristics of tumour motion and tumour size. Such will be discussed in the following studies.

Figure 4.2 Defining the iITV with the dose volume enclosed by D_{min}. The 100% target coverage with prescription dose of 20Gy is obtained by applying 20Gy to D_{min}, by increasing the prescription dose from 20Gy to 20/14.02 = 28.6Gy.

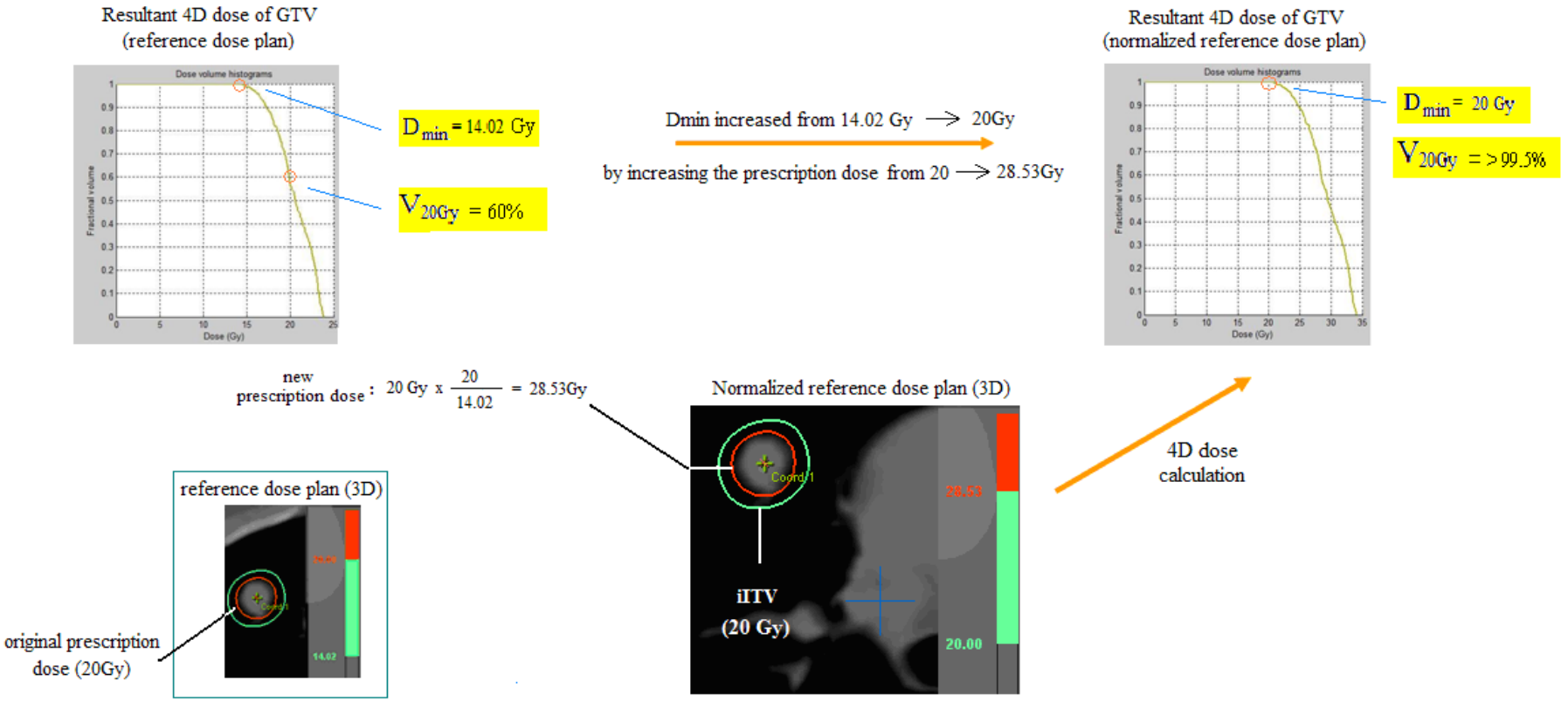

4.3 Effect of Phase-Specific Dose Planning on Target Coverage and the Volume of iITV

4.3.1 Introduction

In general, the amount of target coverage is significantly associated with the magnitude of tumour movement, however a well-chosen CT phase from the 4D CT scan for treatment planning plays an important role in optimizing dose planning Previous studies (Engelsman et al. 2001; Witte et al. 2004) have shown that if the tumour is irradiated at its average position during the respiratory cycle, optimal dose coverage would be obtained even if the tumour is not fully within the high-dose region during certain parts of the breathing cycle due to the presence of the wide-beam penumbra. However, dose planning is usually performed at the end-inhale or end-exhale phases. Whilst the inhale phase creates a larger lung volume which would minimize normal tissue irradiation, the exhale phase would result in the most stable and reproducible target position (Balter et al. 1998; Wu et al. 2010). In our study, the most effective respiratory phase for dose planning was assessed with the maximized target coverage and the minimized iITV volume.

4.3.2 Methods

For each case, three dose studies were performed with the planning CT selected at end-inhale ($PLCT_{in}$), end-exhale ($PLCT_{ex}$) phases and at the temporal mean tumour position ($PLCT_{mean}$). The V_{20Gy} and iITV at the corresponding phases, namely $V_{in\ 20Gy,}$ $V_{ex\ 20Gy}$, $V_{mean\ 20Gy,}$ and $iITV_{in}$, $iITV_{ex}$, $iITV_{mean}$, respectively, were then determined. For the dose plan performed at the temporal mean tumour position, the planning CT was selected among all CT bins using the average intensity projected (AIP) CT images as reference. Thus, the tumour position shown on each CT phase was compared with that of the AIP set, the CT set with the tumour at the most comparable position was selected for the planning CT. The dose volumes $iITV_{in}$, $iITV_{ex}$ and $iITV_{mean}$ were consequently compared with each other.

4.3.3 Results

For all cases, the mean GTV volumes of the three phase-specific dose plans ranged from 1.42 cc to 17.89 cc (2nd column, Table 4.1) and the standard deviations were relatively small. The peak to peak tumour movements were 0.5 mm – 5.8 mm, 0.5

mm – 8.3 mm, 0 mm – 9.0 mm in the lateral, anterio-posterior and cranio-caudal directions, respectively, and the resultant displacement ranged from 1.2 mm to 10.5 mm. (3^{rd} column, table 4.1). The inadequate target coverage as a result of tumour motion was clearly revealed by the 4D dose distribution. The V_{20Gy} and the volume of iITV obtained in the phase-specific dose plans for all cases are varied and depicted in columns 2 – 4 and columns 8 – 10 of table 4.2, respectively. Among all phase-specific dose plans, the $V_{20Gymean}$ provides the maximum or over 93% target coverage in majority of the cases (cases 1 -7) and the $iITV_{mean}$ which has the smallest volume for all the case suggests that dose planning performed at the tumour mean position generally provides the optimal target dose coverage. The reasons for maximum target coverage maximizations not obtained with $V_{20Gymean}$ in cases 8 and 9 are explained in chapter 5.2.

Table 4.1 Treatment planning parameters for phase-specific dose studies

Patient	GTV (cc) mean ± std	max Pk-Pk (mm)	cITV (cc) mean ± std	$PLCT_{in}$ (%)	$PLCT_{ex}$ (%)	$PLCT_{mean}$ (%)
1	1.42 ± 0.07	5.8 (LAT) 1.6 (AP) 0.3 (CC) 6.0 (RES)	3.17± 3.3%	`0	50	20
2	1.93 ± 0.06	0.5 (LAT) 2.6 (AP) 3.5 (CC) 4.4 (RES)	2.80 ± 0.6%	0	60	30
3	3.00 ± 0.14	0.5 (LAT) 2.6 (AP) 3.0 (CC) 4.0 (RES)	4.42 ± 4.1%	0	50	80
4	6.74 ± 0.19	1.1 (LAT) 0.5 (AP) 0 (CC) 1.2 (RES)	8.66 ± 1.4%	0	60	60
5	4.06 ± 0.18	1.1 (LAT) 3.2 (AP) 3.0 (CC) 4.5 (RES)	6.36 ± 2.4%	0	60	20
6	17.89 ± 0.33	2.1(LAT) 1.6 (AP) 6.0 (CC) 6.6 (RES)	22.23 ± 1.4%	0	60	60
7	12.80 ±0.54	1.5(LAT) 3.5 (AP) 0 (CC) 3.8 (RES)	17.04 ± 1.9%	0	50	80
8	5.5 ± 0.47	1.5 (LAT) 1.5 (AP) 9.0 (CC) 9.2 (RES)	10.74 ± 4.3%	0	50	33
9	12.40 ± 1.47	2.4(LAT) 8.3 (AP) 9.2 (CC) 10.5 (RES)	18.52 ± 1.7%	0	50	16

GTV: gross tumour volume.

cITV: classical internal target volume.

max pk-pk: maximum peak to peak tumour movement; LAT, AP, CC and RES denotes lateral, anterior-posterior, cranio-caudal and resultant displacements., respectively.

$PLCT_{in}$, $PLCT_{ex}$, $PLCT_{mean}$: planning CT selected for the phase-specific studies at inhale, exhale and tumour mean position, respectively.

Table 4.2

CASE	Vin_{20Gy} (%)	Vex_{20Gy} (%)	$V_{mean\ 20Gy}$ (%)	$Dmin_{in}$ (Gy)	$Dmin_{ex}$ (Gy)	$Dmin_{men}$ (Gy)	$iITV_{in}$ (cc)	$iITV_{ex}$ (cc)	$iITV_{mean}$ (cc)	$cITV_{100\%}$ (cc)	Diff (%) $iITV_{mean}$ vs $cITV_{100\%}$	% coverage of cITV by $iITV_{mean}$
1	63.1	57.4	71.5	14.02	14.72	15.92	4.76	5.03	3.90	4.86	- 19.8	86.4
2	91.0	85.2	95.9	18.02	17.02	17.88	4.23	4.58	3.96	4.39	-9.8	94.6
3	73.0	80.0	89.2	12.57	17.27	17.48	11.75	6.64	5.17	7.38	-29.9	90.8
4	96.6	97.7	97.7	18.13	18.27	18.27	12.06	11.1	11.1	13.64	-18.6	98.3
5	92.8	94.6	92.9	16.42	17.45	18.42	13.63	10.43	7.34	10.16	-27.7	92.4
6	90.7	96.7	96.7	14.82	18.67	18.67	37.93	26.81	26.81	28.16	-4.8	98.6
7	95.7	99.1	95.6	17.17	18.77	18.48	28.00	24.44	23.93	24.49	-2.3	98.8
8	83.2	60.4	79.5	15.47	13.13	17.5	20.17	20.99	14.18	17.49	-19.3	84.6
9	66.9	90.4	84.0	8.23	13.63	14.77	79.85	38.5	28.5	26.36	+8.1	97.0

V_{20Gy}: accumulated dose coverage of GTV by 20Gy (prescription dose) as a result of 4D dose evaluation. V_{20Gy} expressed in terms of percentage of GTV volume

D_{min}: minimum dose received by the GTV as a result of 4D dose evaluation.

iITV: inverse internal target volume

cITV: classical internal target volume.

$cITV_{100\%}$: prescription dose volume to the cITV.

In, ex, mean: values obtained in the phase-specific studies performed at inhale, exhale and tumour mean position, respectively.

4.4 Internal Target Volume Comparison – between iITV and cITV

4.4.1 Methods

To demonstrate whether the internal target volume could be effectively minimized according to the concept of iITV, the dose volume defined by the iITV was compared with the dose volume generated by the classical ITV (cITV) during 3D dose planning. The $cITV_{100}$% which defines the dose volume generated by the cITV with >99.5% prescription dose coverage was compared with the volume of the $iITV_{in}$, $iITV_{ex}$ and $iITV_{mean}$.

4.4.2. Results

Depending on the magnitude of tumour movement, the volume of cITV were 2 to 3 times that of the GTV volume, ranging from 2.80 cm^3 to 22.23 cm^3 (column 4, table 4.1). As considering that if there would be significant variation between the volumes of cITV derived from different respiratory phases could affect the result of the study. The cITV volumes generated from three studied reference phases were evaluated and discrepancies among those were found to be small. The variations (SD / mean volume) among the three studies were ranged from 0.6% to 4.1% for all cases. Our results show that the iITV reduces the internal target volume compared with that defined classically. The $iITV_{mean}$, which has the minimum volume among all iITVs was found to be smaller than the dose volume of $cITV_{100\%.}$ The volume reduction ranged from 2.3 % to 29.9% (mean: 16.5%) for all cases except case 9, in which the dose volume of $iITV_{mean}$ was 8.1% greater than that of $cITV_{100\%}$ (the cause is addressed in chapter 6.2). The results are shown in columns 8 – 12 of table 4.2. The difference between the GTV, cITV, iITV and $cITV_{100\%}$ is illustrated geometrically in figure 4.3. The iITV (in green) defining 100% dynamic dose coverage of the GTV (in red) did not completely cover the cITV (in orange). This incomplete coverage was observed in all cases. The volume coverage of cITV by the $iITV_{mean}$ ranged from 84.6% to 98.8% (93.5 ± 4.6%) of the cITV volume (column 13, table 4.2). Such a result demonstrates that dose coverage of the entire range of the tumour motion which would be applied in classical ITV during dose planning may not be necessary.

Figure 4.3 The geometric difference between the GTV, cITV, iITV and $cITV_{100\%}$ is illustrated.

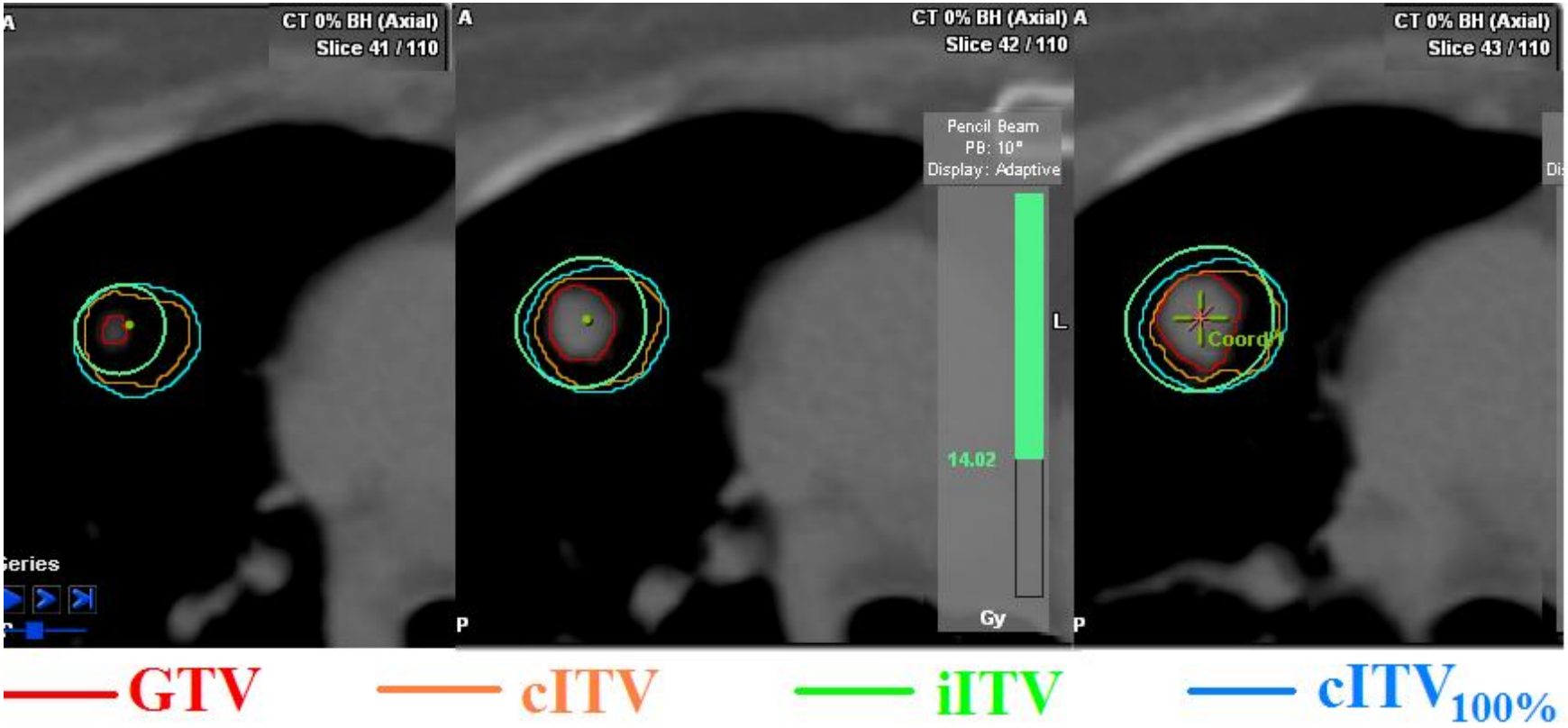

4.5 Dose Properties Comparisons between Studies with Dosimetric Indices

To enable unbiased comparison of the dose studies, the 3D dose planning protocol for all studied dose plans was conformed to the RTOG 0236 guidelines (Michaiski et al 2009). These guidelines suggest that planning doses are normalized to the centre of the target volume and prescribed to between the 60% – 90% isodose level. The conformity of target coverage defined as the ratio of the volume of the prescription isodose to the volume of planning target should be less than 1.2. The protocol recommends that at least 95% of the planning target volume (PTV) should be covered by the prescription isodose surface, and that 99% of the PTV receive at least 90% of the prescription dose. However, in our study, the proposed iITV was inversely derived from the resultant 4D dose accumulated in the moving tumour. Hence, dose was prescribed directly to the GTV with a target coverage of more than 99.5%.

Although similar dose planning parameters were attempted for all four plans (ie iITVin , iITVex , $iITV_{mean}$, cITV), the shape, size and location of the planning target were not the same because of the non-rigid transformation of the tumour during the breathing cycle. The planning parameters (eg. beam aperture margin, number of conformal arcs, etc) inevitably had to vary in order to achieve the optimal dose plan for each study. Similarity in dose properties between the four plans was however confirmed by employing the following dosimetric indices; target coverage index (TCI) (Lomax et al, 2003), conformity index (CI) (Lomax et al, 2003; Shaw et al, 1993) and dose heterogeneity index (HI) (Lomax et al, 2003; Shaw et al, 1993). The TCI specifies the percentage coverage of the prescription dose, whereas the CI indicates the amount of prescription dose volume as a function of the planning target. The HI defines the ratio of the maximum target dose to the prescription dose.

The similarity in dose properties among the four dose plans was verified with the dosimetric indices. The CI values at 95% and 99.5% target coverage were assessed. The mean CI values of the three phase-specific dose plans ranged from 1.50 to 1.80 and 1.20 to 1.62 at 99.5% and 95% target coverage, respectively (1^{st} column of table 4.3). The CI values of cITV ranged from 1.15 to 1.67 and 1.12 to 1.31 at 99.5% and 95% target coverage respectively (5^{th} column of table 4.3). The mean and standard deviation of TCI and HI of the four dose plans for all cases are listed in columns 3 - 4

of table 4.3. The very low standard deviation of the TCI for the four studied plans confirms that all 3D dose plans are similar in terms of target coverage for dose comparison. In addition to equivalent target coverage, the small standard deviations of CI and HI were 2% – 3% and 0 – 1% of their respective mean values suggesting that the dose properties and the dose distributions were similar among all dose plans.

Table 4.3 The dose properties among the phase-specific dose plans and dose plans of cITV were compared with the dosimetric indices of CI, TCI and HI.

Patient	CI (CI $_{95\%}$) of 3 phase-specific dose plans (mean ± std)	TCI (%) of all dose plans (mean ± std)	HI of all dose plans (mean ± std)	CI (CI $_{95\%}$) of cITV
1	1.80 ± 0.04 (1.33 ± 0.15)	99.7 ± 0.1	1.21 ± 0.01	1.53 (1.28)
2	1.95 ± 0.18 (1.24 ± 0.08)	99.8 ± 0.2	1.22 ± 0.02	1.57 (1.26)
3	1.86 ± 0.04 (1.62 ± 0.12))	99.5 ± 0.0	1.20 ± 0.01	1.67 (1.31)
4	1.65 ± 0.04 (1.20 ± 0.06)	99.8 ± 0.0	1.19 ± 0.00	1.58 (1.19)
5	1.84 ± 0.04 (1.39 ± 0.03)	99.8 ± 0.0	1.22 ± 0.01	1.39 (1.29)
6	1.50 ± 0.03 (1.29 ± 0.11)	99.8 ± 0.2	1.21 ± 0.01	1.15 (1.18)
7	1.67 ± 0.05 (1.50 ± 0.07)	99.6 ± 0.1	1.20 ± 0.01	1.39 (1.30)
8	1.69 ± 0.01 (1.34 ± 0.05)	99.8 ± 0.1	1.22 ± 0.00	1.63 (1.20)
9	1.53 ± 0.01 (1.26 ± 0.11)	99.8 ± 0.2	1.24 ± 0.02	1.42 (1.12)

CI: Conformity index evaluated at 99.5% target coverage.

CI $_{95\%}$: Conformity index evaluated at 95% target coverage

TCI: Target coverage index.

HI: Dose heterogeneity index

CHAPTER 5

DOSIMETRIC EFFECT OF TUMOUR MOTION

5.1 Factors Associated with Tumour Size and Magnitude of Movement

5.1.1 Introduction

In general, the magnitude of tumour motion is considered to be the prime factor in obtaining target coverage. A motion-related treatment margin (Balter et al. 1998; Wong et al. 2010) is generally applied for treatment planning. Several studies have suggested that the treatment margin may be derived from 4D contouring or the probability distribution of the target positions. Rietzel et al (2006) used 4D CT to characterize tumour motion in order to define the treatment volume. Ekberg et al (1998) suggested a margin formula of 1.64σ, where σ denotes the combined deviation of tumour motion and treatment setup corresponding to the nominal probability of the target position of 90% in each of the three dimensions. van Herk et al (2000) introduced a margin recipe of $2.5\Sigma + 0.7\sigma$', where Σ denotes systematic errors introduced by treatment preparation variations due to setup error on CT scan and organ motion as well as delineation error, and σ' denotes random errors occur due to tumour motion and day-to-day setup error. The recipe was derived from the dose-population histograms to ensure that 90% of the patient population receive 95% of the prescription dose. Both formulae were applied regardless of the tumour size. The dosimetric effects on factors associated with tumour size and tumour motion are examined in this section.

5.1.2 Methods

To assess the efficiency of margin determination based on the magnitude of tumour motion, the correlation between actual target coverage as a result of 4D dose evaluation and the magnitude of tumour displacement was studied. The minimum V_{20Gy} of all phase-specific dose plans which indicates the extremity of target missing encountered during the respiratory cycle was plotted against the resultant magnitude of tumour displacement and the degree of correlation between the two factors was

assessed by using a linear least –squares fit and the Pearson correlation coefficient (R^2).

5.1.3 Results

The low value of R^2 of 0.4671 as shown in Figure 5.1 indicates poor linear correlation between the target coverage and the magnitude of tumour movement. However, the degree of target coverage was found to be associated with the combined factors of motion magnitude and tumour size. Significant target missing was found for smaller tumours with similar movement to large tumours as can be seen in table 5.1. For instance, more severe target missing was found with case 1 with a tumour size of 1.42 cc compared with case 6 with tumour size of 17.89cc while in both cases the resultant movement was about 6 mm. The difference in target coverage between the two cases was found to be 35.4% (Vex $_{20Gy}$ of 57.4 % for case 1, Vin $_{20Gy}$ of 92.8% for case 6) by comparing the minimum V_{20Gy} obtained in the two cases. Similar findings were observed between case 3 (tumour size of 3.0 cc) and case 7 (tumour size of 12.8 cc), case 2 (tumour size of 1.42 cc) and case 5 (tumour size of 4.06 cc) with differences in target coverage of 22.7% and 7.6% with tumour movement of ~4.0 mm and ~4.5 mm, respectively (see Table 5.1). The phenomenon was found to be more apparent for cases with a large discrepancy in tumour size and with the same magnitude of motion.

Figure 5.1 The minimum target coverage plots against the magnitude of tumour movement.

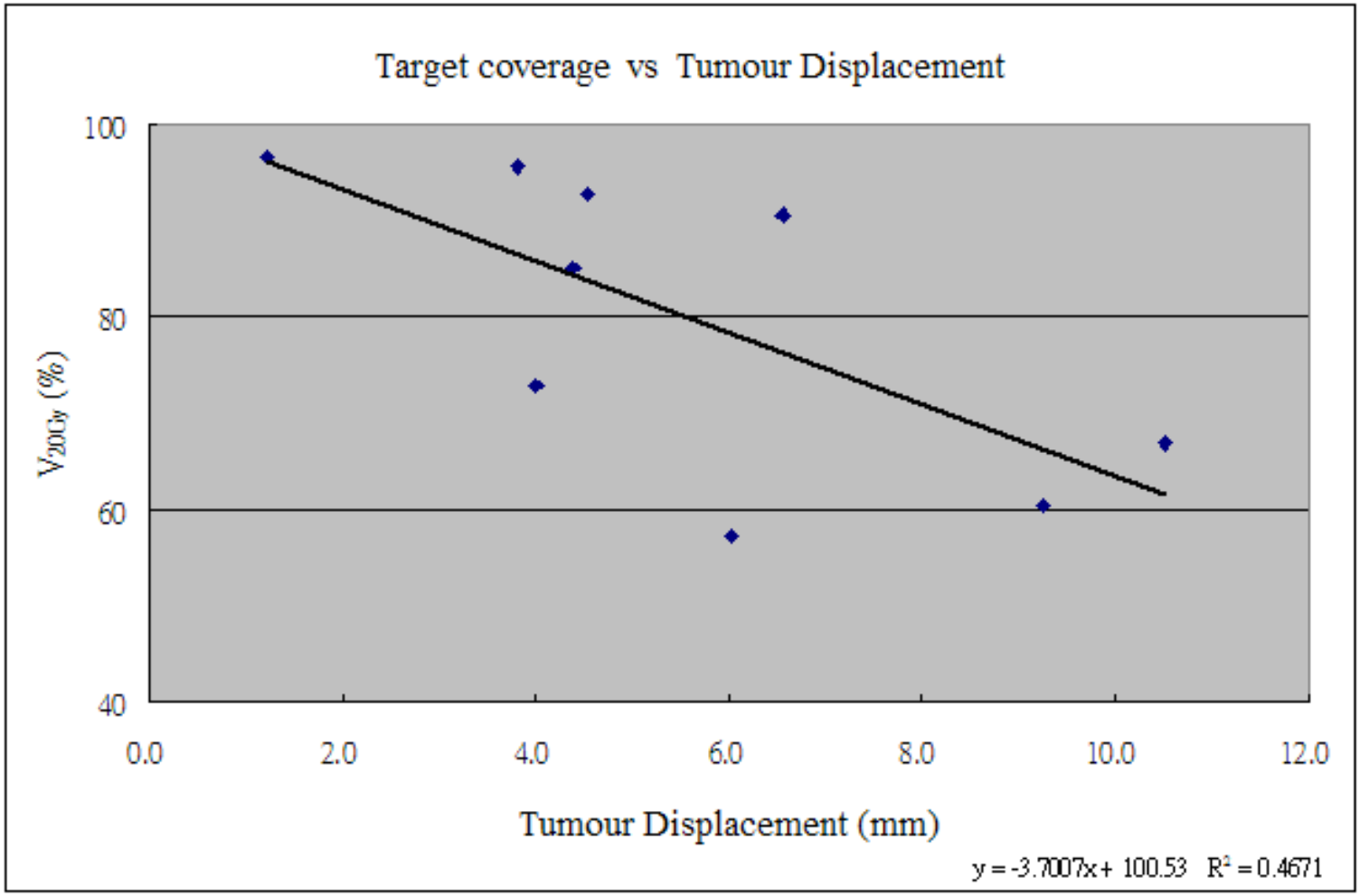

Table 5.1 The relationship between target dose coverage and tumour size and magnitude of tumour movement.

Case	resultant movement (mm) $\sqrt{(AP_{max}^2 + LR_{max}^2 + SI_{max})^2}$	tumour size (cc)	Least target Coverage (V_{20Gy})
4	1.2	6.74	96.6%
7	3.8	12.8	95.7%
3	4.0	3.0	73.0%
2	4.4	1.93	85.2%
5	4.5	4.06	92.8%
1	6.0	1.42	57.4%
6	6.6	17.89	90.7%
8	9.2	5.5	60.4%
9	10.5	12.4	66.9%

5.2 Factors Associated with Characteristic Motion Trajectory

5.2.1 Introduction

To further explore the factors involved in target coverage maximization, the influence on target coverage in relation to the characteristic of the tumour trajectory was also assessed. This was performed by studying V_{20Gy} obtained from the three phase-specific dose plans with respect to the nature of tumour motion trajectory for each case.

5.2.2 Method

The tumour trajectory was determined from tumour motion vector plots, which was set at the peak along the direction with maximum displacement, as a function of the respiratory phase. The path of maximum displacement was selected in order to maximize the trajectory effect on dose coverage.

5.2.3 Results

The degree of target coverage maximization was demonstrated to be affected by the characteristics of the tumour motion. Figure 5.2 shows the V_{20Gy} obtained from the three phase-specific dose plans of all cases (except case 4 due to the insignificant tumour movement) and with tumour trajectories illustrated in each case. The results indicated two types of tumour trajectory; the sinusoidal-like and a "flat-top" sinusoidal. Substantial target coverage maximization was found with the latter type, as shown in cases 2 – 7 with $V_{mean\ 20Gy}$ ranging from 89.2% – 95.9% compared to 71.5% to 84.0% for cases 1, 8, 9, in which tumours moved in a sinusoidal-like trajectory. This can be explained, for the case of a sinusoidal-like trajectory full target irradiation is obtained only over a relatively small fraction of the respiration cycle, however, for the flat-top sinusoidal trajectory, the tumour stays near the end-exhale position for most of the respiration cycle which corresponds to the position of the temporal mean. Hence the temporal-mean dose plan is most advantageous for cases with tumour movement in flat-top sinusoidal trajectory. This phenomenon is illustrated in Figure 5.3. A similar effect would be expected where hysteresis in tumour motion is evident. Such limitation could become more apparent with larger tumour displacement, as even smaller portion of respiration would receive full target irradiation. As shown in case 9, where tunmor has the largest magnitude of displacement among all cases and in sinusoidal-like movement,

treatment volume was not optimized with dose plan performed at the temporal mean tumour position, resulting with similar volume of $iITV_{mean}$ (28.5 cc) and $cITV_{100\%}$ (26.4cc). Moreover, the volume of iITV is directly related to the value of D_{min}, the lower the D_{min}, the larger the iITV volume. Target with irregular shape is often associated with low D_{min} due to the low dose received at the pointed area of the treatment target, it therefore significantly reduces the D_{min} and consequently enlarges the iITV volume. Thus apart from the nature of the tumour movement, the degree of tumour uniformity may also affect the significance of the target coverage maximization using iITV. In cases 9, the shape of GTV was irregular and contained a few spikes. The minimum target dose of 14.77 was received at one of the spike, and enclosed 28.5 cc dose volume. Considering that if the spike was not existed, then the minimum dose would be increased to 15.5Gy which enclose 26.5 cc dose volume, that is almost the same as $cITV_{100\%}$ (26.4 cc). The geometric factor concerning the significance of iITV for cases 3 was explained in figure 5.4.

Figure 5.2 shows the V_{20Gy} obtained from the three phase-specific dose plans of all cases (except case 4 due to the insignificant tumour movement) and with tumour trajectory illustrated in each case. The tumour trajectory is plotted with vector magnitude (1division = 1mm) against breathing phase ranged from 0% to 100% in 20% interval.

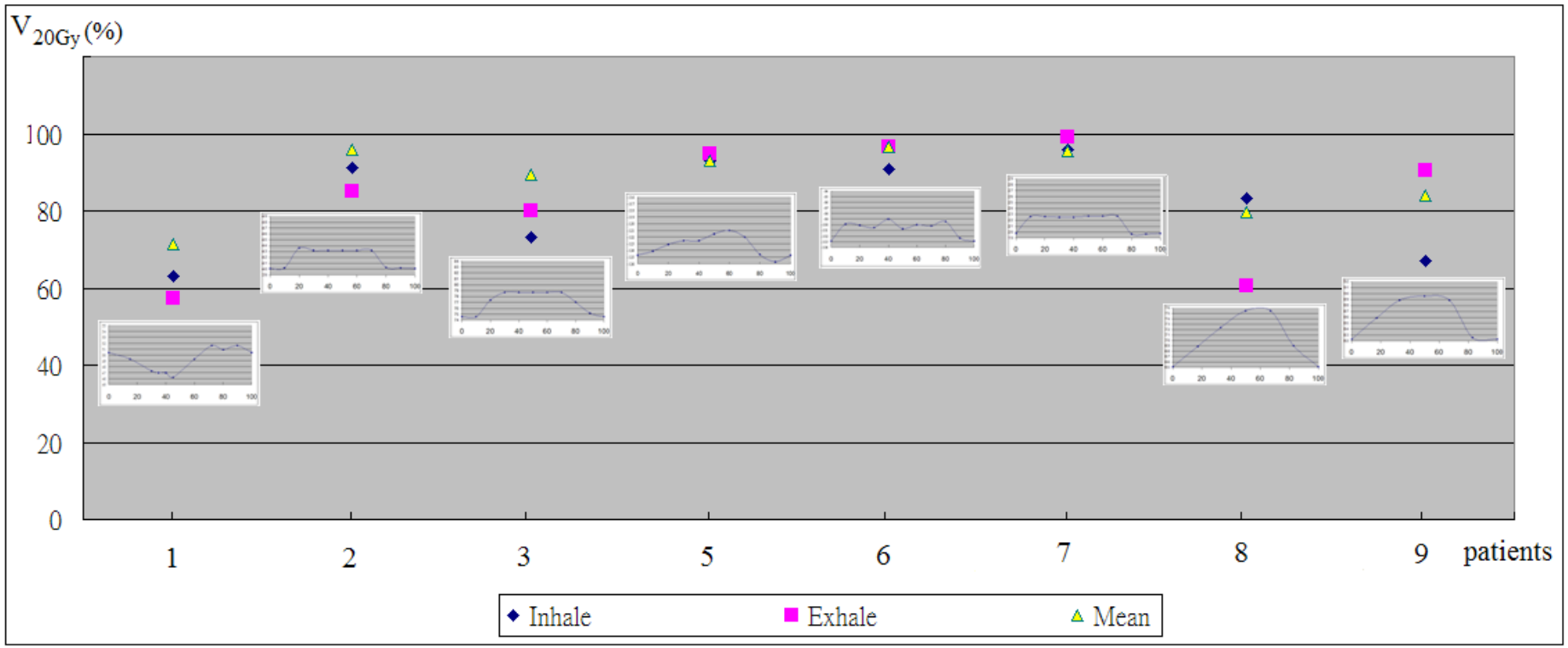

Figure 5.3 Diagram illustrates the temporal irradiation of the target for cases with sinusoidal-like (top) and flat-top sinusoidal (bottom) tumour motion trajectory during a breathing cycle. The top diagram shows when the target (in orange) is moving across the radiation filed (region confined by the blue dotted line) in a sinusoidal-like trajectory, full target irradiation is obtained in a relatively small fraction of the respiration cycle, while more irradiation is received in the lower diagram.

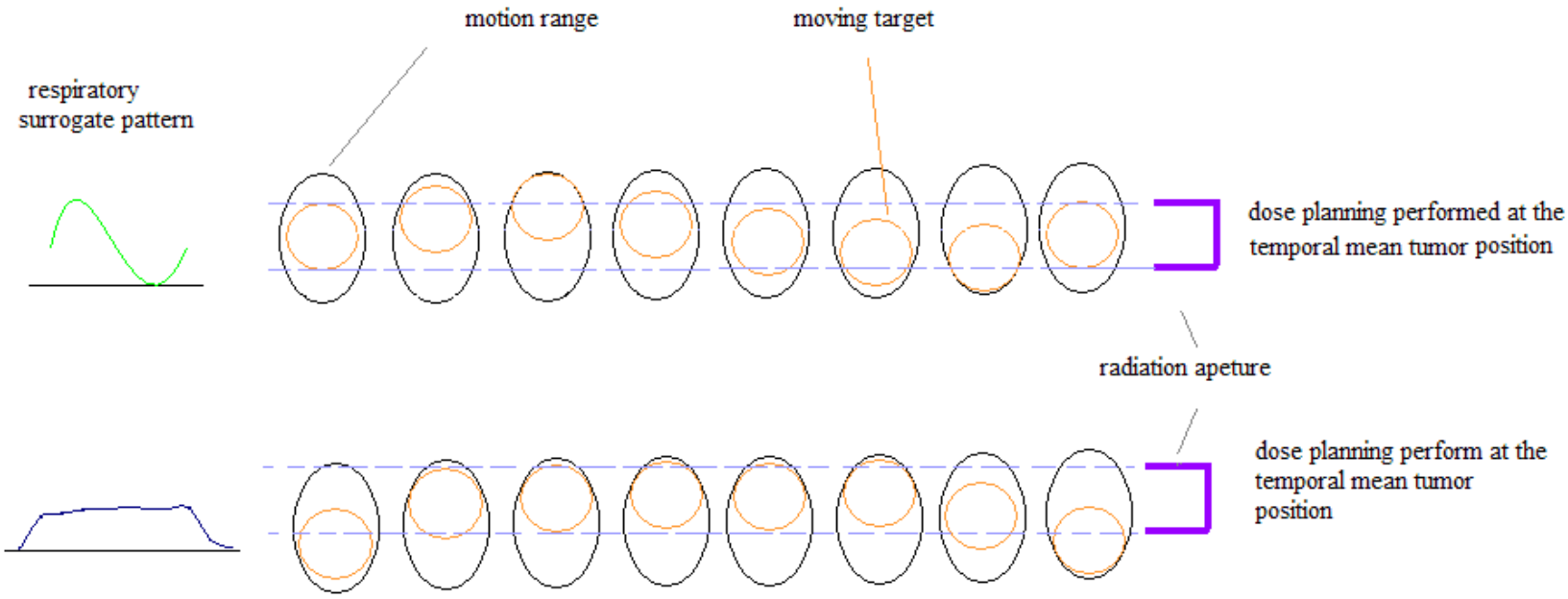

Figure 5.4 The upper diagram shows the D_{min} of 14.77 located at the superior spike enclosing 28.5 cc dose volume. The bottom diagram shown Dmin increased to 15.5 Gy if the spike is not existed. The % difference in dose volume enclosed by the Dmin of14.77 and of 15.5 Gy could be deduced using dose volume histogram.

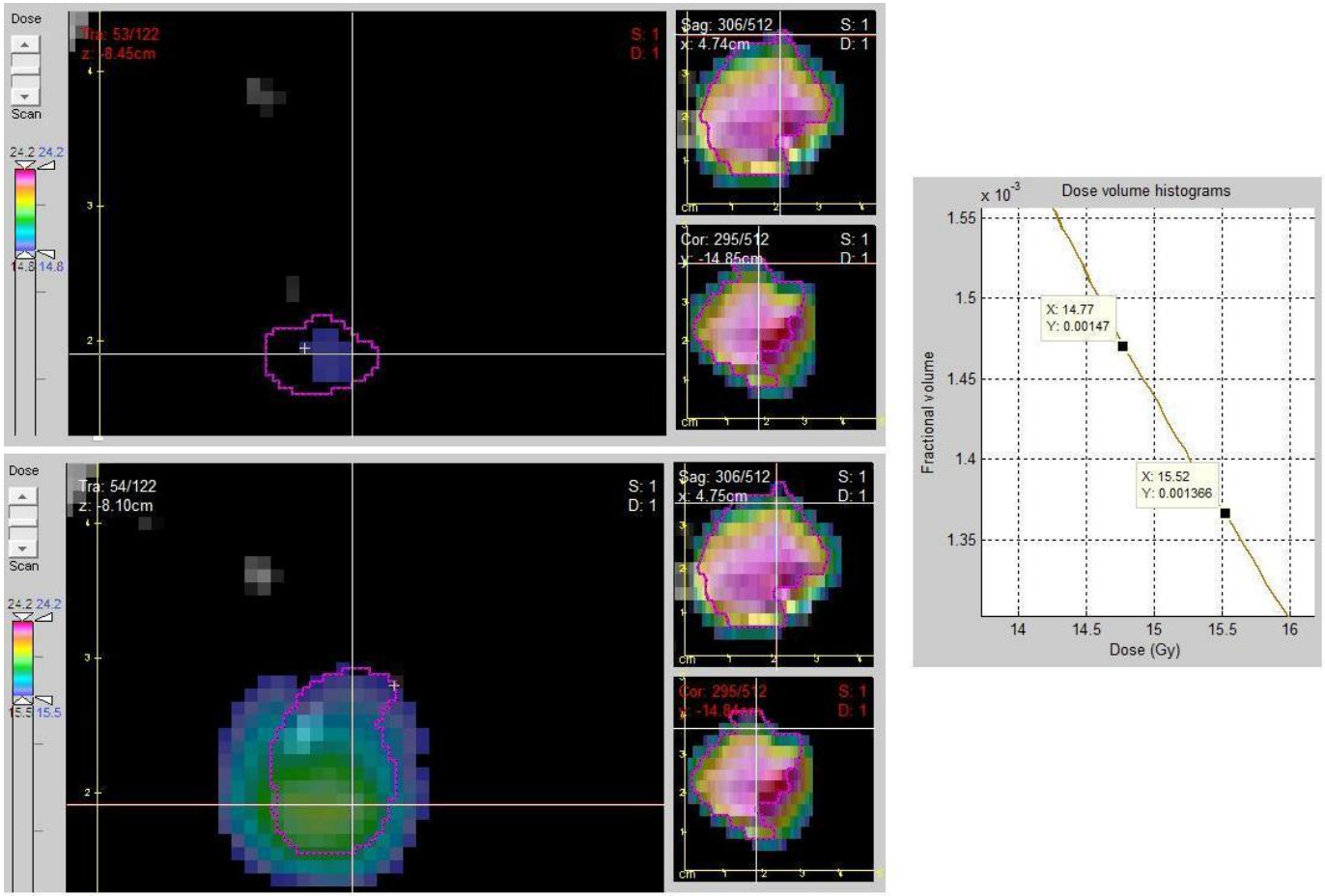

CHAPTER 6

INTRODUCTION OF OPTIMIZED 4D TREATMENT PLANNING

6.1 Determination of Effectual 4D Planning Technique using iITV

6.1.1 Introduction

The definition of iITV derived from a 4D dosimetric approach is proposed in this study, it minimizes the treatment volume by reducing the conventionally defined internal treatment margin. The results of the study indicate that the effectiveness of margin minimization depends on the planning (or reference) phase where the iITV was generated. Although dose planning performed at the temporal mean tumour position was confirmed to provide the most optimal dose plan with over 95% target coverage or the maximum target coverage among all phase-specific dose studies (see column 2^{nd} - 4^{th} , Table 4.2), however, the degree of target coverage maximization was found to be related to the nature of the target motion trajectory. The temporal-mean dose plan is most advantageous for target travels with a flat-top sinusoidal trajectory but is less effective for cases with sinusoidal-like trajectory. As for the cases with sinusoidal-like moving trajectory, tumour continuously travels along the moving track with initial deceleration until reach to the end inhale and followed by acceleration to the end exhale. Hence similar amount of receiving doses to the target would be expected with the reference field of radiation defined at any phase. Therefore, there would be no advantage in selecting the planning phase as explained in figure 5.3.

Due to the above reasons, the radiation field must cover the entire motion range of the tumour in sinusoidal-like movement to ensure the full target coverage (ie. > 99.5% target volume encompassed by the prescription dose). Hence instead of using GTV, the cITV is applied for the planning target during the 3D dose planning. In such an approach, the tumour (ie GTV) would receive a higher radiation dose than the prescription dose while it travelled along the high dose region within the beam aperture. As a result, a lower prescription dose would be required to achieve the full target dose coverage resulting in a reduction of treatment dose volume. This hypothesis is explained in figure 6.1.

Figure 6.1 In the case of sinusoidal-like tumour motion trajectory, cITV applied as the planning target providing entire target coverage and higher dose irradiation to the tumour (in orange) while it travels across the high dose region (in red)

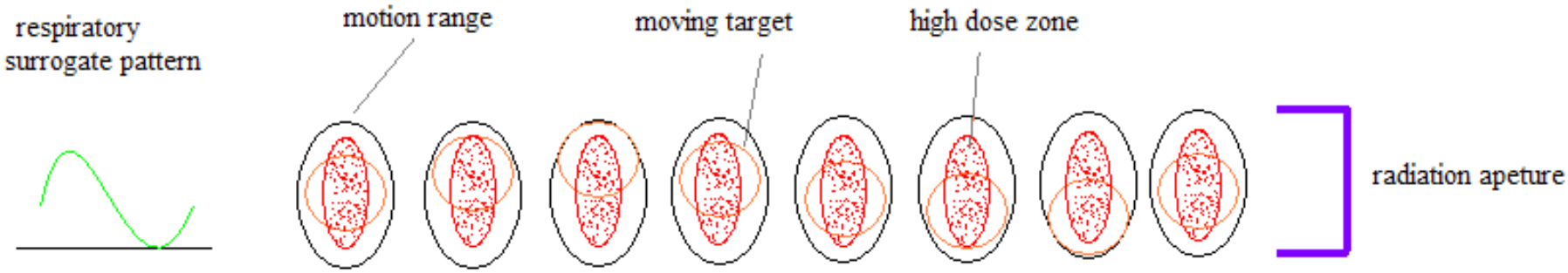

6.1.2 Methods

To test the hypothesis and its implications for treatment volume optimization, dose planning was studied using cITV as the planning target which encompasses the entire dynamic coverage of the tumour, for all cases. The 3D dose plans as described in Chapter 4.1 were re-employed for this study. Since the generated volume of cITVs has been evaluated and shown to be similar with the source image selected from different planning phases (column 4, Table 4.1), the planning reference was thus selected arbitrarily at the inhale phase for this study. For the evaluation of 4D dose distributions in the target, the 3D target dose at each respiratory phase was obtained by re-applying the planning parameters and the monitor units obtained from the reference plan to each set of 4D-CT images and recalculating the dose with a heterogeneity correction. The 4D dose distribution over the GTV was traced according to the voxel displacement of the GTV during respiration and determined by IM as described in Chapter 3.2.2

6.1.3 Results

The phenomenon described in figure 6.1 was observed in the study. Figure 6.2 shows the 3D dose plan of case 9, in which the tumour was displaced uniformly along the motion range during respiration (figure 6.2a). The radiation field covers the entire motion range (ie cITV) and the hot dose zone was located near the centre of the radiation field (figure 6 2.b). The dose-volume histogram indicates that the GTV received excessive dose above the prescribed dose (20Gy), as over 60% of the GTV volume received radiation dose higher than 23.5 Gy at any breathing phases (figure 6.2c).

Figure 6.2 shows the 3D dose plan of Case 9. In figure 6.2a, GTV of phases 0%, 16%, 33%, 50%, 67%, 83% shown in yellow, green, orange, red, blue, purple, respectively, displace uniformly along the motion range during respiration cycle. Excessive high dose irradiation to GTV volume during most of the respiration cycle is shown in figure 6.2b. At the breathing phases of 0%, 50% and 33%, the GTV volume of 63%, 76% and79% respectively received radiation doses of ≥23.5Gy. The yellow, red and orange colour-wash denote the GTV at breathing phases of 0%, 50% and 33%, respectively in figure 6.2b.

Figure 6.2 a

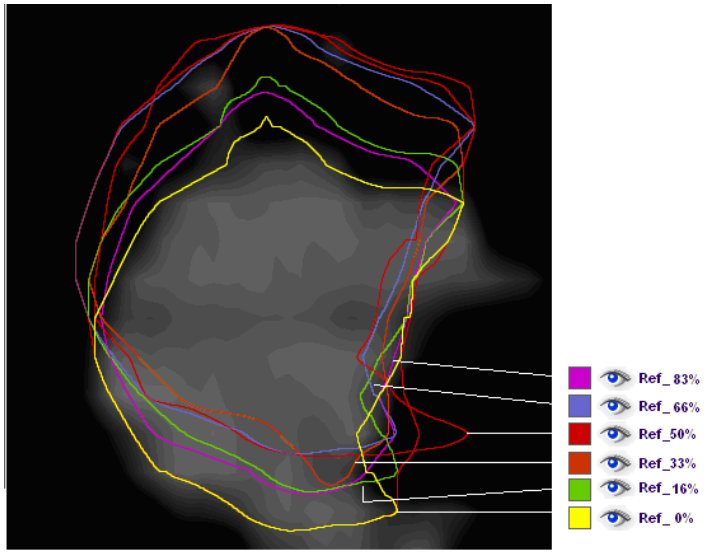

Figure 6.2 b

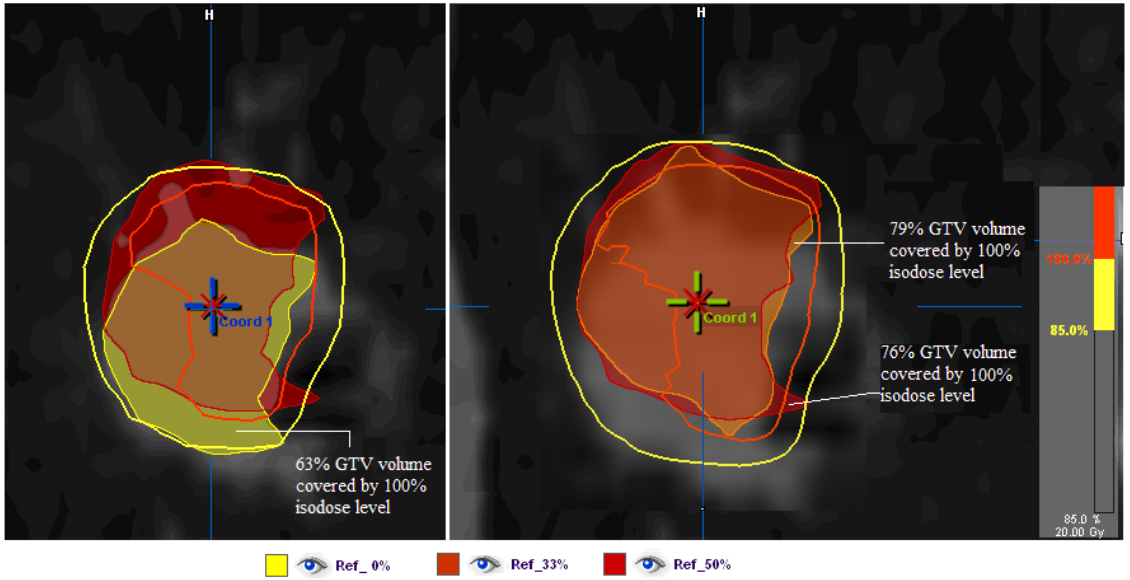

Figure 6.2c The 3D dose volume histogram depicts the temporal dose distribution of GTV. At each breathing phases the GTV volume ranged from 63% to 79% receiving radiation dose of ≥ 23.5Gy during the respiration cycle. (The print out of "violated DVH constraint" referred to the constraints of dose planning setting).

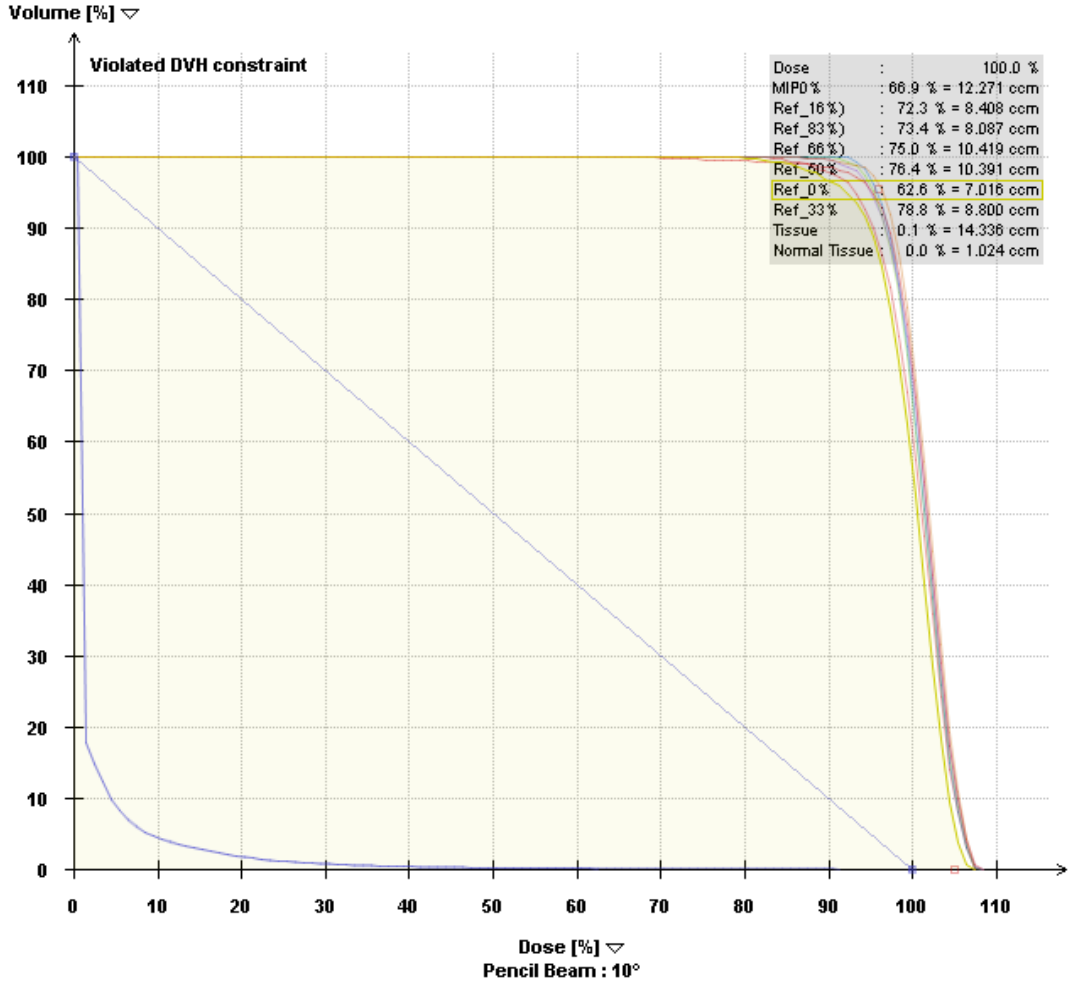

Figure 6.3 compares the 3D and 4D dose volume histogram for the GTV (green line) for case 9. The D_{min} of 21.02Gy being higher than the prescription dose suggests that the overwhelming tumour dose resulted from the excessive irradiation at the high dose zone. Using cITV as the planning target, the D_{min} was found in all cases to be higher than or equal to the prescription dose (20Gy) (column 4, Table 6.1). By prescribing at the isodose level of D_{min}, the dose volume encompassed by 20Gy on the re-normalized 3D dose plan defines the new internal target volume, denoted $iITV_{all}$. As suggested by the higher dose values of D_{min} compared to 20Gy in most of the cases, the $iITV_{all}$ is expected to be smaller than the $cITV_{100\%}$. Table 6.1 compares dose volumes among the $iITV_{mean,}$ $cITV_{100\%}$ (data were extracted from columns 10 – 11, Table 4.2) and $iITV_{all}$ for all cases, and showed that the $iITV_{mean}$ reduced the dose volume by 16.5% (range from 2.3% to 29.9%) (column 6, table 6.1) and $iITV_{all}$ reduced the dose volume by 8.7% (ranged from 0% to 24.9%) (column 7, table 6.1), as compared to $cITV_{100\%.}$ Moreover, although the $iITV_{mean}$ reduced dose volume in most of the cases, further reduction in volume could be obtained with $iITV_{all}$ for the cases with targets in sinusoidal-like motion trajectories (case 1 and case 9, see column 8, table 6.1). This result suggests that $iITV_{mean}$ may be more effective for flat-top sinusoidal motion trajectory and $iITV_{all}$ for sinusoidal-like trajectory for minimizing treatment volume.

Figure 6.3 The comparison between 3D and 4D dose volume histogram of the GTV in case 9.

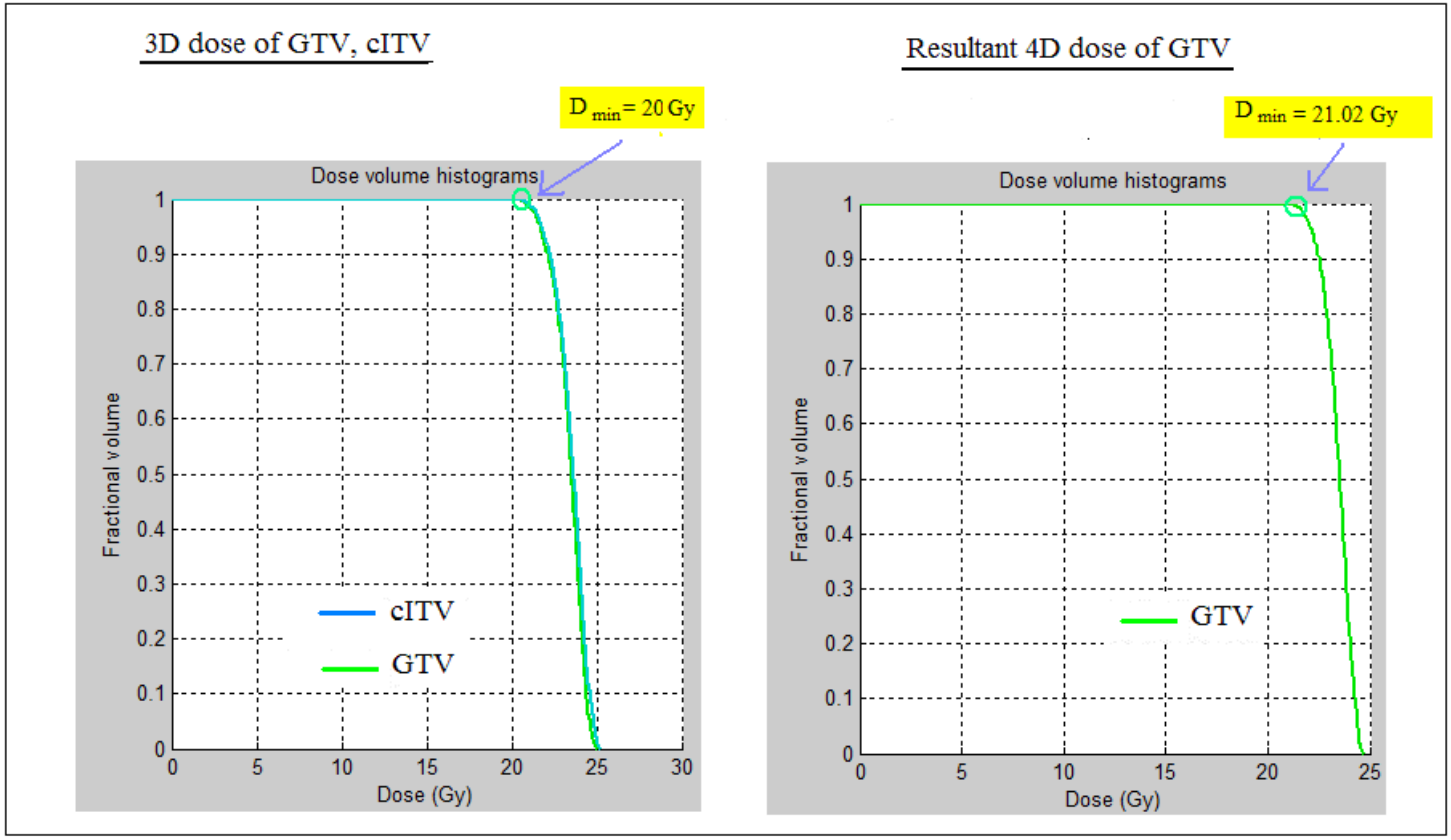

Table 6.1 Dose volume comparison among the $iITV_{mean,}$ $cITV_{100\%}$ and $iITV_{all}$ for all cases.

Case	$cITV_{100\%}$ (cc)	$iITV_{mean}$ (cc)	D_{min} (Gy)	$iITV_{all}$ (cc)	$iITV_{mean}$ vs $cITV_{100\%}$	$iITV_{all}$ vs $cITV_{100\%}$	$iITV_{all}$ vs $iITV_{mean}$
1	4.86	3.90	20.56	3.65	- 19.8	-24.9	-6.4
2	4.39	3.96	19.96	4.39	-9.8	0	+10.9
3	7.38	5.17	20.46	5.87	-29.9	-20.5	+13.5
4	13.64	11.1	21.36	11.08	-18.6	-18.8	-0.2
5	10.16	7.34	20.00	10.16	-27.7	0	+38.4
6	28.16	26.81	20.03	28.16	-4.8	0	+5.0
7	23.69	23.93	20.02	23.69	-2.3	0	-1.0
8	17.49	14.18	20.32	16.70	-19.3	-4.5	+17.8
9	26.36	28.5	21.02	23.75	+8.1	-9.9	-16.7

$cITV_{100\%}$: prescription dose volume to the cITV.

$iITV_{mean}$: inverse internal target volume derived from the dose plan performed at the temporal mean of tumour movement.

D_{min}: minimum dose received by the GTV as a result of 4D dose evaluation whereas cITV was applied as the planning target for 3D dose planning.

$iITV_{all}$: inverse internal target volume derived from the dose plan with cITV as the planning target

$cITV_{100\%}$: prescription dose volume of the cITV.

6.2 4D Treatment Planning Implementation – with treatment margins considered

6.2.1 Introduction

In this study, the concept of iITV has been proposed to optimize treatment by minimizing the treatment volume. In order to simplify the explanation of the concept and for the purpose of easy validation (image morphing), at the beginning of the study, the GTV was applied as the planning target without accounting for clinical (microscopic spread) and setup margins. To verify whether the concept of iITV could be effectively applied for clinical practice where such margins are required, the 4D doses were evaluated with the planning target including both clinical and setup margin. In the following studies, the treatment doses developed according to the proposed 4D planning technique were assessed and compared with those obtained using the conventional 3D planning technique, as well as with the immobilized treatment techniques using Deep-Inspiration- Breath-Hold which had been applied clinically in TMH.

According to the results of the iITV study, the smallest ITV volume was obtained with $iITV_{all}$ for cases 1, 4, 7, 9 and $iITV_{mean}$ for case 2, 3, 5, 6, 8 (Table 6.1). One case from each group was re-applied for 4D dose planning study in this section with the PTV containing both clinical and setup margins. The planning target dose and the lung dose were evaluated and compared with that obtained from the conventional and DIBH techniques. Since cases 1 and case 3 from each group had undergone DIBH treatment, they were selected for this study.

6.2.2 Method

6.2.2.1 Definition of PTV for the studies

A.. Conventional PTV

The conventional PTV *(cPTV)* is defined according to ICRU 62. The GTVs which are delineated on each phase of the four-dimensional computed tomography (4D-CT) image date set were expanded with a clinical margin to form the CTVs (5 mm margin was applied in this study). To explicitly account for the variations in tumour position, size and shape, the ITV is constructed by combining the CTVs and expanded with setup margin (2 mm was applied in this study) to form the cPTV (figure 6.4)

Figure 6.4 Definition of cPTV for conventional 3D dose planning

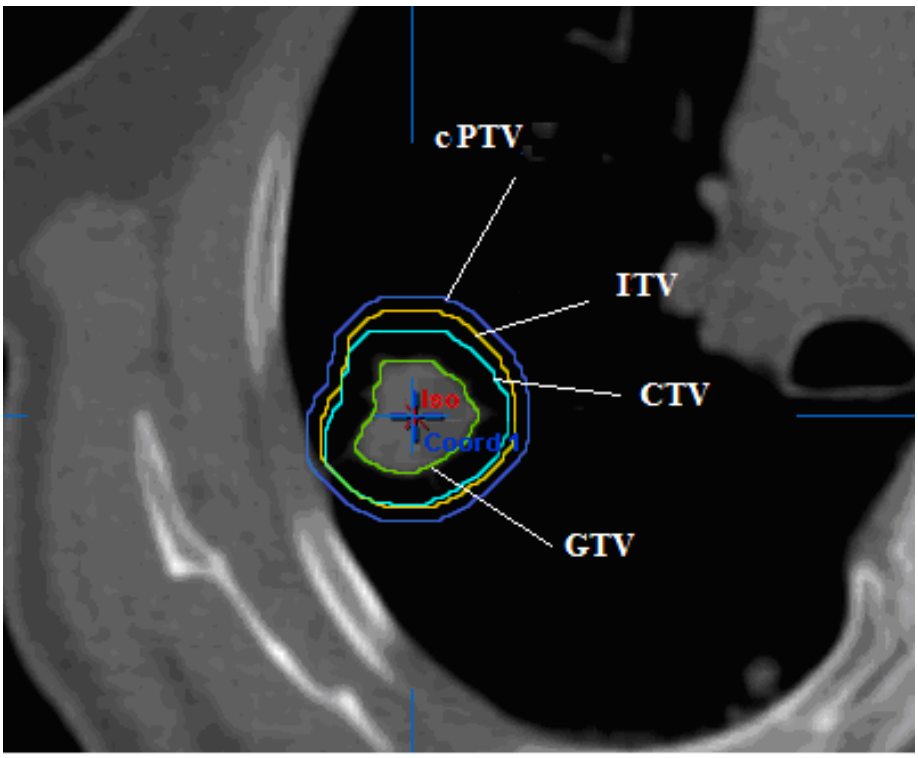

B. PTV for Case 1

As shown by the results of the previous study (on iITV), since the tumour of this case moved in a sinusoidal-like pattern, using the cITV as the planning target volume had provided the least resultant treatment volume ($iITV_{all}$). A similar result was therefore presumed for treatment while the clinical and setup margins were included for dose planning. The cPTV, defined previously (section A), covering the entire motion range was employed as the PTV for this case. The cPTV was delineated on the planning CT selected at the inhale phase. The volume of GTV, CTV and PTV defined at the reference CT were denoted as GTV_ref, CTV_ref and PTV_ref, respectively (figure 6.5). The resultant 4D doses received by the cPTV and PTV_ref were evaluated for the effective treatment volume comparison.

Figure 6.5 cPTV applied as planning target for 4D dose planning study in case 1

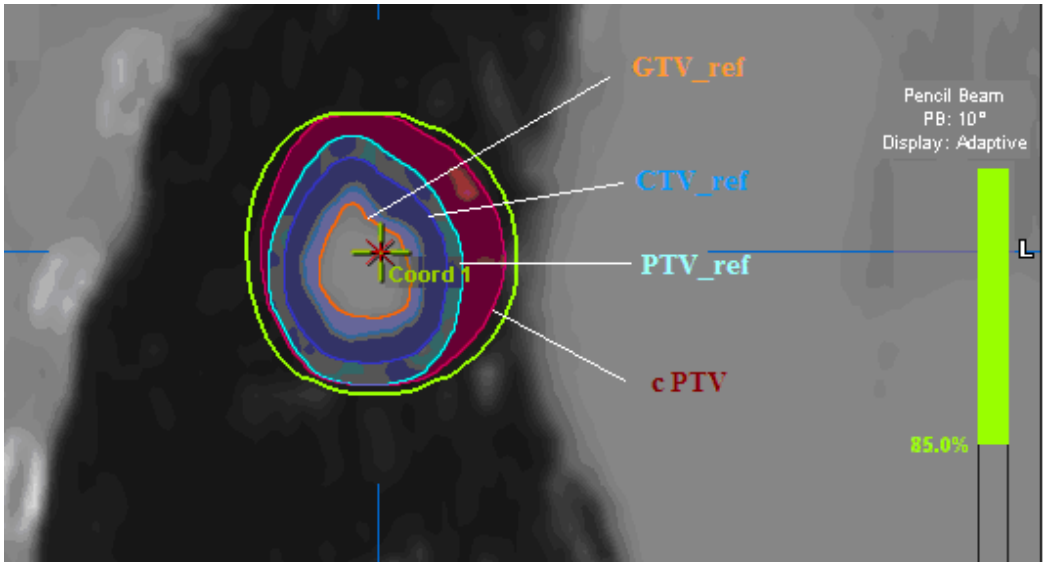

C. PTV for Case 3

The tumour in this case displaced in a flat-top sinusoidal trajectory during breathing. As indicated by the results of previous study, the planning reference taken at the temporal mean position achieved the most optimal treatment volume among studies. Hence, for the 4D planning study, the planning target volume, denoted PTV_ref, was defined with the GTV delineated at the temporal mean tumour position (ie GTV_ref), and expanded by 5 mm to form the CTV (ie CTV_ref) and further 2 mm to account for setup error. However, the margin accounting for tumour motion is not included

within the treatment volume. For the purpose of dosimetric comparison with the conventional technique, conventional dose planning was performed using cPTV as the planning target. (see figure 6.6)

Figure 6.6 The yellow circle indicates the defined planning volume for the dose studies of conventional planning and 4D dose planning

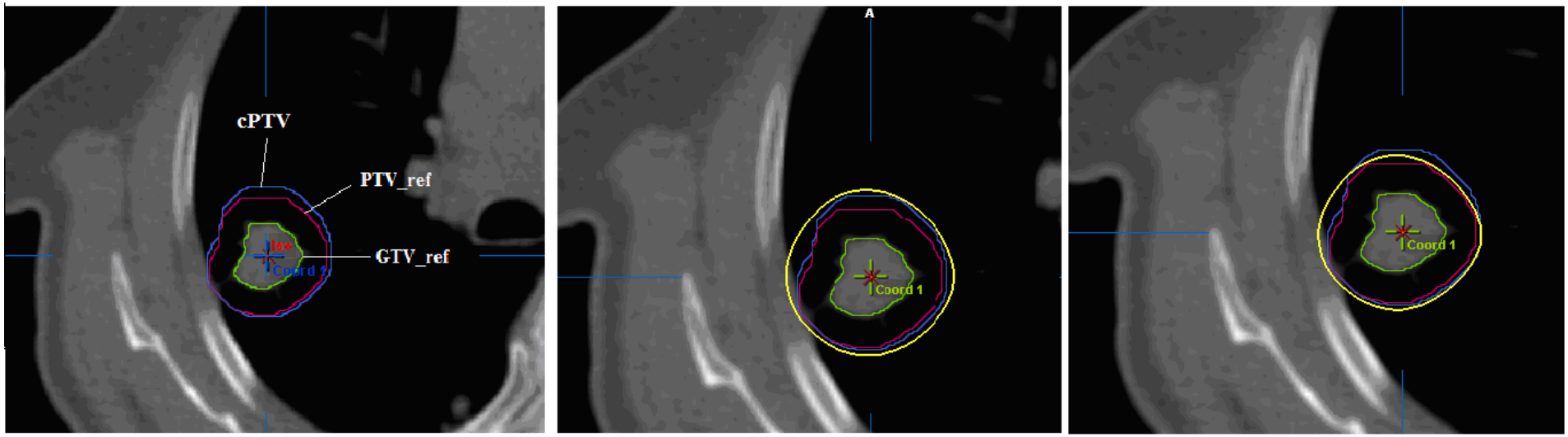

A. PTV definition of case 3

B. conventional planning

C. 4D dose planning study

6.2.2.2 4D Dose Planning

The 4D dose was calculated based on the procedure described in Chapter 3.2.2, and with the PTV described above for case 1 and case 3 as the planning target. The 3D dose planning was initially performed on one of the 4D CT sets (reference planning phase at 0% for case 1, 30% for case 3). A prescription of 20Gy was applied to the 85% or 90% isodose to enclose ≥ 99.5% of the PTV volume. To evaluate the 4D dose over the planning target volume, the PTV_ref at the reference CT served as the source data for deformable image registration using IM. However, the source data confined to the PTV_ref region would not be sufficient to look up the eventual 4D dose volume enclosed by the D_{min} of the PTV_ref. Thus the 4D dose distribution beyond the PTV_ref was assessed with source data of IM extended to a region of approximately 1 cm from the extremity of the PTV_ref (1cm is determined according to the tumour displacement magnitude) in the three dimensions. The 4D dose calculation was processed with the 3D dose distribution obtained at each respiratory phase by re-applying the planning parameters and the monitor units employed in the reference plan to each set of 4D-CT images, and recalculating the 3D doses with a heterogeneity correction. The 4D dose was then calculated using the 4D dose tool box. As a result of the 4D dose calculation, the D_{min} of the PTV_ref can be determined by prescribing at Dmin on the original 3D dose plan, complete PTV_ref coverage by 20Gy would be achieved. The new dose volume enclosed by 20Gy presented on the renormalized 3D dose plan was compared with the planning dose volume obtained from conventional treatment plan with cPTV as the planning target.

6.2.2.3 Lung dose evaluation

Apart from the evaluation of the effective size of treatment volume, the amount of radiation dose delivered to the lung volume was also assessed. The small variation between lung volumes measured at different respiratory phases of within 5% of its mean value (Table 6.2) implies that the deformation effect on dosimetric influence on lung volume during breathing was insignificant. Thus, the dosimetric influence caused by geometrical changes of lung volume was not accounted for lung dose evaluation. The volume of lungs was assumed to remain constant during the breathing cycle. The mean physical lung dose (LD_{mean}) was calculated based on the dose-volume histogram, in which both lungs were considered as one organ and the GTV was excluded. LD_{mean} is given by equations (1) and (2) :

$$\overline{LDi} = \sum_{j=0\%}^{m} \frac{LDi, j}{m} \quad (1)$$

$$\mathrm{LD}_{\mathrm{mean}} = \Sigma_i \, v_i \, . \, \overline{LDi} \quad (2)$$

Where $\overline{LDi}$ is the physical mean dose received by the partial lung volume (v_i) in dose bin i of the dose plans obtained from the mth respiratory phases (m=10 for both cases).

Table 6.2 Lung volume of case 1 and case 3.

	Case 1	**Case 3**
0%	2583 cc	3315 cc
10%	2543 cc	3292 cc
20%	2395 cc	3238 cc
30%	2324 cc	3195 cc
40%	2424 cc	3142 cc
50%	2260 cc	3092 cc
60%	2253 cc	3054 cc
70%	2323 cc	3019 cc
80%	2425 cc	3054 cc
90%	2555 cc	3231 cc
mean +/- stdev	2409 +/- 121 cc	3163 +/- 106 cc
variation	5.0%	3.3%

6.2.3 Results

Case 1

The cPTV was assigned as the PTV in this case. The physical dose received by the cPTV and PTV_ref evaluated in 3D and 4D are listed in Table 6.3. Due to the motion effects, the dose distributions over the cPTV of the 4D dose plan were different from that shown on the 3D plan especially for the minimum dose. The volume dose histogram of the 3D and 4D dose plans (figure 6.7) reveals the minimum dose received by the cPTV was 20.3 Gy and 16.4 Gy and enclosed 26.3 cc and 35.5 cc dose volume, respectively (column 2^{nd} , 4^{th} Table 6.3). As a result of 4D dose evaluation, the PTV_ref with D_{min} of 21.4 Gy indicates that the original 3D dose plan using conventional planning technique could be optimized by prescribing at the 21.4Gy isodose level to achieve complete coverage of PTV_ref . This leads to reduction of treatment volume by 17%, as the 21.4 Gy enclosed 21.8 cc dose volume versus 26.3 cc enclosed by the original planning dose of 20Gy according to the 3D dose distribution (column 4 , Table 6.3). Moreover, the maximum dose of PTV_ref was reduced by 6.6% (from 24.3Gy to 22.7Gy). In terms of 4D accumulated dose, the new prescription dose volume obtained from the re-normalized dose plan was 20.1cc. And the LD_{mean} was reduced from 1.10 to 1.03 Gy.

Figure 6.7 Radiation dose of 20.3 Gy represents the minimum dose received by the cPTV in 3D dose planning. The 4D dose evaluation indicates the actual minimum dose to the cPTV and PTV_ref were 16.4Gy and 21.4 Gy, respectively.

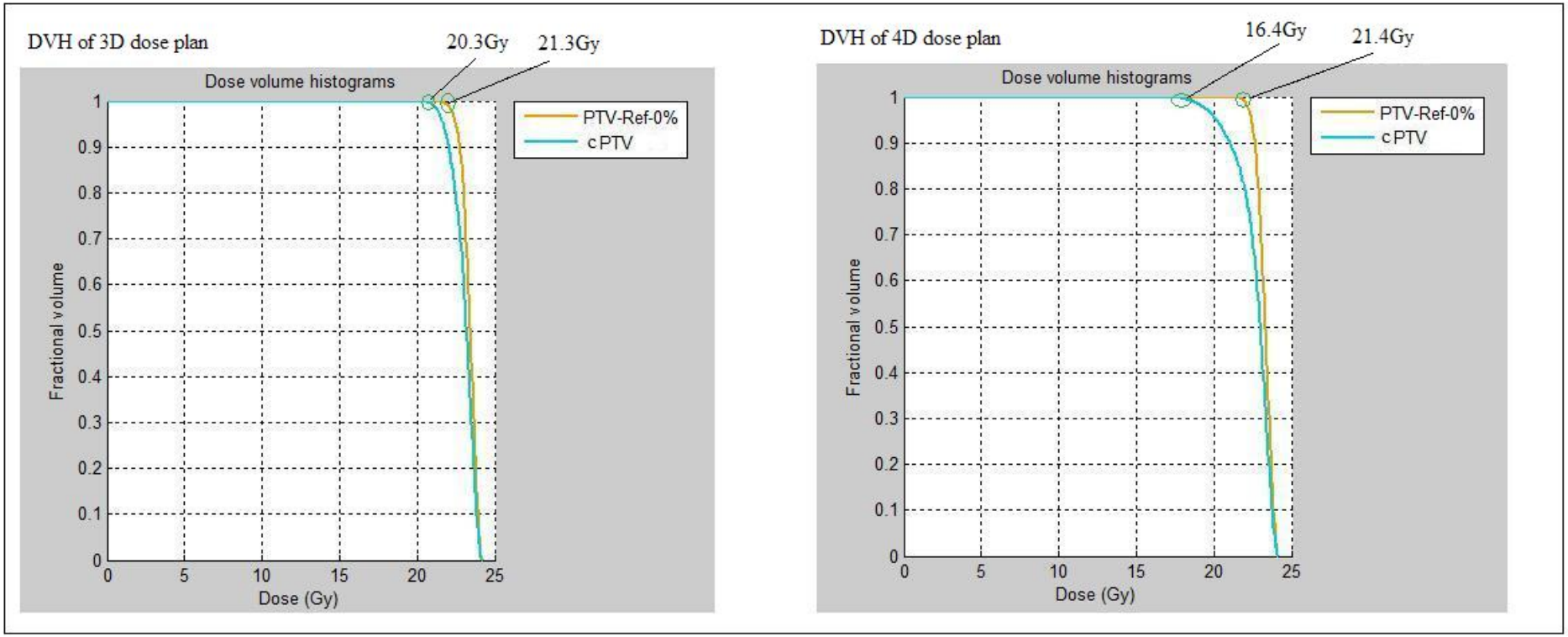

cPTV: The conventional PTV volume defined according to ICRU 62

PTV_ref: PTV volume defiend in reference planning CT

Table 6.3 Dosimetric comparison between 3D and 4D dose planning for Case 1

Case 1	Target Dose (Gy)						Dose volume (cc)		Lung Dose (vol. = 2615 cc)	
	cPTV (vol. = 19.9 cc)			$PTV_{\_ref}$ (vol.=12.6 cc)						
	max	min	mean	max	min	mean	V_{PD}	V_{Dmin} ($V_{21.4}$)	max	LD_{mean}
3D dose	24.2	20.3	23.1	24.5	21.3	23.3	26.3	21.8	24.2	1.10
4D dose	24.2	16.4	22.7	24.3	21.4*	23.3	24.9	20.1		
4D dose (renormalized dose plan - prescribed at Dmin)	22.6	15.3	21.2	22.7	20.0	21.8		20.1	22.6	1.03 #

cPTV: The conventional PTV volume defined according to ICRU 62

PTV_ref: PTV volume defined in the reference planning CT

V_{PD}: Total dose volume encompassed by prescription dose (PD) of 20Gy

V_{Dmin}: Dose volume encompassed by Dmin isodose

LD_{mean}: Mean physical lung dose

*Dmin: the minimum 4D dose of PTV_ref, which was 21.4 Gy

The lung dose was evaluated in 3D (refer to section 8.2.1.3 for calculation)

Case 3

As in case 1, dose plans were generated using the cPTV and PTV_ref as the planning target for dosimetric comparison between the conventional and 4D planning techniques, respectively. The same CI value of 1.22 was obtained in both cases. According to the results of 4D dose evaluation, the minimum accumulated dose over the PTV_ref was 18.7 Gy (figure 7.8b, 7.8c), it enclosed 29.1 cc and 28.0 cc dose volume according to the 3D and 4D dose evaluations, respectively (column 4^{th}, Table 6.4). Hence, by prescribing at the D_{min} (18.7Gy) the entire target dose coverage to the PTV_ref would be achieved. As compared to the conventional dose plan using cPTV as the planning target, of which, 20Gy enclosed 31.2 cc dose volume, the prescription dose volume was found to be reduced by 6.7 % (= 29.1 / 31.2). However, the maximum dose of PTV_ref was increased by 6.8% (from 23.5Gy to 25.1 Gy).

Figure 6.8 3D and 4D dosimetric comparison on PTV_ref. Figure 6.8c indicated the PTV_ref (contoured in red) was entirely encompassed by Dmin (18.7Gy)

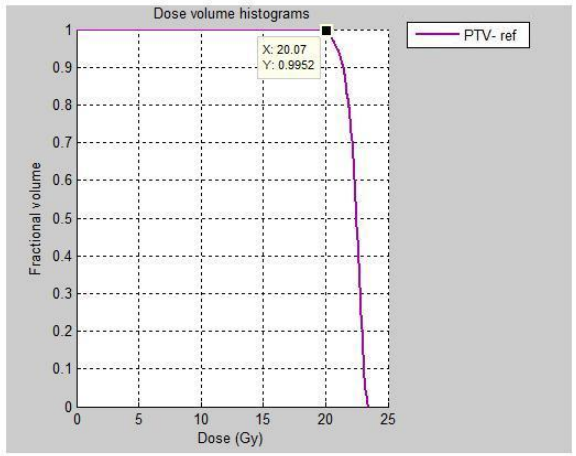

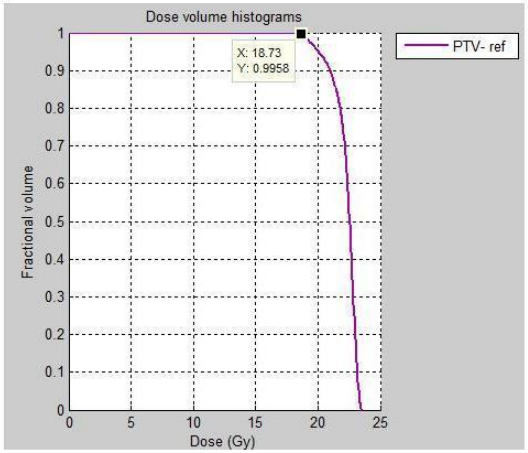

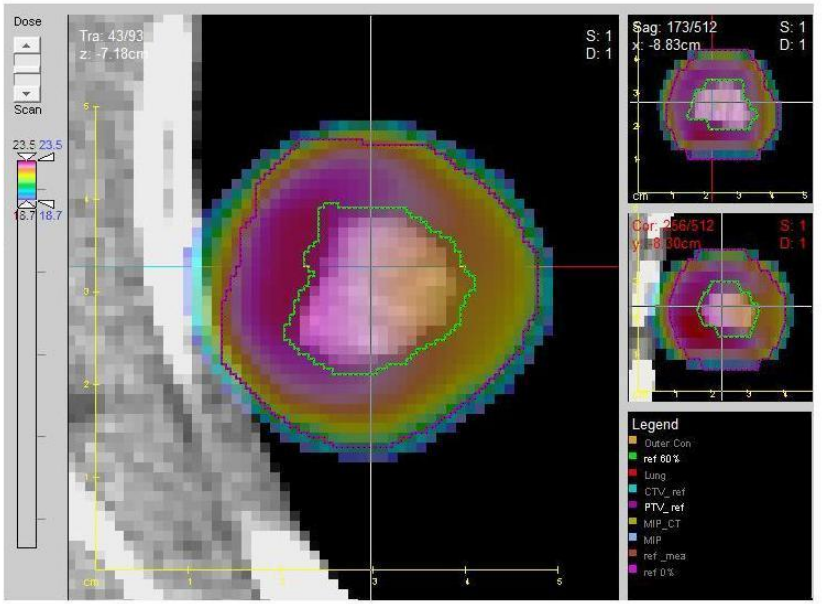

A. DVH of 3D dose plan B. DVH of 4D dose plan C. 4D dose distribution — $V_{Dmin\ /\ 18.7\ Gy}$ of PTV_ref

PTV_ref: PTV volume defiend in reference planning CT

Dmin: minimum 4D dose received by PTV_ref

Table 6.4 Dosimetric comparison between 3D and 4D dose planning for Case 3

Case 3	Target Dose (Gy)						Dose volume (cc)			Lung Dose (vol. = 3049 cc)	
	cPTV (vol. = 25.6 cc)			$PTV_{\_ref}$ (vol.= 20.9cc)							
	max	min	mean	max	min	mean	V^{c}_{PD}	V_{PD}	$V_{18.7Gy}$	max	LD_{mean}
3D dose	23.0	20.0	22.1	23.5	20.0	22.4	31.2	25.5	29.1	23.1	0.94
4D dose	not calculated			23.5	18.7*	22.3	not calculated		28.0		
4D dose (renormalized dose plan - prescribed at Dmin of $PTV_{\_ref}$)				25.1	20.0	23.8			28.0	24.7	1.01 #

cPTV: The conventional PTV volume defined according to ICRU 62

PTV_ref: PTV volume defiend in reference planning CT

V_{PD}: Total dose volume encompassed by prescription dose (PD) of 20Gy

$V_{18.7Gy}$: Total dose volume encompassed by isodose of 18.7Gy

LD_{mean}: Mean physical lung dose

*18.7: the minimum 4D dose received by PTV_ref

The lung dose was evaluated in 3D (refer to section 8.2.1.3 for calculation)

V^{c}_{PD} : The prescription dose volume (V_{PD}) obtained from the conventional dose plan.

CHAPTER 7

BREATH-HOLD VS FREE BREATHING TECHNIQUES FOR LUNG CANCER

7.1 Introduction of Deep Inspiration Breath Hold (DIBH) Techniques

In the past decade, several sophisticated treatment delivery methods such as gating, tracking and tumour immobilization with breath-hold have been developed for better treatment localization for lung cancer (Hanley et al. 1999; Balter et al. 1998; Barnes et al. 2003; Brown et al. 2007). Various studies (Engelsman et al. 2005; Mageras et al. 2004; Berbeco, 2005) have compared the gating and breath-hold techniques and these indicate that more margin may be required to allow for the residual tumour motion during respiratory gating. The Deep Inspiration Breath Hold (DIBH) technique has two distinct features namely deep inspiration, which reduces lung density and breath-hold, which immobilizes lung tumours. The reduction of tumour motion using DIBH should permit the field aperture to be reduced for the same target coverage. The lower density of normal lung relative to tumour can further decrease the amount of normal lung tissue in the high-dose region, thus reducing morbidity and improving the possibility of dose escalation. Despite the distinctive therapeutic advantages of using the DIBH technique, it however may not be compliable to every patient, training must be provided prior to treatment. For patients who are not able to comply their unstable or lack of breath-hold control may lead to unsuccessful target immobilization and possible treatment failure. At the Radiation Oncology Centre of TMH, the breath-hold and gating concepts were combined. The tumour movement was immobilized using DIBH and the breath hold consistency and stability were monitored and controlled by the gating technique. In such an approach the benefits from both techniques are extracted. The gated-DIBH technique for lung cancer radiotherapy has been applied in fifteen cases in TMH since 2004. Since the gated-DIBH dose plan of case P47 (table 3.1) was corrupted, the DIBH dose planning evaluation was not applied. The disease characteristic for the DIBH group patients can be found in table 3.1.

7.2 Clinical Application using Gated-DIBH Technique in TMH

During treatment, DIBH was conducted using the active breathing coordinator device (ABC) (Elekta, Ltd). The treatment position and the amount of tumour movement during breath-hold were controlled according to the abdominal surface tracking using the ExacTrac stereotactic positioning system (v.3.5, BrainLab Ltd). This system was developed for automated treatment positioning and is based on optical detection utilising IR-reflective markers (figure 7.1). The theory of the gated-DIBH technique is based on the assumption that good tumour immobility relies on the consistent performance of breath-hold and this could be confirmed by the geometric configuration of the abdomen. Such hypothesis is in-line with the principle of the ExacTrac system in which the 3D configurations are analyzed for performing automated positioning. In addition to the validation of breath-hold stability, the ExacTrac system was also applied for the treatment set up. Considering that the setup process was actually performed in a static mode (during breath-hold), the sub milli-meter positioning accuracy using the ExacTrac system as reported in the literature was therefore expected. The control of tumour immobility was investigated inter- and intra- fractionally.

Figure 7.1 Treatment setup of Gated-DIBH using the ExacTrac stereotactic positioning system

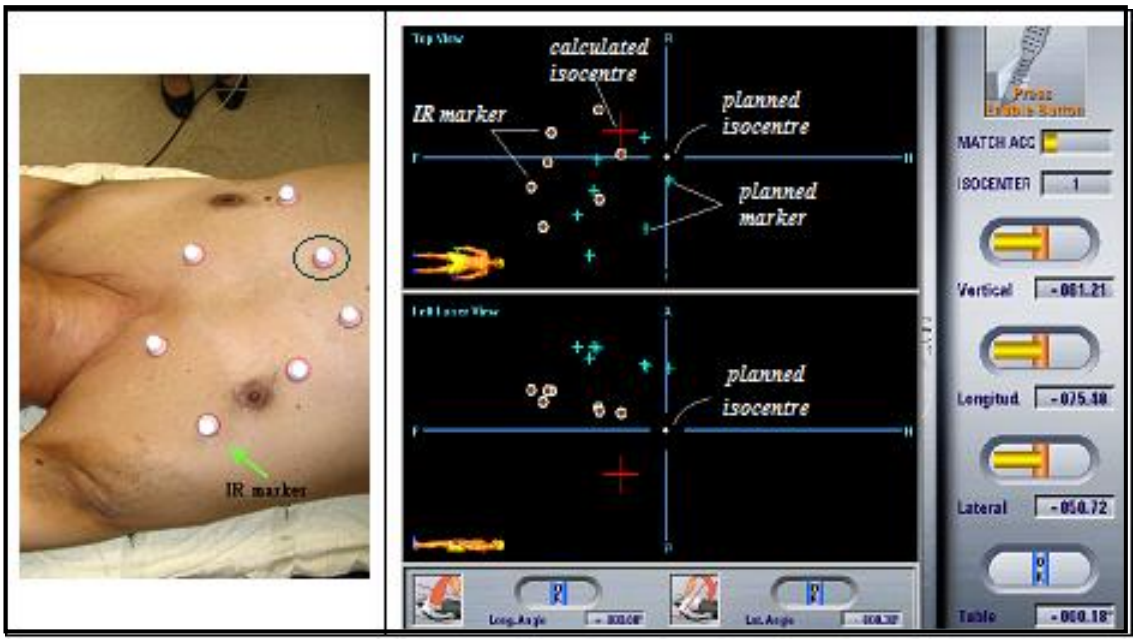

7.2.1 Treatment Setup using ExacTrac System

The principle of treatment setup and the applications of the ExaTrac system are well documented and the positioning accuracy of within 1 mm for localization of static target has been reported [13 – 15]. The procedure is briefly described here, during the treatment, the IR markers were placed onto the positions which had been labeled during the CT planning simulation. The markers were tracked on-line with a pair of infrared cameras and the three-dimensional (3D) displacement of the markers was recorded in a sample rate of 5 Hz. The treatment position was determined by least square fit optimization; a matrix was computed on-line to achieve the best mapping between the IR markers and the markers recorded on the treatment plan. The treatment isocentre was calculated according to the result of mapping and consequently aligned with the Linac isocentre (fig. 7.1). The discrepancy between the calculated and the planned isocentres was computed in 3D and updated at 0.2 s interval. When the breath-hold control was consistent, the positions of the IR markers would be the same as those recorded on the treatment plan (ie identical surface curvature). However, if breath-hold was unstable, the discrepancy between the calculated and planned isocentres will gradually increase. A warning was set for discrepancy of greater than 2 mm in any direction, and the treatment would then be interrupted manually.

7.2.2 Treatment Margin of the Gated-DIBH Technique

The margin of the planning target volume (PTV) was evaluated based on 2 factors: 1) The treatment setup errors to account for patient setup variation and inter-breath hold variation (σ_s), and 2) the intra-breath hold tumour motion (σ_t) in which the residual tumour motion during irradiation under breath hold was studied. From clinical evaluations in fourteen patients, the group systematic error and group random error of the treatment setup measured at the isocentre were 0.2(R) ± 1.6 mm, 1.0(A) ± 2.0 mm, 0.3(S) ± 1.5 mm in the left-right (LR), anterior-posterior (AP) and caudal-cranial (CC) directions, respectively. The PTV margin of individual patients (M_{ptv}) was calculated by the quadratic sum of σ_s and σ_t. The group PTV margin (GM_{ptv}) was evaluated by the mean of individual's margins (M_m) and twice the SD of individual margins (Σ_m) to cover 95% of the population to receive the prescribed

dosage. The group PTV margins of 3.8 (LR), 4.6 (AP) and 4.8 (CC) mm were evaluated and applied clinically. The clinical implementation of using gated-DIBH technique and its efficacy in terms of tumour immobility and treatment set up accuracy were reported in the previous study (Wong et al. 2010). The details of margin evaluation of for gated-DIBH technique are listed in Appendix II.

Table 7.2 Intra -breath-hold tumour motion, individual and group margin.

Patient	Intra-breath hold tumour variation σ_t (mm)			Individual Margin M_{PTV} (mm) $M_{PTV_i} = \sqrt{(\sigma_{s_i})^2 + (3\sigma_{t_i})^2}$.		
	LR	AP	CC	LR	AP	CC
1	0.6	0.3	0.5	3.6	2.5	2.1
2	0.2	0.3	0.4	0.7	2.7	2.1
3	0.2	0.2	0.7	0.5	0.7	2.1
4	0.1	0.2	0.4	0.3	2.3	3.8
5	0.2	0.3	0.7	1.1	2.1	2.0
6	0.2	0.3	0.4	2.1	3.6	1.1
7	0.1	0.5	0.9	0.3	1.4	2.8
8	0.1	0.3	0.6	2.0	2.2	3.5
9	0.2	0.3	0.9	0.7	1.3	2.8
10	0.1	0.1	0.1	0.2	0.3	0.3
11	0.3	0.5	0.9	1.0	4.7	2.7
12	0.3	0.1	0.5	3.6	0.4	1.6
13	0.4	0.5	0.5	2.3	3.1	1.7
14	0.3	0.2	1.6	0.9	0.7	5.2
Group Mean (mm)	0.2	0.3	0.7	1.4	2.0	2.4
Group SD (mm)	±0.2	±0.1	±0.4	±1.2	±1.3	±1.2
Group Margin (GM_{PTV}) = $M_m + 2\Sigma_m$ (mm)				3.8	4.6	4.8

σ_t: Intra-breath hold tumour variation

σ_s: treatment setup error

M_m: Group mean of individual margins

Σ_m: Group std of individual margins

7.3 Dosimetric Comparison between Gated-DIBH (3D Dose Planning) and Free Breathing (4D Dose Planning) Techniques

Among the fifteen cases treated with the Gated-DIBH technique, four (cases 1, 3, 4, 5) were included in this study. Comparison of dosimetric advantages between treatments delivered with DIBH technique based on 3D dose planning and with free breathing based on 4D dose planning (ie results presented in Chapter 6) were assessed for the four cases. However, the DIBH dose plan of case 5 was corrupted and case 4 with minimal tumour motion, thus only case 1 and case 3 with relatively large tumour movement were selected for dosimetric comparison.

To allow unbiased comparison, equivalent dosimetric properties were verified for similarity in dosimetric indices (ie. CI, HI and TCI). The same dose prescription and delivery technique as those applied in the 4D dose study described in Chapter 6.2.2 (20Gy at the 85% (case 1) and 90% (case 3) isodose level to enclose ≥ 99.5% of the PTV volume) was used for the gated-DIBH dose plan. The GTV was delineated on the clinical dose plan using a lung CT window (HU = -500, 1000). The Clinical Target Volume (CTV) was defined with a 5 mm margin expanded evenly from the GTV to cover the microscopic extent of tumour. The evaluated PTV margins of 3.8 mm, 4.6 mm and 4.8 mm in the LR, AP and CC directions were applied. To eliminate dosimetric variation resulting form discrepancy in dose grid between planning systems (BrainScan and CERR), the gated-DIBH dose plan was imported into CERR for dose evaluation. The physical dose received by the PTV, GTV and both lungs were assessed. For consistent dosimetric comparison with the 4D dose study performed in Chapter 6.2, the terminology was synchronized by renaming the GTV, CTV and PTV to GTV_ref, CTV_ref and PTV_ref, respectively..

7.3.1 Conversion of Physical Dose to Normalized Dose for Lung Dose Evaluation

Symptomatic pneumonitis occurs in approximately 0-20% of patients irradiated with conventional doses of radiation (Cox et al. 1990; Gross, 1997). The incidence of this side effect appears to be dependent on irradiated lung volume and dose, although the exact relationship is not well defined (Lawrence et al, 2010). In this study, the dose was delivered via hypo-fractionation in order to correlate the clinical outcome with that of a conventional study. The physical dose distribution was converted into the biologically equivalent dose (BED) distribution (Williams et al. 1985) of 2 Gy

per fraction to define the normalized total dose (NTD) distribution. By using the linear quadratic model (Maciejewski, et al. 1986), with an α/β ratio of 3 Gy, the NTD for lung was defined by equation (3):

$$NTD = \frac{nd\,[1+d/(\alpha/\beta)]}{[1+2/(\alpha/\beta)]} \qquad (3)$$

where n is equal to the number of fractions (n=3), d the dose per fraction and α/β for the specific end point. Base on the dose-volume histogram, in which both lungs were considered as one organ and the GTV was excluded for dose calculation, the normalized mean lung dose (NTD_{mean}) was calculated using equation (4)

$$NTD_{mean} = \Sigma_i\, v_i \,.\, NTD_i \qquad (4)$$

Wherev_i is the partial lung volume in dose bin i, which received a biological dose NTD_i. The percentage of total lung volume receiving NTD ≧20 Gy (V_{NTD20}) and NTD_{mean} were assessed and compared between the FB and DIBH groups.

7.3.2 Dosimetric Comparison for Treatment Target and Lungs

Dose planning using the gated-DIBH (section 7.4) and FB techniques (section 6.2.2), respectively were compared for case 1 and case 3. Table 7.3 and Table 7.4 lists the radiation doses received by the PTV_ref, GTV_ref and the resultant dose volume encompassed by the prescribed dose (20Gy per fraction) planned with the two techniques for case 1 and case 3, respectively. The nominal total dose (NTD) of the lung volume was also evaluated for assessment of radiation induced pneumonitis. Lung dose which was evaluated with the GTV excluded. The FB techniques using cPTV and PTV_ref as the planning target, for cases 1 and case 3, respectively were discussed in Chapter 6.2, the data of the results was applied here for comparison.

Table 7.3 Dosimetry comparison between 3D dose planning with DIBH and 4D dose planning with free breathing for case 1

CASE I											
Physical Dose (all fractions)	PTV_ref					GTV_ref				Lung	
	max. (Gy)	min (Gy)	mean (Gy)	V_{PD} (CC)	$V_{PTV\_ref.}$ (cc)	max. (Gy).	min (Gy)	mean (Gy)	V_{GTV_ref} (cc)	LD_{mean} (Gy)	Lung volume (cc)
DIBH (3D)	74.0	60.0	70.2	27.9	20.5	73.4	69.2	71.2	1.30	3.72	3210
FB (4D)	69.7	60.0	65.5	20.1	12.6	67.7	64.0	65.7	1.28	3.3	2409
NTD (all fractions)	Lung ($\alpha/\beta = 3$)										
	NTD_{mean} (Gy_3)					V_{20Gy} (%)					
DIBH (3D)	17.5					14.3					
FB (4D)	17.5					15.8					

DIBH (3D): 3D dose planning using gated-DIBH technique.

FB (4D): 4D dose planning with treatment performed under free breathing.

PTV_ref: PTV volume defiend in reference planning CT

GTV_ref: GTV volume defiend in reference planning CT

$V_{GTV\_ref.}$: Volume of GTV_ref

$V_{PTV\_ref.}$: Volume of PTV_ref

V_{PD}: Total dose volume encompassed by prescription dose (PD=20Gy)

LD_{mean}: Mean physical lung dose NTD_{mean}: mean nominal total dose

Table 7.4 Dosimetry comparison between 3D dose planning with DIBH and 4D dose planning with free breathing for case 3.

CASE 3											
Physical Dose (all fractions)	PTV_ref					GTV_ref				Lung	
	max. (Gy)	min (Gy)	mean (Gy)	V_{PD} (CC)	$V_{PTV\_ref.}$ (cc)	max. (Gy).	min (Gy)	mean (Gy)	V_{GTV_ref} (cc)	LD_{mean} (Gy)	Lung volume (cc)
DIBH (3D)	69.9	60.0	66.6	45.5	37.5	69.3	64.8	67.2	3.92	2.94	5049
FB (4D)	75.3	60.0	71.4	28.0	20.9	75.0	70.8	72.9	2.92	3.03	3163
NTD (all fractions)	Lung ($\alpha/\beta = 3$)										
	NTD_{mean} (Gy_3)					$V_{NTD=20Gy}$ (%)					
DIBH (3D)	18.2					19.8					
FB (4D)	17.5					18.2					

Abbreviations as in Table 7.3

As the results show the target doses were found to be more homogenous using DIBH(3D) technique than FB(4D) technique for case 3 and vice versa for case 1. This can be explained by the differentiated target volume, as more uniform dose distribution tends to be attained for a larger target volume. In case 3, the planning target volume employed in the DIBH(3D) dose plan (PTV_ref = 37.5 cc) was 1.79 times that of the FB(4D) dose plan (PTV_ref = 20.9 cc). For case 1, although the treatment volumes (cPTV=19.9 cc for FB, PTV_ref = 20.5 cc for DIBH) of both techniques were similar and comparative dose uniformities (max: 74.2 Gy, 73.6 Gy; mean: 70.2 Gy, 71.0 Gy for the DIBH and FB dose plans, respectively) were initially obtained. However, after the prescription dose was normalized to Dmin (21.4 Gy) by a factor of 1.07 (21.4 Gy / 20 Gy), the maximum and the mean doses were dropped to 68.8 Gy and 66.4 Gy, respectively, that certainly improved the dose homogeneity.

Although the setup margin of the gated-DIBH technique has been substantially reduced compared with the data reported in the literature, still more margin was required for the gated-DIBH technique than FB technique as shown in this study. A larger irradiated volume (27.9cc, 45.5cc) was obtained using the gated-DIBH technique than FB (20.1cc, 28.0cc) in both cases. The relatively large dose volume obtained in the DIBH dose plans was however compensated by the expansion of the lungs volume during DIBH, and as a result comparative lung doses were found for both techniques in the two cases. In chapter 6, adequate dose coverage to the planning target (PTV_ref) has been demonstrated using the 4D planning technique, together with the comparative lung doses ($NTD_{mean,}$ V_{NTD20}) to that obtained from the DIBH studies which had been reported with no symptomatic peumonitis (Ng et al 2008). Such results implies that the 4D planning technique proposed in this study for clinical application are encouraging. Dosimetry comparison between disffernt treatment techniques as demonstrated in this chapter is recommended to be performed clinically for the choice of optimal treatment for individual cases.

CHAPTER 8

DISCUSSIONS AND CONCLUSION

8.1 Discussions

Respiratory motion is a significant challenge in targeting the tumour during radiation therapy. With the availability of 4D imaging, the latest research on 4D treatment planning (Birkner et al. 2003; Zhang et al. 2008; Colgan et al. 2008; Wolthaus et al. 2008) which takes into account the temporal changes in anatomy suggests that this could be an optimal technique for treatment of lung cancer. However, despite its appeal, the concept of 4D planning is not yet widely available. This is because the process of 4D planning is rather complex as demonstrated in our study, with the work flow containing deformable image registration, automated propagation of target delineation and dose transformation between phases and involves 10-20 times more processing data than would be required in a standard plan (Rietzel et al. 2005). Moreover, validating the accuracy of deformable image registration is difficult due to the frequent lack of identifiable physical landmarks. Several studies (Lin et al. 2008; Rietzel et al. 2005; Wink et al. 2008) have been published on 4D dose calculation using different algorithms of deformable image registration (Chao et al. 2006; Harten et al. 2002; Thirion, 1998). (eg. voxel-based affine non-rigid image registration, optical-flow-based demons registration etc), and the evaluation of DIR in clinical studies was generally performed using visual comparison (Chao et al. 2006; Wink, Chao, et al. 2008) or quantitative comparison (Lin et al. 2008) between the morphed and the manual contours. In our study, the DIR was evaluated quantitatively, with the matching indices for lung mapping of around 0.94 – 0.95 (Table 2.3) which is comparable with previously published results (Lin et al. 2008). Since most of the DIR algorithms including IM apply voxel based registration, in which the similarity of the voxel intensity is compared, it is therefore imperative to employ low-noise 4D CT images obtained from regular breathing in order to achieve constructive 4D dose evaluation. To validate the stability of the 4D-CT images employed in our study, the studied cases were screened for the regularity of breathing rate. Moreover, the difference in the GTVs' volume which had been manually contoured in the three phase-specific dose plans (inhale, exhale, mean-tumour-position) was studied, the small standard deviations in GTV volumes

ranging from 2% to 5% (Table 3.2) suggest that the potential cause of unstable image leading to variation in delineated GTV volumes is minimal.

In this study, dose plans performed at different phases were compared for the size of iITV volume. Dosimetric indices such as conformity index (CI), target coverage index (TCI) and heterogeneity index (HI) were employed to assess similarities in dose distributions among plans for constructive comparisons. The values of CI were found to be lower (better) for cITV than GTV (column 2^{nd}, 5^{th}, table 5.3), this is because CI is a volume dependent factor, which suggests a better CI value is more achievable for the larger target volume. In this study, the CI values of around 1.2 at 95% target coverage recommended by RTOG 0236 were achieved for all cases indicating that optimal dose planning was attained.

As a result of the study, the 4D dose evaluation on the nine clinical cases has given us insights into a possible approach to radiation planning where a moving target is encountered, these are summarized as follows.

8.1.1 Treatment planning

It is widely recognized that there are unavoidable positional variation due to tumour motion, leading to uncertainties in delivery of radiotherapy for lung cancer. It is difficult to entirely eliminate the potential dosimetric errors caused by these uncertainties. However, a good knowledge of dosimetric effect on tumour motion can facilitate selection of optimum treatment technique for individual cases. The treatment planning technique proposed in this study is based on the resultant dosimetry by taking into account both geometric and temporal factors, and the dosimetric influence of a tumour's characteristic.

The magnitude of tumour motion is an important factor which contributes significantly to under dose coverage of the target, therefore a motion-related treatment margin is usually required for treatment planning (Witte et al. 2004; Wu et al. 2010; Ng et al. 2008; Rietzel et al 2006; Ekberg et al, 1998). Several studies have suggested that the treatment margin should be derived from the 4D contouring or probability distribution of the target positions. Rietzel et al (2006) used 4DCT to characterize tumour motion to define the treatment volume. Probability based

margin was also applied recently. Ekberg et al (2008) suggested a margin formula of 1.64σ (where σ is the combined deviation of tumour motion and treatment setup) for nominal probability of 90% in each of the three dimensions. van Herk et al (2000) introduced the margin recipe: 2.5Σ+ 0.7σ' (Σ: SD of systematic error, σ': SD of random error) to ensure 90% of the patient population would received 95% of the prescription dose. Both formulae were applied regardless of the tumour size. Our results, however, show that the degree of target coverage is associated with both factors of displacement magnitude and tumour size; more severe target missing was found with a small tumour than with a large one with comparable magnitude of target movement. If only the motion magnitude is considered for margin determination, the margin could be over-estimated for the case of large sized target. Such a finding can be deduced from the data shown on table 5.1. The minimum target coverage of 73.0% and 95.87% was found with cases 3 and 7 both with tumour movement of about 4 mm but with tumour size of 3.0 cc and 12.8 cc, respectively. The 95.7% target coverage obtained in case 7 demonstrating the goals of target coverage assigned by the two formulae had been fulfilled even before any margin was applied. This implies that if motion magnitude only is considered for margin determination, this would result in excessive treatment volume.

Although, dose planning performed at the temporal mean tumour position has been well demonstrated for dose coverage maximization (Engelsman et al. 2001; Witte et al 2004; Colgan et al. 2008), and substantiated by the results of this study (treatment volumes were shown to be optimized with $iITV_{mean,}$ see table 5.2). It is however noteworthy that the degree of maximizations is governed by the characteristics of the motion of the tumour. For instance, if the target travels in a sinusoidal-like trajectory during the respiratory cycle, the maximization of target coverage would be limited. This is because full target irradiation is obtained only over a fraction of the respiration cycle (figure 5.3), no additional gain would be obtained even with the temporal-mean dose-plan. On the other hand, for cases with flat-top sinusoidal trajectory, the tumour stayed near the end-exhale position for most of the respiration cycle which corresponds to the position of temporal mean. Hence, the temporal-mean dose plan is more advantageous for cases with such a tumour movement trajectory. In these cases, the treatment volume would be substantially reduced using $iITV_{mean}$ compared to cITV. Such findings demonstrate the

limitation of the classical ITV in regard to excessive normal tissue irradiation since it is defined only from geometrical aspect without accounting for the temporal nature of the tumour motion. Nevertheless, to delineate the mean target position is a challenge and image-guided positioning may be necessary to implement the desired treatment. For cases with targets having sinusoidal-like trajectories dose planning at the exhale phase is recommended for minimizing the setup uncertainty as no substantial benefit is gained by using the temporal mean dose plan. Moreover using cITV as the planning target, treatment volume could be optimized with the excessive target irradiation during its oscillation along the high-dose-region within the beam aperture (table 6.1).

Numerous studies (Hurkmans et al. 2001; Erridge et al. 2003) have described the effect of respiration motion on the shape of dose distribution by blurring the planned dose with a Gaussian distribution. Similar to our study, Wolthaus et al (2008) evaluated the treatment margin from GTV to PTV (CTV was not applied) based on the internal target volume, however dose-probability-based margin recipe (van Herk et al 2000, 2003, 2004; Witt et al 2004) was applied for the evaluation. In their study, with the provision of on-line correction, the systematic errors contributed from setup and respiration was negligible, and only the random errors and the penumbra width of dose distribution were accounted for margin calculation. Their results showed that the total treatment margin of less than one third of the peak-to-peak amplitude of tumour motion was suggested for the typical respiration motion of up to 1.5 cm amplitude. To compare their results with this study, the suggested one-third-amplitude margin was applied using the data of this study to hypothetically evaluate the total treatment volume. The calculation for the treatment volume based on van Herk et al' s study (2000, 2004) and the deduced dose volume is described in Figure 8.1. As shown by the results, the planning target volume defined by iITV which provided 100% prescription dose coverage was only 3.5% in average (range: -19.2% – 19.5%) larger than the deduced dose volume defined using probability-based margin recipe of which the 95% prescription dose coverage was aimed (Table 8.1). The relatively large CI (CI=1.67) applied in case 3 indicates the planning target was irregular in shape, and the result of comparative large probability-based planning among all cases leading to a question whether the iITV defined in 4D basis would be more favorable to the irregular shaped target, such

presumption requires more data to confirm. Our preliminary findings however suggest that iITV provided good target coverage compared to that using probability-based margin recipe in terms of volume and coverage specificity. Such encouraging results could be due to iITV accounting for the non-rigid anatomical displacement on the dose distribution during breathing (both temporal and spatial factors are considered), whereas only spatial factor is considered for the static dose convolution with translational displacement probability. 4D dose planning using DIR and dose convolution with PDF for determination of treatment volume are increasingly applicable. A thorough evaluation to determine the effectiveness of both techniques, in terms of treatment volume optimization and target coverage specificity, would be practically useful. Since probability-based margin is evaluated based on patient statistic, further investigation is not possible at the present stage due to insufficient patient data.

Figure 8.1 According to van Herk et al's study (2000, 2004), with the tumour position well defined during treatment, the volume of PTV(Vp_{TV}) provided a minimum dose of 95% to the tumour (ie GTV) could be defined by expanding the tumour with a SD of respiration motion. The SD of respiration motion was determined by one-third of peak-to-peak amplitude of tumour motion. The equivalent diameter of GTV was calculated by assuming the GTV was in spherical shape and the V_{PTV} was derived in oval volume using Equation (5). The V'_{PTV} denotes the planning dose volume of the PTV, derived by multiplying the V_{PTV} with the conformity index (CI listed in Table 4.3).

Planning Target Volume (PTV) deduced from a SD of respiration motion

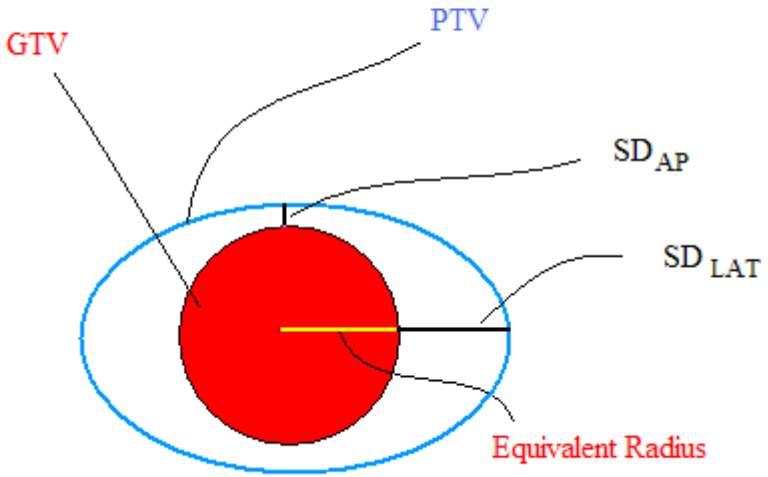

$$V\,p_{TV} = 4/3\ \Pi \times (SD_{LAT} + Req) \times (SD_{AP} + Req) \times (SD_{cc} + Req) \quad (5)$$

$$V'_{PTV} = V_{PTV} \times CI$$

SD_{LAT}: SD of respiration motion in lateral direction

SD_{AP}: SD of respiration motion in anterio-posterior direction

SD_{CC}: SD of respiration motion in cranial-caudal direction

Table 8.1. Treatment volume comparison between V'_{PTV} and iITV. The volumes of iITV were larger than V'_{PTV} by an average of 4.4%.

Case	GTV (cc)	R_{eq} (mm)	Displacement (pk – pk) (mm)			SD of Respiration motion (mm)			V_{PTV} (cc)	V'_{PTV} (V_{PTV} x CI) (cc)	iITV (cc)	$iITV_{mean}$ - V'_{PTV} (% difference)
			LAT	AP	CC	SD_{LAT}	SD_{AP}	SD_{CC}				
1	1.42	6.9	5.8	1.6	0.3	1.9	0.5	0.1	2.0	2.0 x 1.53 = 3.1	3.7*	+ 19.5
2	1.93	7.7	0.5	2.6	3.5	0.2	0.9	1.2	2.5	2.5 x 1.57 = 3.9	4.0#	+ 2.5
3	3.0	8.9	0.5	2.6	3.0	0.2	0.9	1.0	3.7	3.7 x 1.67 = 6.2	5.2#	-19.2
4	6.74	11.7	1.1	0.5	0.0	0.4	0.2	0.0	7.0	7.0 x 1.58 = 11.1	11.1#	0
5	4.06	9.9	1.1	3.2	3.0	0.4	1.1	1.0	5.1	5.1 x 1.39 = 7.1	7.3#	+ 2.7
6	17.89	16.2	2.1	1.6	6.0	0.7	0.5	2.0	21.6	21.6 x 1.15 = 24.8	26.8#	+ 7.5
7	12.8	14.5	1.5	3.5	0.0	0.5	1.2	0.0	14.3	14.3 x 1.39 = 19.9	23.9#	+ 15.7
8	5.5	11.0	1.5	1.5	9.0	0.5	0.5	3.0	7.7	7.7 x 1.63 = 12.6	14.2#	+ 11.2
9	12.4	14.4	2.4	8.3	9.2	0.8	2.8	3.1	18.9	18.9 x 1.42 = 26.8	23.8*	-3.0
											Average	+3.5

$iITV_{mean}$ was used, data was extracted from Table 6.1

* $iITV_{all}$ was used, data was extracted from Table 6.1

SD_{LAT}: 1/3 x LAT (peak-to-peak motion amplitude in lateral direction)

SD_{AP}: 1/3 x AP (peak-to-peak motion amplitude in anterio-posterior direction)

SD_{CC}: 1/3 x CC (peak-to-peak motion amplitude in cranio-caudal direction)

Req: equivalent radius of GTV

8.1.2 Concerns for Radio-Biological Dose Influence

The possible influence of the biological effect on dose distribution of a moving target was not within the scope of this study. However, the recent study carried out by van Herk et al (2003) indicates that the biologic fractionation effect on dose distribution for the concerns of additional margin is negligible. In their study, the physical and biologic fractionation effects of random geometric errors and respiration motions were assessed; the resulting dose distributions were compared using Gaussian blurring with the planned dose. Due to the non-linear relationship between the physical dose and BED, the total dose distribution was slightly wider; with 0.2 mm for α/β ratio of 3Gy. The widening was reduced with α/β ratio and increased with random error of more than 1 cm motion amplitude. Moreover, they concluded that there was no additional margin requirement due to the biologic effect of fractionation, as errors that shift the target towards higher dose levels completely cancel the effect of errors that shift the dose toward lower levels. Hence, the proposed planning volume for performance of hypofractionated treatment should be entirely safe. Nevertheless, a more detailed analysis of the biological effect of random and systematic errors by van Herk et al (2002) pointed out that the effect of insufficient geometrical margin can lead to significant lost of Tumour Control Probabily (TCP). In their study, a threshold margin was defined, below which, the TCP of the population will start to decrease sharply. It is therefore important to verify the evaluated treatment margin carefully before clinical implementation.

In this study, the 4D dose planning deduced from the concept of iITV has been demonstrated to be effective for optimizing dose coverage of a moving target. However, complications such as radiation-induced puemonitis may limit the clinical application of the technique. The lung doses evaluated in the 4D dose plans were found comparable with that using gated-DIBH techniques. Although there is no evidence of a dosimetric threshold level for inducing symptomatic pneumonitis, V_{NTD20} limited to $\leq$30-35% and $NTD_{mean,}$ to $\leq$20-35Gy were suggested by QUANTEC (Lawrence et al, 2010) to lower the risk level of radiation-induced puemonitis to within 20% of the treated patients. Such criteria were well achieved in the 4D dose planning study (NTD_{mean} was 17.5 Gy andV_{NTD20} ranged from 16% to 18 %, for both cases). Although only two cases were selected for the assessment, the relatively acceptable lung dose values obtained in both cases indicate that the

proposed 4D planning technique are encouraging.

Since the resultant dosimetry can be complex under different circumstances; for instance the volumes of lung and tumour, the nature of tumour motion, the planning phases, the selected planning target volume, etc, which have been discussed in the study, performing the various planning techniques are advised and the choice of treatment technqiue should be based upon the adequate target coverage and the result of lung dose evaluation to account for the probability complication. If similar dosimetry is obtained with both FB and gated-DIBH techniques, FB treatment with 4D planning technique would have an implementation advantage over the DIBH technique.

8.1.3 Future Studies

8.1.3.1 Treatment Implementation

In this study, the possibility of 4D dose planning offers a solution on how to maximize the planning dose to the target volume by revealing the dynamic dose distribution in the presence of motion. Our results demonstrate that iITV reduces the dose volume in all cases compared with that derived from the classical technique (Table 5.2). The discrepancy in geometric coverage between the iITV and cITV implies that treatment margin to cover the entire range of tumour motion is not necessary. Nevertheless, the concept of iITV has not yet considered the variation in tumour motion, which may occur between simulation and treatment caused by unstable breathing. The accuracy of the delivered dose using iITV for clinical application could however be assessed according to the concept suggested in Seppenwoolde et al's study (2007), in which the dosimetric uncertainties due to breathing motion was simulated. In this study, the 4D dose of each voxel in the different phases was stored in the corresponding order by TD_x (see figure 2.4), based on the assumption of consistent correlation between the internal and external movement as obtained during CT planning simulation, the resultant 4D doses over the target volume during treatment can be estimated on-line or off-line with provision of real-time respiratory surrogate data. The concept of on-line 4D dose evaluation is presented in Appendix III. In common with other respiratory gating or tracking techniques, the treatment technique proposed in this study also require stable breathing of the patient during treatment, however the total dose received by the

patient could be estimated at any time during or after treatment. The technique of 4D dose evaluation in real time using the tool-box would be investigated following this study.

8.1.3.2 Application

A tool box written in MATLAB in conjunction with CERR was developed for 4D dose calculation in this study. The 4D dose Tool Box allows the 3D treatment dose plans, generated either commercially or in-house developed treatment planning system, with planning data contained in DICOM-RT format, to process 4D dose calculation using deformable dose registration approach. However, the algorithm of the tool box is restricted to the DICOM image format in grid resolution of 1.0-1.01 mm and slice thickness of 3 mm. Moreover, the processing time of 4D dose calculation depends on the size of the target volume and the resolution of the dose grid. The study was performed with a computer with 4GB of RAM and 2.5 GHz processor speed. For instance, to work out the 4D dose distribution of a cubic volume of 2 cm in dimension, the processing time was approximately 48 hours for the dose grid of 1 mm. The processing time and the application flexibility of the tool box can be improved by modifying the 4D dose calculation algorithm, which will be performed after this study.

8.1.3.3 Limitations

The study relies on good quality 4D CT images for effectual dynamic image registration and therefore patients with regular and stable breathing is a pre-requisite in order to perform low-noise image reconstruction. The technique is therefore restricted to the cases where stable breathing is achieved or breath coaching is effective. In this study, the 4D dosimetry was evaluated based on DIR and although the accuracy of IM has been validated by good contour matching, absolute registration accuracy based on point to point correspondence may be needed to further ensure the robustness of the technique.

Numerous studies have reported the limitation of PB algorithm in heterogeneous media (Krieger et al. 2004, Nisbet et al. 2004, Irvine et al. 2004, Ahnesjo et al. 1999). This is because the PB algorithm uses a one-dimensional path density correction which does not model the distribution of secondary electron in the media. Doses are

calculated according to the radiological depth along a ray line from the radiation source to the calculation point, and does not account for the effect of side and backscattered radiation. Krieger et al (2004) evaluated the accuracy of dose predicted in heterogeneous media by a PB, a collapsed cone (CC) and a Monte Carlo (MC) algorithm, using a simple phantom consisted of Styrofoam and white polystyrene. Doses were measured in the central layer of white polystyrene. It was found that, in white polystyrene, both MC and CC calculations agreed satisfactorily with the measurements whereas the PB algorithm calculated 12% higher doses on average. Nisbet et al (2005) studied the dosimetric accuracy of the CC algorithm based on phantom study and obtained good agreement between measured and calculated dose to within 2%, for most of the homogeneous and heterogeneous cases. Their study suggested that CC algorithm was preferable to PB algorithm despite the fact that there may still be some discrepancy between calculation and measurements. The possible errors with CC algorithm are discussed in recent studies where the published results are mainly governed by the particular phantom geometry and set-up (Klein et al 1993, Sauer 1995). In this study, the PB algorithm was applied for relative dose comparison, however for absolute 4D dose evaluation the gold standard of MC algorithm or CC algorithm is used.

8.2 CONCLUSION

The uncertainty in target coverage arising from the motion effects has been a major obstacle in applying escalated dose treatment for better therapeutic gain, as excessive irradiation is often traded for the possible marginal miss. In this study, a new concept of internal target volume, namely iITV, was defined from the 4D dosimetry. The iITV precisely identifies the required treatment volume and offers the adequate dosimetric coverage for the dynamic target (tumour). The proposed 4D planning techniques based on the iITV approach has proved to be useful for significant reduction of the irradiated volume without compromising the target coverage. However, the accumulated dose distribution of 4D radiotherapy is dynamically complex and the control factors such as tumour size, magnitude of tumour displacement, tumour motion characteristic and the reference phases for dose planning etc., are interactively affecting the resultant dose distribution. Hence there are no definite solutions to the treatment or planning techniques for 4D radiotherapy such as those applied in 3D radiation treatment; for example, better dose conformity dynamic conformal radiation techniques (eg. intensity modulation radiation therapy (IMRT), volumetric modulation arc therapy (VMAT)) would be preferred to static conformal radiation. As demonstrated in the study, the reference dose plan performed at the temporal mean tumour position does not necessarily provide the optimal dose plan since the resultant dose distribution depends on the motion nature of the tunour. Moreover, the geometric-defined treatment margin could over emphasize the required treatment volume for actual target coverage, consequently leading to potential restriction in dose escalation by the excessive irradiation.

In this study, a DICOM-RT based toolbox was developed to enable 4D dose calculation based on deformable image registration. The toolbox provides an user friendly platform for 4D dose calculation. Once the compatible DICOM-RT data is input, the 4D dose distribution over the treatment regions is automatically computed and the results are presented and analyzed schematically (eg. 3D dose distribution map, accumulated and differential volume dose histogram, etc). Upon the choice of adequate dosimetry, the most suitable and optimal treatment modalities and planning techniques can be determined for an individual case.

Apart from using DIR, a modeling technique which based on the convolution of the

static dose distribution with the probability distribution function (PDF) of the organ motion was also applied for 4D-dose planning recently. As the result of comparison between the two techniques, though the application of iITV are encouraged, however due to the lack of sufficient clinical data, the results and course are prelimarily and further investigations are required.

Despite the technology for 4D imaging and dose calculation is becoming increasingly available but 4D planning and delivery are still in their initial phase of research and development. This study demonstrates a novel 4D dose planning platform which not only offers realistic treatment dosage analysis, but also facilitates optimal dose plan by minimizing the treatment volume.

APPENDIX I

A1.1 A program code for *DE_DOSE_REG*

```
%%%%%%%%%%%%%%%%%%%%%%%%%%%%%%  DE_DOSE_REG %%%%%%%%%%%%%%%%%%%%%%%%%%%%%%%%%%%%%%%%%%%%%%%%%%%%%%%%
%%   A code to register the pixel dose at each breathing phase corresponding to the IM order          %%%
%%   [sort_morphdata] contains image morphing data in 1 mm resolution                                  %%%
%%   [fullsetdose_done] contains dose data in 1 mm resolution                                          %%%
%%   [index_dose] stored doses in the order corresponding to target source coordinates                %%%
%%   save full set of dose in the file name of "completedose_x" for xth phase                          %%%
%%%%%%%%%%%%%%%%%%%%%%%%%%%%%%%%%%%%%%%%%%%%%%%%%%%%%%%%%%%%%%%%%%%%%%%%%%%%%%%%%%%%%%%%%%%%%%%%%%%%%%


for i = 1 : size(fullsetdose_done)
   if sort_morphdata(1, 1:3)== fullsetdose_done(i, 1:3)
      p = i
   end;
end;
for w = 1 : size(sort_morphdata)
for m = p : size(fullsetdose_done)
if sort_morphdata (w, 1:3) == fullsetdose_done(m, 1:3)
index_dose(sort_morphdata(w,7))= fullsetdose_done(m,4);
p = p+1;
end;
end;
end;
t2 = clock;
etime(t2, t1)
save completedose_x
```

A1.2 A program code for *ADD_ALL_DOSE*

```
%%%%%%%%%%%%%%%%%%%%%%%%%%%%%%   ADD_ALL_DOSE %%%%%%%%%%%%%%%%%%%%%%%%%%%%%%%%%%%%%%%%%%%%%%%%%%%%%%%%%%%%%%%%%%%%%%%%
%%   A code to attain time-weighted dose summation of TDx                                   %%%%%%%%%%%%%%%%%%%%%
%%   The accumulated dose over a breathing cycle = Index_dose1 + Index_dose2 + … Index_dose10  %%%%%%%%%%%%%%%%%%%%%
%%%%%%%%%%%%%%%%%%%%%%%%%%%%%%%%%%%%%%%%%%%%%%%%%%%%%%%%%%%%%%%%%%%%%%%%%%%%%%%%%%%%%%%%%%%%%%%%%%%%%%%%%%%%%%%%%%%%
load completedose_0.mat
Buffer_index_dose = index_dose*0.1;
clear index_dose;
load completedose_10.mat
Buffer_index_dose = index_dose*0.1 + Buffer_index_dose;
clear index_dose;
load completedose_20.mat
Buffer_index_dose = index_dose*0.1 + Buffer_index_dose;
clear index_dose;
load completedose_30.mat
Buffer_index_dose = index_dose*0.1 + Buffer_index_dose;
clear index_dose
load completedose_40.mat
Buffer_index_dose = index_dose*0.1 + Buffer_index_dose;
clear index_dose;
load completedose_50.mat
Buffer_index_dose = index_dose*0.1 + Buffer_index_dose;
clear index_dose;
load completedose_60.mat
Buffer_index_dose = index_dose*0.1+ Buffer_index_dose;
clear index_dose;
load completedose_70.mat
Buffer_index_dose = index_dose*0.1 + Buffer_index_dose;
clear index_dose;
load completedose_80.mat
Buffer_index_dose = index_dose*0.1 + Buffer_index_dose;
clear index_dose;
load completedose_90.mat
Buffer_index_dose = index_dose*0.1 + Buffer_index_dose;
index_dose = Buffer_index_dose;
save completedose_all
```

APPENDIX II

A2 TREATMENT MARGIN VERIFICATIONS FOR THE GATED-DIBH TREATMENT

A2.1 Treatment Setup error (σ_s)

Treatment setup error (σ_s) which accounts for patient setup variation and inter-breath-hold variation was evaluated prior to the first treatment. This was verified in the treatment room by simulating the entire set up procedure. The stereotactic couch tray was placed on the top of the treatment couch; patient lied on the tray with the same posture as during the CT scan. Breath-hold was repeated several times to ensure the consistency of the positioning. Data were recorded throughout the whole procedure by the ExacTrac. Once the treatment isocentre was confirmed, it was marked on the patient according to the LINAC lasers. The patient was then transferred to CT for isocentre displacement verification. To avoid any skin movement which may displace the skin marks, the patient was instructed to maintain in the same posture and was carefully transferred together with the stereotactic couch tray to the CT for displacement verification. The CT was located approximately 10 meters away from the treatment room. To identify the isocentre position on the CT image, three radio-opaque markers were attached on the skin marks of the patient, two on the lateral and the third on the anterior part. A CT scan was performed with breath-hold with a slice thickness of 3 mm and the central slice positioned at the isocentre plane. To assess the amount of isocentre shift, the verified CTs were fused with the treatment plan using the tumour as a reference. The treatment setup error σ_s was determined from the displacement between the planning and the treatment isocentres indicated by the radio-opaque markers. The systematic setup error for the group (M_s) is given by the mean of individual errors, and the group random set up error (Σ_s) by the standard deviation (SD) of individual errors.

The treatment setup error was assessed prior to the first fraction of the treatment. The displacements at the isocentre of individual patients are listed in Table A2.1. The ranges of displacement were -2 – 3.5 mm, -1.7 – 3.6 mm and -2.7 – 4.4 mm in the direction of LR, AP and CC, respectively. The group systematic errors Ms of 0.2 (LR), 1.0 (AP) and 0.3 (CC) suggest that the setup errors in the preparation

processes (eg. the setup error on the CT scanner, the offset error of laser alignment, etc.) were small. On the other hand, the group random errors Σs of ±1.6 (LR), ±2.0 (AP), ±1.5 (CC), indicate the discrepancy in tumour immobility among individuals.

Table A2.1 The inter-fractional treatment setup displacement (σ_s) measured at the isocentre in the left-right (LR), anterio-posterior (AP) and cranio-caudal (CC) directions of all cases.

Patient	Treatment setup error σ_s (mm)		
	LR	AP	CC
1	3.0	-2.3	1.5
2	0.1	2.6	-1.7
3	0	0	0
4	0	-2.2	3.6
5	-1	2	0
6	-2	3.5	0
7	0	0	0
8	-2	2	3
9	0	1	0
10	0	0	0
11	-0.2	4.4	0.2
12	3.5	0.1	-0.3
13	2	2.8	0.3
14	0	0	-2
Group systematic error (M_s)	0.2	1.0	0.3
Group Random error (Σ_s)	±1.6	±2.0	±1.5

A2.2 Intra-breath-hold tumour motion evaluation

Despite of the numerous debates on correlation between internal and external movement (Koch et al, 2004, Hoisak et al 2004, Ahn et al 2004), the surface movement was stringently restricted in attempt to strive for the minimum tumour motion. In 2006, Stock et al (2006) decisively demonstrated the correlation between tumour and external markers movement on 16 lung/liver cancer patients. In their study, the movements during several respiratory cycles in 1) stable breathing, 2) DIBH and 3) deep expiration breath-hold were investigated using a multi-slice CT

scan in the dynamic 3D scan mode (fixed table position) every 3s, with the total scan volume of 24 mm length. Good tumour – marker correlation was reported with the tracking marker placed above tumour or at the xiphoid process; the mean Pearson correlation coefficient was reported of 0.83±0.17 (0.77 – 0.89).

A2.2.1 Tumour – marker correlation study

In the study of DIBH technique, the relationship between tumour movement and external marker movement during DIBH was assessed retrospectively. The tracking marker was selected according to Stock et al's method. It was primarily selected with the marker located close to the tumour, for the case with all the markers positioned far from the tumour, the marker near to the xiphoid process was selected. The relative movement between the tracking marker and the tumour was determined from their positions on the two sets of planning CT images. Since the patient was kept in the same position during the two CT scans, the stereotactic tray was considered integrated with the patient, the fiducial markers which embedded at the bottom of the stereotactic tray was applied as a measurement reference for the tumour and marker movement. Since the set of fiduical markers consists of 3 columns, which laid in a pattern of "N" along the cranial-caudal direction, of which the fiduical markers located at the middle column can be found as a single spot on the axial view and travelling along the lateral direction while slicing through the CT set. A specific fiducial marker shown on the axial CT was selected and identified from both CT sets by the same distance measured from the fixed markers located at the left or right column and used as a reference point (P) for measurement (fig.A2.1a). The tumour – marker correlation was evaluated by comparing the differences in tumour movement (ΔT) and the tracking marker movement (ΔTM) between the 2 planning CT sets in x (left-right), y (anterior – posterior) and z(caudal- cranial) directions. The ΔT and ΔTM were defined in all 3 directions as follows:

$$\Delta T_i = \left[T_{1_i} - P_{1_i} \right] - \left[T_{2_i} - P_{2_i} \right] \qquad i \in (x, y, z) \qquad \text{(A1)}$$

$$\Delta TM_i = \left[TM_{1_i} - P_{1_i} \right] - \left[TM_{2_i} - P_{2_i} \right] \qquad \text{(A2)}$$

where T, TM denotes the tumour and tracking marker positions, respectively. The subscript “1” and “2” indicate data acquired from CT1 and CT2, respectively. The details of measurement are depicted in figure A2.1. To improve the measurement accuracy, the variations in GTVs delineation between the two CT sets must be minimized as this could affect the localization of the tumour centroid. This can be achieved if the two GTVs are accurately aligned since the centroid of the GTVs would coincide on the aligned CTs. Accurate alignment of the GTVs was achieved in the study by using intensity based image fusion. In assumption of no distortion on the GTV volume, based on maximum intensity similarity in voxel based comparison, image registration was performed using rigid transformation (image was aligned with one to the other with translational and rotational adjustments). As a result, the T1 and T2 would be the same, and with varied TM and P between the two CT sets if the tumour position was not the same. Moreover, in order to improve the measurement spatial resolution, in the case where the centre of the tracking marker or the point P did not appear on the CT image, interpolation between neighboring slices was performed. The centre of the TM was traced by the size of TM measured on the consecutive CTs and interpolated based on the 2^{nd} order polynomial correlation as demonstrated in figure A2.1c

Figure A2.1 Two planning CT scans performed with DIBH were fused with reference to GTV; the different sizes of TM indicate position discrepancy of GTV. The reference point P (in circle) of measurement was selected at the isocenter slice, which was identified on two CT sets by the same distance measured from the fixed fiducial marker (right). The center of TM was interpolated according to the size of TM measured on (b) the consecutive CT images using the (c) second order polynomial fit. The TM's center lied at Z =152.3 mm in above case.

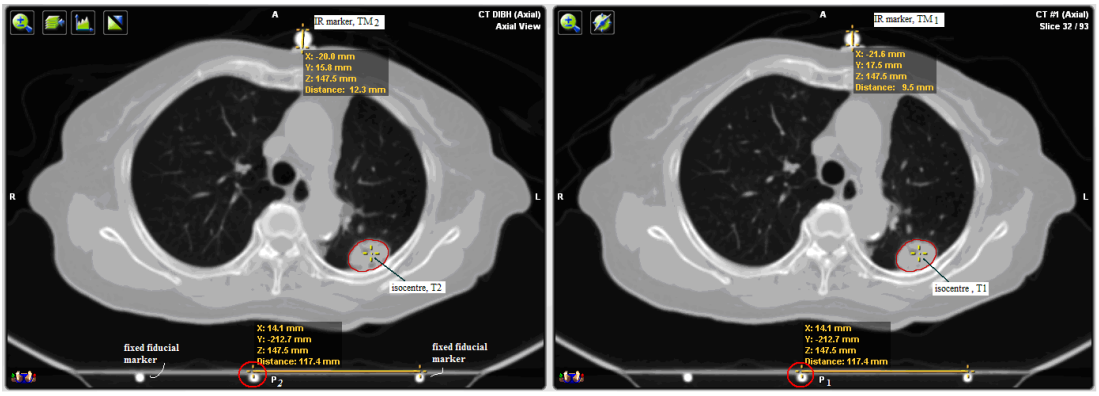

(a)

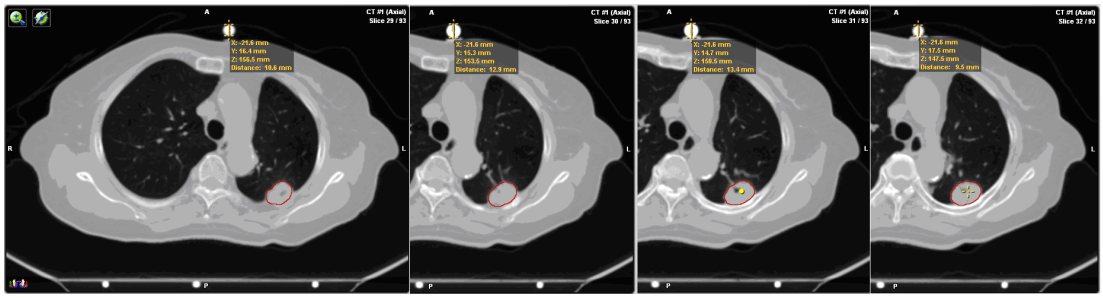

(b)

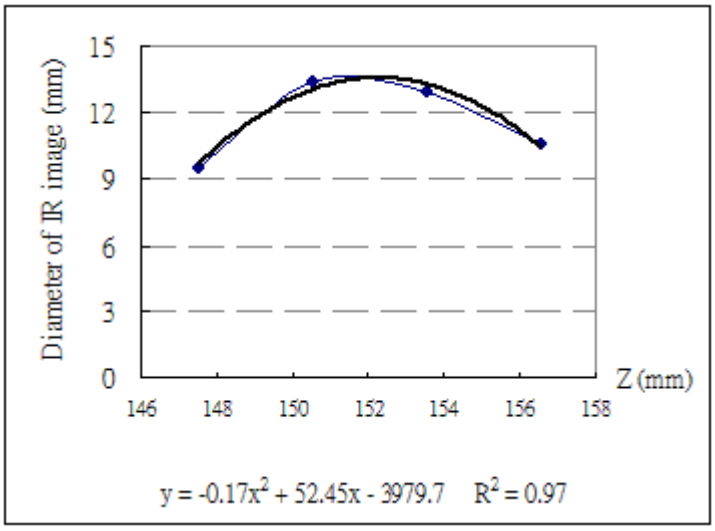

(c)

ΔT was plotted against ΔTM and the degree of correlation was assessed using linear least squares fit and the Pearson product-moment correlation coefficient (R^2) as shown in equation A3 where (β_1) is the gradient and (β_2) the intercept

$$\Delta T_i = \left[\beta_{1_i}\right] \times \left[\Delta TM_i\right] + \beta_{2_i} \qquad \text{(A3)}$$

The relationship between the tumour movement and the tracking marker movement during breath-hold is demonstrated in figure A2.2. Values of R^2 of 0.81, 0.76 and 0.85 obtained in LR, AP and CC directions, respectively suggest a linear correlation as reported by Stock et al. The values of β1 being 0.61 (LR), 0.46(AP) and 0.87(CC), were all less than unity indicating that the magnitude of tumour movement were generally less than the marker movement during breath-hold. The β2 (range: 0.06 – 0.28) are closed to zero in all directions.

Figure A2.2. Tumour-marker correlation in LR, AP, and CC directions based on the linear least square fit evaluation was shown in Figs. A2.2(a) – (c), respectively.
The Pearson correlation coefficient (R2) expressed the degree of linearity.
The characteristic of the linear relationship can be derived from the slope
and the intercept of the equation.

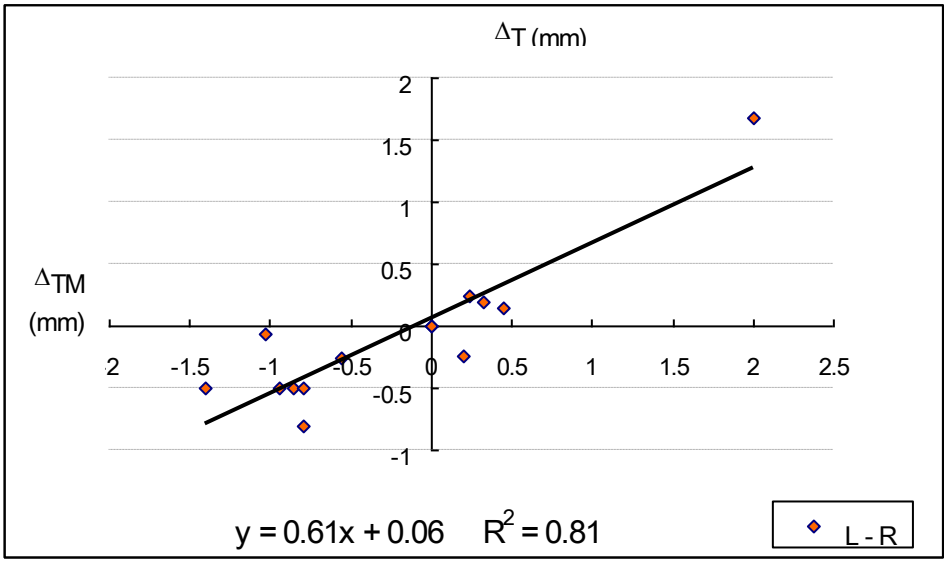

(a)

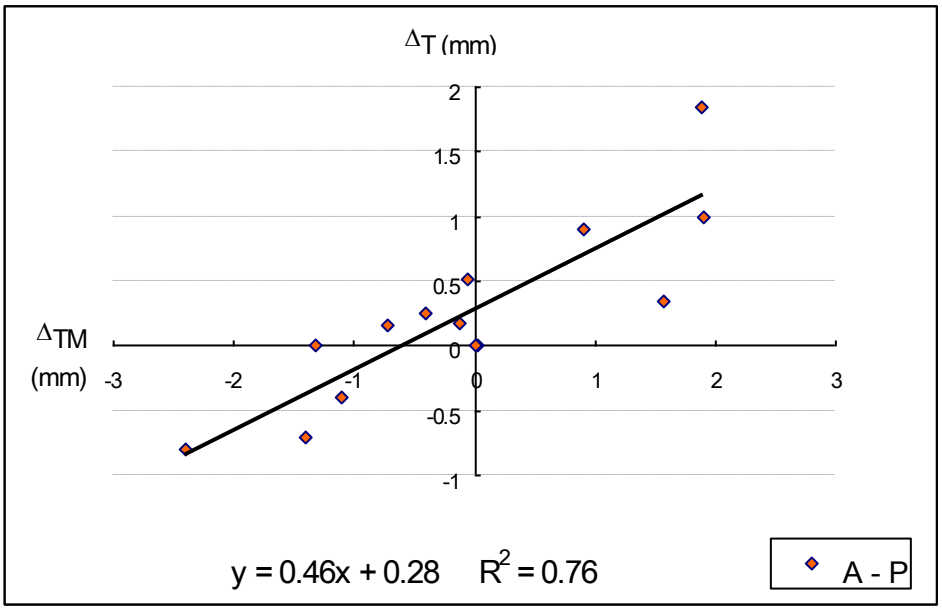

(b)

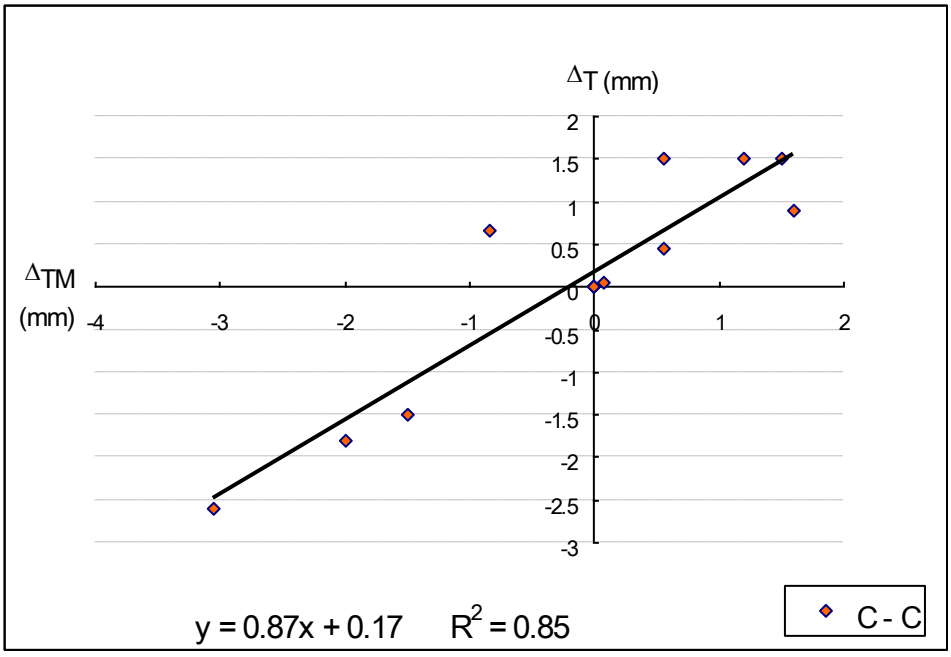

(c)

A2.2.2 Intra-breath-hold motion

Since intra-breath hold tumour motion could be caused by the quiet excursion of abdominal diaphragm or unsteady breath-hold. Such motion will introduce an extra treatment variation in addition to the previously defined set up error. The

intra-breath-hold tumour movement, which was constrained with a pre-defined tolerance (< 2mm at isocentre as estimated with ExacTrac), varied around its mean position, and in a standard normal distribution. The range of variations of the tumour motion was defined by the standard deviation of the tumour movement (σ_t), which was interpreted by the tracking marker movement. The standard deviation of tracking marker movement is defined (σ_{TM}) as follow:

$$\sigma_{TM} = \sqrt{\sum_{j=1}^{n} \frac{(a_j - \bar{a})^2}{(n-1)}} \qquad \text{(A4)}$$

The evaluation was applied with data recorded in the process of treatment set up verification. Where n is the total number of sample data of the recorded tracking marker positions of all successful breath holds. a_j is the position of the jth sample, $\bar{a}$ is the mean position of the tracking marker calculated from all successful breath-holds.

The standard deviation of the intra-breath-hold tumour motion σ_t was determined by combining equation (A3) and (A4). It is also assumed that β_2 is close to zero and can therefore be ignored. Derivation of the resulting equation (A5) had been depicted in the Wong et al's study (2010) .

$$\left[\sigma_{t_i}\right] = \left[\beta_{1_i}\right] \times \left[\sigma_{\mathrm{TM}_i}\right] \qquad \text{(A5)}$$

The amount of intra-breath-hold tumour movement was evaluated by the marker movement weighted by the slope of regression β1 as suggested in equation A5. The intra-breath-hold tumour movements in all three directions were found to be small compared to σ_s (column 6^{th} – 8^{th} , Table A2.2).

PTV Margin Estimation

In 1993, the international Commission on Radiation Units and Measurements (ICRU

50) published definitions for target volume for photon radiotherapy. The gross tumour volume is the confirmed tumour that is palpable or visible by physical or radiological examination. The clinical target volume is the GTV plus a margin for sub-clincial disease. The PTV is the CTV plus a margin to allow for geometrical uncertainty in its shape and variations in its location relative to the radiation beams due to organ mobility, organ deformation, and patient setup variation. In our study, both of the inter- and intra-fractional organ mobility were taken into account for margin evaluation. However, since the treatment setup was performed under breath-hold, the inter-fractional organ mobility and setup variation were genuinely integrated during evaluations. The tumour deformation was not studied as it was assumed to be consistent under stable DIBH control and can be ignored during the intra-fractional tumour motion. The PTV margin of individual (M_{ptv}) was defined by 2 factors: 1) the treatment setup error σ_s and 2) the variation of intra-breath-hold tumour motion σ_t. Assuming that the tumour oscillates around a mean position during breath-hold, the range of intra-breath-hold movement was partially overlapped with the range of movement defined by σ_s. σ_s and σ_t were therefore considered not to be linearly related. M_{ptv} was calculated by the quadratic sum of the 2 factors as follow:

$$M_{PTV_i} = \sqrt{\left(\sigma_{s_i}\right)^2 + \left(3\sigma_{t_i}\right)^2} \quad \text{(A6)}$$

Three standard deviations σ_t was used to include the 99.9% of the tumour movement. Despite of the small sampling group, the group PTV margin (GM_{ptv}) was evaluated by the mean of individual's margins (M_m) and twice the standard deviation of individual margins (Σ_m) to cover 95% of the population to receive the prescribed dosage.

$$GM_{ptv} = M_m + 2\,\Sigma_m \quad \text{(A7)}$$

The evaluated group PTV margin (GM_{ptv}) of the study were listed in Table A2.2.

TABLE A2.2 The Intra-breath hold tumour motion was derived from the movement of the tracking marker. The position of tracking marker w.r.t. the tumour is listed in column 2. The standard deviations (SDs) of tracking marker movement (σTM) in 3D are depicted in 3^{rd} – 5^{th}. The tumour movement was interpreted according to tumour-marker correlation and the SDs of tumour motion (σt) in 3D were evaluated based on equation 5 and the results are listed in 6^{th} – 8^{th}. PTV margin of individual (M_{PTV}) and of group margin (GM_{ptv}) in 3D are listed in column 9^{th} – 11^{th} .

Patient	Tracking marker from tumour (cm)	Intra-breath hold tracking marker variation $\pm\sigma TM$ (mm)			Correlated Intra-breath hold tumour variation $\pm\sigma t$ (mm)			Individual Margin (M_{PTV}) (mm)		
		LR	AP	CC	LR	AP	CC	LR	AP	CC
1	2	1.0	0.7	0.6	0.6	0.3	0.5	3.6	2.5	2.1
2	0.3	0.4	0.6	0.4	0.2	0.3	0.4	0.7	2.7	2.1
3	Xiphoid	0.3	0.5	0.8	0.2	0.2	0.7	0.5	0.7	2.1
4	0.6	0.2	0.5	0.4	0.1	0.2	0.4	0.3	2.3	3.8
5	0.3	0.3	0.6	0.8	0.2	0.3	0.7	1.1	2.1	2.0
6	1.5	0.3	0.7	0.4	0.2	0.3	0.4	2.1	3.6	1.1
7	0.3	0.2	1.0	1.1	0.1	0.5	0.9	0.3	1.4	2.8
8	0.3	0.2	0.6	0.7	0.1	0.3	0.6	2.0	2.2	3.5
9	0	0.4	0.6	1.1	0.2	0.3	0.9	0.7	1.3	2.8
10	Xiphoid	0.1	0.2	0.1	0.1	0.1	0.1	0.2	0.3	0.3
11	1	0.5	1.2	1.0	0.3	0.5	0.9	1.0	4.7	2.7
12	0.3	0.5	0.3	0.6	0.3	0.1	0.5	3.6	0.4	1.6
13	1.5	0.7	1.0	0.6	0.4	0.5	0.5	2.3	3.1	1.7
14	4	0.5	0.5	1.9	0.3	0.2	1.6	0.9	0.7	5.2
Group Mean (mm)		0.4	0.6	0.8	0.2	0.3	0.7	1.4	2.0	2.4
Group SD (mm)		±0.3	±0.3	±0.4	±0.2	±0.1	±0.4	±1.2	±1.3	±1.2

Group Margin (GM_{PTV}) = $M_m + 2\Sigma_m$ (mm)	3.8	4.6	4.8

APPENDIX III

The variation in tumour motion which may occur between simulation and treatment caused by unstable breathing is not accounted for in the 4D dose planning technique proposed in the study. Based on the assumption of consistent correlation between the internal (tumour) and external movement (marker placed on the xiphoid) during simulation and treatment, the amount of delivered dose could be estimated on-line or off-line according to the breathing pattern. Figure A2 below shows the variations of the breathing pattern acquired during CT simulation and treatment. Since the 4D dose was calculated by summation of TDx which defines the 4D dose received by the planning target at the xth breathing phases, the 4D dose received during treatment could be estimated from the TDx used in the dose planning according to the amplitude of the breathing. TDx can be extrapolated for the breathing amplitude that are larger than that used for the planning CT,

Figure A1 demonstrates the insignificant dose variations caused by unstable breathing between CT simulation and treatment, using case 3 as an example. Due to the flat top sinusoidal tumour movement (figure 5.2), even there is the small breathing variation at the exhale phase between CT simulation and treatment, the resultant dose is shown being insignificantly affected. Similar receiving dose was estimated by the DVHs of PTV_ref obtained from dose planning and treatment.

Figure A.3. The upper diagram shows the breathing pattern obtained during CT simulation and treatment, the small variation in breathing amplitude was shown at the exhaled region. The resultant 4D dose during treatment is estimated by summing the TDx weighted with time. The minimum accumulated dose of the PTV_ref during dose planning and treatment were estimated using the 4D volume dose histograms (lower diagram).

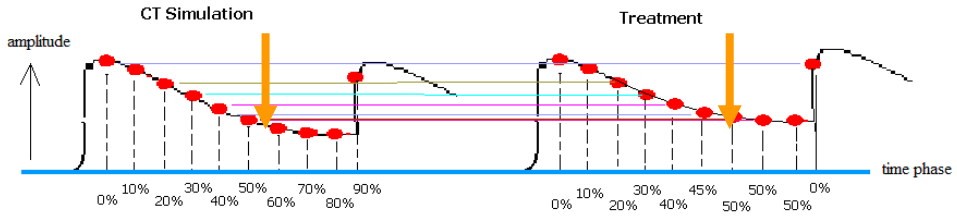

evaluated 4D planning dose:

$$\sum_{x=0\%}^{x=90\%} TD_x$$

evaluated treatment dose :

$$2\times TD_{0\%} + TD_{10\%} + TD_{20\%} + TD_{30\%} + TD_{40\%} + TD_{45\%} + 3\times TD_{50\%}$$

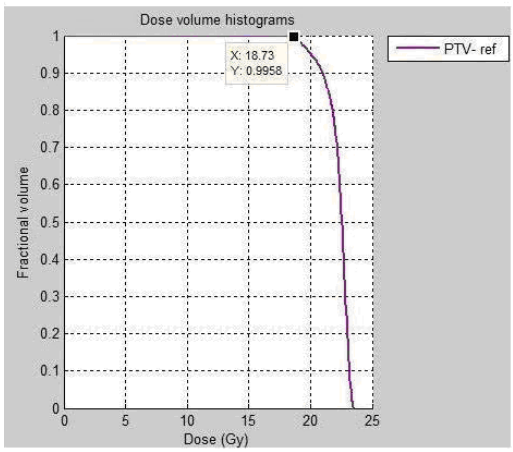

Planning Dose

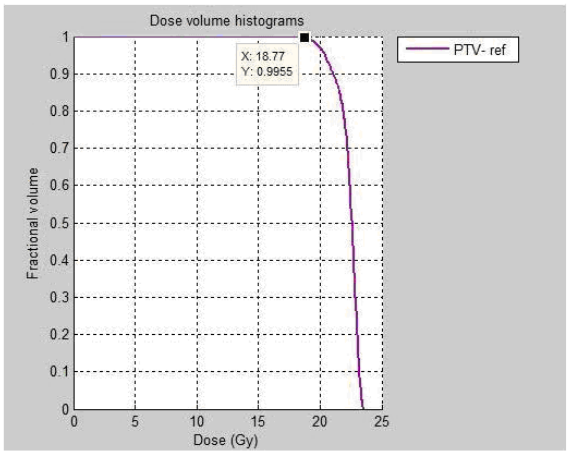

Treatment Dose

$TD_{45\%}$: interpolate between $TD_{40\%}$ & $TD_{50\%}$

REFERENCES

1. Ahn S., Yi B., Kim J. (2004). "A feasibility study on the prediction of tumour location in the lung from skin motion," Br. J. Radiol. 77, 588-596.
2. Ahnesjo A., Aspradakis M.M., et al. (1999). „ Dose calculation for external photon beams in radiotherapy". Phys. Med. Biol. 44: R99-155.
3. Alavanja M. C., Lubin J. H. et al. (1999). Residential radon exposure and risk of lung cancer in Missouri. American Journal of Public Health. 89(7): 1042 – 1048.
4. Armstrong B., Hutchinson E., et al. (2004). "Lung cancer risk after exposure to polycyclic aromatic hydrocarbons: a review and meta-analysis." Environ Health Perspect. 112(9): 970-8
5. Barnes E.A., Murray B.R., et al. (2003). "Dosimetric evaluation of lung tumour immobilization using breath hold at deep inspiration," Int J Radiat Oncol. Biol. Phys 57:1437–1442
6. Balter J.M, Lam K.M., et al. (1998). "Improvement of CT-based treatment planning models of abdominal targets using static exhale imaging. Int. J. Radiat. Oncol. Biol. Phys 41: 939-43.
7. Bradley J.D., Nofal A.N., et al. (2006). "Comparison of helical, maximum intensity projection (MIP), and average intensity (AI) 4D CT imaging for stereotactic body radiation therapy (SBRT) planning in lung caner. Radiother Oncol 81: 264-268.
8. Brown W.T., Wu A.., et al (2007). "Cyber knife radiotherapy for stage 1 lung cancer: results at 36 months" Clin Lung Cancer 88(8): 488 – 492.
9. Berbeco R.I. (2005). "Residual motion of lung tumours in gated radiotherapy with external respiratory surrogates," Phys Med Biol 50, 3655–3667.
10. Berbeco R.I., Neicu T., et al. (2005). "A technique for respiratory-gated radiotherapy treatment verification with an EPID in cine mode." Phys Med. Biol. 50: 3669–3679.
11. Blomgren H., Lax I., et al. (1995). "Stereotactic high dose fraction radiation therapy of extracranial tumours using an accelerator." Acta Oncol. 34: 861-870.
12. Blomgren H., Lax I., et al. (1998). "Radiosurgery for tumour in the body: clinical experience using a new methods." J Radiosurg 1: 63–74.

13. Birkner M., Yan D, et al. (2003). “Adapting inverse planning to patient and organ geometrical variation : Algorithm and implementation”. Med Phys 30: 2822-2831.

14. BrainLab Ltd, White paper. “iPlan automatic segmentation”.

15. Cai J., Read P.W., et al. (2007). “ Estimation of error in maximal intensity projection based internal target volume of lung tumours: A simulation and comparison study using dynamic magnetic resonance imaging.” Int J Radiat Oncol Bio Phys 69: 895-902.

16. Chao M., Schreibmann, E, et al. (2006). “Knowledge based auto-mapping of contours in 4D radiation therapy” Med Phys 33: 2171.

17. Colgan R, McClelland J, et al. (2008). “Planning lung radiotherapy using 4D CT data and a motion model”. Phys Med Biol. 53(20): 5815-30.

18. Cox J. D., Azarnia N., et al. (1990). “A randomized phase I/II trial of hypofractionated radiation therapy with total dose of 60.0 Gy to 79.2 Gy: Possible survival benefit with >69.9Gy in favorable patients with Radiation Oncology Group Stage III non-small cell lung carcinoma: Report of Radiation Oncology Group 83-11. J. Clin. Oncol. 8: 1543 – 1555.

19. Darby S., Hill D., et al. (2005). “Radon in homes and risk of lung cancer: collaborative analysis of individual data from 13 European case-control studies.” Bmj, 330(7485): 223.

20. Doll R., Fraumeni Jr. J., et al. (1994) “Trends in Cancer Incidence and Mortality.” In: Sidebottom E, ed. Cancer Surveys. Vol. 19/20. New York: Cold Spring Harbor Laboratory Press.

21. Donnelly E.D., Parikh P J, et al. (2007). “Assessment of intrafractional mediastinal and hilar lymph node movement and comparison to lung tumour motion using four-dimensional CT.” Int J Radiat Oncol Biol Phys 69: 580–588.

22. Dosoretz D., Katin M. J., et al. (1992). “Radiation therapy in the medically inoperable carcinoma of the lung: Results and implications for future treatment strategies.” Int J Radiat Oncol Biol Phys 24(1): 3-9.

23. Engelsman M., Sharp G.S., et al. (2005) “How much margin reduction is possible through gating or breath hold?” Phys Med. Biol. 50, 477–490.

24. Engelsman M, Damen E.M., et al. (2001). “The effect of breathing and setup errors on the cumulative dose to a lung tumour. Radiother Oncol 60: 95-105

25. Ekberg L., Holmberg O., et al. (1998). “What margin should be added to the clinical target volume in radiotherapy treatment planning for lung cancer?” Radiother Oncol 48: 71-77.

26. Erridge SC, Seppenwoolde Y. et al. (2003). Portal imaging to assess set-up errors, tumour motion and tumour shrinkage during conformal radiotherapy of non-small cell lung cancer. Radiother Oncol 66:75-85.

27. Ezhil M., Vadam S., et al. (2009). “Determination of patient specific internal gross tumour volume for lung cancer using four-dimensional computed tomography” Radiat Oncol. 27: 4:4.

28. Frumkin H., Samet J.M., et al. (2001). “Radon.” CA Cancer J Clin. 51(6): 337-344.

29. Fukumoto S., Shirato H., et al. (2002). “Small-volume image guided radiotherapy using hypofractionated, coplanar, and noncoplanar multiple fields for patients with inoperable stage I nonsmall cell lung carcinoma.” Cancer 95: 1546–1553.

30. Germain F., Beaulieu L, et al. (2008). “Individual margins in 3D conformal radiotherapy planning for lung cancer: analysis of physiological movements and their dosimetric impacts.” Med. Dosim. 33: 48 – 54.

31. Green B., Miles J.C.H., et al. (2002). “Radon Atlas of England and Wales.” Chilton. NRPB-W26; Report No. NRPB-W26.

32. Gross N. J. (1997). “Pulmonary effects of radiation therapy”. Ann Intern Med 86:81-92.

33. Haffty B., Goldberg N.B., et al. (1988). “Results of radical radiation therapy in clinical stage1, technically operable non-small cell lung cancer.” Int J Radiat Oncol Biol Phys 15(1): 69-73.

34. Hanley J, Debois M.M., et al. (1999). Deep inspiration breath-hold technique for lung tumours: the potential value of target immobilization and the reduced lung density in dose escalation. Int J Radiat Oncol Biol Phys 45: 603–611.

35. Harkness E.F., Brewster D.H., et al. (2002). “Changing trends in incidence of lung cancer by histologic type in Scotland.” Int J Cancer, 102(2): 179-183.

36. Harten T., Rueckert D., et al. (2002). “VTK CISG Registration Tool kit : An open source software package for affine and non-rigid registration of single and multimodal 3D images”. In: Meiler M, Saupe D, Kruggel F, et al. Eds. Bildverarbeitung für die Medizin 2002: Algorithmen System Anwendungen. Leipzig, Germany: Springer-Verlag, 2002:409 – 412.

37. Herk van M., Remeijer P, et al. (2000). “The probability of correct target dosage: Dose-population histograms for deriving treatment margins in radiotherapy”. Int. J. Radiat. Oncol. Biol. Phys 47: 1121-1135.

38. Herk van M., Remeijer P, et al. (2002). “Inclusion of geometric uncertainties in treatment plan evaluation”. Int. J. Radiat. Oncol. Biol. Phys 52: 1407-1422.

39. Herk van M., Witte M., et al. (2003). “Biological and physical fractionation effects of random geometric errors” Int. J. Radiat. Oncol. Biol. Phys 57: 1460-1471.

40. Herk van M. (2004). “Errors and Margins in Radiotherapy. Seminars in Radiation Oncology 14: 52-64.

41. Hemminki K., Li X. (2005). “Familial risk for lung cancer by histology and age of onset: evidence for recessive inheritance”. Experimental Lung Research. 31 (2): 205-215.

42. Hoisak J.D., Sixel K.E., Tirona R. (2004) “Correlation of lung tumour motion with external surrogate indicators of respiration,” Int J Radiat Oncol Biol Phys. 60, 1298-1306.

43. Hoyer M., Roed H., et al. (2006). “Prospective study on stereotactic radiotherapy of limited-stage non-small-cell lung cancer. Int J Radiat Oncol Biol Phys 66: S128–135.

44. Hurkmans C. W., Remeijer P. et al. (2001). “Setup verification using portal imaging; review of current clinical practice”. Radiother Oncol. 58:105-120.

45. ISD Online (2009). “Cancer Mortality in Scotland, 2008” http://isd.scot.nhs.uk/isd/3535.html

46. Irvine C., Morgan A., Crellin A. et al. (2004). “The clinical implication of the collapsed cone planning algorithm.” Clin. Oncol. 16: 148 - 154.

47. Janssen-Heijnen M.L., Coebergh J.W., et al. (2003). “The changing epidemiology of lung cancer in Europe.” Lung Cancer 41(3): 245-258.

48. Jin J. Y., Yin F. F., et al. (2008). “Use of the BrainLab ExacTrac X-ray 6D system in image-guided radiotherapy” Med. Dosim, 33: 124-134.
49. Kang Y., Zhang Z., et al. (2007). “4D proton treatment planning strategy for mobile lung tumours” Int J Radiat Oncol Biol Phys 67, 906 – 914 (2007).
50. Krieger T., Sauer O. A. (2005). „Monte Carlo- verus pencil-beam-/collapsed-cone-dose calculation in a heterogeneous multi-layer phantom”. Phys. Med. Biol. 50: 859-868.
51. Koch N., Liu H.H., Starkschall G., M. et al. (2004). “Evaluation of internal lung motion for respiratory-gated radiotherapy using MRI: part I. Correlating internal lung motion with skin fiducial motion” Int J Radiat Oncol Phys. 60, 1459-1472.
52. Korreman S.S., Juhler-Nottrup T., et al. (2008). “Respiratory gated beam delivery can not facility margin reduction, unless combined with respiratory related image guidance.” Radiother. Oncol. 86: 61-68
53. Kubo H.D., Hill B.C., et al. (1996). “Respiration gated radiotherapy treatment: a technical study.” Phys Med. Biol. 41: 83-91.
54. Keall P.J., Kini V. R., et al. (2001). “Motion adaptive x-ray therapy: a feasibility study.” Phys Med. Biol. 46: 1-10.
55. Klein E. E. Chin L. M., Rice K. J., et al. (1993). “The influence of air cavities on interface doses for photon beams”. Int J Radiat Oncol Biol Phys 27, 419 – 427(2007).
56. Lawrence B.M., Soren M. B., Joseph O., et al. (2010) “Radiation dose – volume effect in the lung” Int J Radiot Oncol Biol Phys 76: S70–76.
57. Li X.A., Keall P.J., et al. (2007). “Point/Counter point. Respiratory gating for radiation therapy is not ready for the prime time.” Med. Phys 34: 867-70
58. Lin L., Shi C.Y., et al. (2008). “Development of novel post-processing treatment planning platform for 4D radiotherapy”. Technol Cancer Res Treat 7(2): 125-132
59. Liu H. H., Balter P., et al. (2007). “Assessing respiration-induced tumour motion and internal target volume using 4DCT for radiation therapy of lung cancer”. Int J Radiat Oncol Biol Phys 68: 531–540.

60. Lomax N. J., Scheib S. G. (2003). Quantifying the degree of conformity in radiosurgery treatment planning. Int J Radiat Oncol Biol Phys 55: 1409-1419.

61. Lubin J.H., Alavanja M.C., et al. (2007). "Cigarette smoking and cancer risk: modeling total exposure and intensity." Am J Epidemiol 166(4): 479-89.

62. Lujan A. E. Larsen E. W., et al. (1999). "A method for incorporating organ motion due to breathing into 3D dose calculations". Med. Phys 26: 715-720.

63. Lujan A.E., Larsen E.W., et al. (2003). "Quality assurance of a system for improved target localization and patient set-up that combines real-time infrared tracking and stereoscopic X-ray imaging," Radiother Oncol. 67, 129–141.

64. Lukanich J.M. (1999). "Tobacco and public health." Chest 116: 486S-489S.

65. Maciejewski B, Talyor J.M., et al. (1986). "Alpha/beta and the importance of the size of dose per fraction for late complications in the surpraglottic larynx". Radiother. Oncol. 7: 323–326.

66. Mageras G.S., Yorke E. (2004). "Deep inspiration breath hold and respiratory gating strategies for reducing organ motion in radiation treatment," Semin Radiat Oncol. 14: 65–75.

67. Mageras G.S. (2001)."Fluoroscopic evaluation of diagrammatic motion reduction with a respiratory gated radiotherapy system." J Appl. Clin. Med. Phys 2: 191-200.

68. Martini N., Bains M.S., et al. (1995). "Incidence of local recurrence and second primary tumours in resected stage I lung cancer." J Thorac Cardiovasc Surg 109: 120–129.

69. McGarry R.C., Papiez L., et al. (2005). "Stereotactic body radiation therapy of early-stage non-small-cell lung carcinoma: phase I study." Int J Radiot Oncol Biol Phys 63: 1010–1015.

70. Michaiski J, Timmerman R. D., et al.(2009). "A phase II trial of stereotactic body radiation therapy (SBRT) in the treatment of patients with medically inoperable stage I/II non-small cell lung cancer" RTOG 0236 of the American College Radiology.

71. Minohara S., Kanai T., et al. (2000). "Respiratory gated irradiation system for heavy –ion radiotherapy." Int J Radiat Oncol Biol Phys 47: 1097-103

72. Morita K., Fuwa N., et al. (1997). “Radical radiotherapy for medically inoperable non-small cell lung cancer in clinical stage I: a retrospective analysis of 149 patients.” Radiother Oncol 42: 31–6.

73. Mountain C.F. (1997). “Revisions in the International System for Staging Lung Cancer.” Chest 111: 1710-171 7.

74. Muirhead R., Featherstone C., et al. (2010). “The potential clinical benefit of respiratory gated radiotherapy (RGRT) in a non-small cell lung cancer.” Radiat Oncol. 95: 172-177.

75. Murphy M.J. Balter J. et al. (2007). “The management of image dose during image-guided radiotherapy: Report of the AAPM Task Group 75. Med Phys 34: 4014-4063.

76. Naruke T., Goya T., et al. (1988). “Prognosis and survival in resected lung carcinoma based on the new international staging system.” J Thorac Cardiovascular Surg. 96: 440-447.

77. National Institute for Clinical Excellence. (2005). “Lung Cancer-The diagnosis and treatment of lung cancer.” Published by the National Collaborating Centre for Acute Care at The Royal College of Surgeons of England.

78. Nisbet A., Beange I., Vollmar H.S., et al. (2004). “Dosimetric verification of a commercial collapsed cone algorithm in simulated clinical situation”. Radiat Oncol. 73: 79-88.

79. Ng A.W.Y., Tung S.Y., et al. (2008). “Hypofractionated stereotactic radiotherapy for medically inoperable stage I non-small cell lung cancer – report on clinical outcome and dose to critical organs.” Radiother Oncol. 87: 24-28

80. Northern Ireland Cancer Registry (2009). “Cancer Mortality in Northern Ireland, 2008”http://www.ons.gov.uk/ons/rel/cancer-unit/cancer-incidence-and-mortality/2007-2009/stb-cancer-incidence-and-mortality.html.

81. Office for National Statistics (2008). “Mortality Statistics: Cause. England and Wales. London TSO 2009”

82. Ohara K., Okumura T., et al. (1989). “`Irradiation synchronize with respiration gate.” Int J Radiat Oncol Biol Phys 17(4): 853-857.

83. Onishi H., Araki T., et al. (2004). “Stereotactic hypofractionated high-dose irradiation for stage I nonsmall cell lung carcinoma. Clinical outcomes in 245 subjects in a Japanese multiinstitutional study”. Cancer 101: 1623–1631

84. Parkin D.M. (2011). “Tobacco-attributable cancer burden in the UK in 2010.” Br J Cancer 105(S2): S6-S13.

85. Richiardi L., Boffetta P., et al. (2004) “Occupational risk factors for lung cancer in men and women: a population-based case-control study in Italy”. Cancer Causes Control 15(3): 285-294.

86. Rietzel E., Liu A.K., et al. (2006). “Design of 4D treatment planning target volumes” Int J Radiat Oncol Biol Phys 66: 287-295

87. Rietzel E., Chen T. Y. G., et al. (2005). “Four-dimensional image-based treatment planning: Target volume segmentation and dose calculation in the presence of respiratory motion”. Int. J. Radiat. Oncol. Biol. Phys 61(5): 1535-1550

88. Riman T, Dickman PW, et al. (2002). “Hormone replacement therapy and the risk of invasive epithelial ovarian cancer in Swedish women”. J Natl Cancer Inst. Apr 3; 94(7):497-504.

89. Sacer O.A. “Calculation of dose distributions in the vicinity of high-Z interfaces for photon beams. Med. Phys. 22: 1685-1690.

90. Schweikard A., Glosser G., et al. (2000). “Robotic motion compensation for respiratory movement during radiosurgery”. Comput. Aided Surg. 5: 77.

91. Seppenwoolde Y., Berbeco R. I., et al. (2007). “Accuracy of tumour motion compensation algorithm from a robotic respiratory tracking system: A simulation study”. Med Phys 34(7): 2774-2784

92. Shaw E., Kline R., Gillin M. et al. (1993). Radiation Therapy Oncology Group: Radiosurgery quality assurance guidelines. Int J Radiat Oncol Biol Phys 27, 1231-1239.

93. Shirato H., Shimizu S., et al. (2000). “Physical aspects of real time tracking system for gated radiotherapy”. Int J Radiat Oncol Biol Phys 48: 95

94. Solberg T. D., Medin P. M., et al. (2008). “Quality assurance of immobilzation and target localization system for frameless stereotactic cranial and extracranial

hypofractionated radiotherapy," Int J Radiat Oncol Biol Phys 71: 131-135.

95. Souhami R. and Tobias J., et al. (2005). "Cancer and its management (5th edition)." Blackwell publishing

96. Spezi E., Lewis D.G., et al (2002). "A DICOM-RT based toolbox for the evaluation and verification of radiotherapy plans". Phys Med Biol 47: 4223-4232.

97. Spoelstra F. O. B., de Koste J.R., et al. (2008). "Analysis of reproducibility of respiration-triggered gated radiotherapy for lung tumours. Radiother Oncol 87: 59-64

98. Stock M., Kontrisova K., Dieckmann K., et al. (2006). "Development and application of a real-time monitoring and feedback system for deep inspiration breath hold based on external marker tracking," Med. Phys. 33, 2868-2877.

99. Taylor R., Cumming R., et al. (2001). "Passive smoking and lung cancer: a cumulative meta-analysis." Aust N Z J Public Health 25: 203-211.

100. Thirion. J. P. (1998). "Image matching as a diffusion process: an analogy with Maxwell's demons". Medical image analysis 2: 243-260.

101. Underberg R.W., Lagerwarrd F.J., et al. (2005). "Use of maximum intensity projections (MIP) for target volume generation in 4DCT scans for lung cancer" Int J Radiat Oncol Biol Phys 63: 253-260.

102. Wild P., Perdrix A., et al. (2000). "Lung Cancer Mortality in a site producing hard metal". Occup Environ Med. 57(8): 568-573.

103. Williams M.D., Sandler A.B., et al. (2001). "The epidemiology of lung cancer." Cancer Treat Res 105: 31-52.

104. Williams MW., Denekamp J., et al. (1985). "A review of alpha/beta ratios for experimental tumours: implications for clinical studies of altered fractionation". Int J Radiat Oncol Biol Phys 11: 87–96.

105. Wink N. M., Chao M, et al. (2008). "Individual gating windows based on four-dimensional CT information for respiration gated radiotherapy" Phys Med. Biol. 53: 1665-157.

106. Witte M., Geer J. Van der, et al. (2004). “The effect of target size and tissue density on the minimum margin for random error”. Med Phys 31: 3068-3079.

107. Wolthaus JW, Sonke JJ, et al. (2008). “Comparison of different strategies to use four-dimensional computed tomography in treatment planning for lung cancer patients”. Int J Radiat Oncol Biol Phys 70(4):1229-38.

108. Wong J.W., Sharpe M.B., et al. (1999).“The use of active breathing control (ABC) to reduce margin for breathing motion.” Int J Radiat Oncol Biol Phys 44: 911–919.

109. Wong V.Y. W., Tung S. Y., et al. (2010). “Real-time monitoring and control on deep inspiration breath-hold for lung cancer radiotherapy – combination of ABC and external marker tracking. Med Phys 37(9) 4673-4683.

110. Wu W.C., Chan C. L., et al. (2010). “A study on the influence of breathing phases in intensity modulated radiotherapy of lung tumours using four-dimensional CT”. Br J Radiol 83: 252-256

111. Wulf J., Baier K., et al. (2005). “Dose–response in stereotactic irradiation of lung tumour.” Radiother Oncol 77: 83–7.

112. Zhang P, Hugo G.D. et al. (2008). “Planning study comparison of real-time target tracking and four-dimensional inverse planning for managing patient respiratory motion”. Int J Radiat Oncol Biol Phys 72(4): 1221-7.